THE
PHYSICAL REVIEW
A journal of experimental and theoretical physics established by E. L. Nichols in 1893

SECOND SERIES, VOL. 65, NOS. 5 AND 6 MARCH 1 AND 15, 1944

Auger Transitions and Widths of X-Ray Energy Levels

JOHN N. COOPER
University of Oklahoma, Norman, Oklahoma
(Received October 29, 1943)

The width of an x-ray energy level depends to a large extent on the probabilities of Auger transitions from that level. Consequently, rapid variations in line width with atomic number are to be expected whenever sudden changes in Auger transition probabilities occur. Atomic number ranges wherein large variations might be expected have been studied. Part of the width variation of $L\beta_3$ for elements $73 \leq Z \leq 92$ is attributed to the Auger transitions $M_{III} \rightarrow M_V N_{IV,V}$. The transitions $N_{II} \rightarrow N_{III} O_{II,III}$, $N_{II} \rightarrow N_{IV,V} N_{IV,V}$, and $N_{III} \rightarrow N_{IV,V} N_{IV,V}$ are shown to explain an intensity anomaly of $M\zeta$ for elements $38 \leq Z \leq 58$. Several other irregular line width variations are correlated with changes in the probabilities of Auger transitions. The evidence supports the theory that Auger transitions are primarily responsible for anomalous changes in line width.

I. INTRODUCTION

IN 1935 Coster and Kronig[1] suggested that the relative diffuseness of the lines arising from transitions from L_I initial states (hereafter called L_I lines) was due to the broadening of the L_I level by Auger transitions. Large probabilities of Auger transitions from a given state decrease the mean life of atoms in this state and lead to an increase in the width of the energy level.[2] Theoretical calculations for gold (79) by L. Pincherle[3] and Ramberg and Richtmyer[4] have shown that Auger transitions account for the greater part of the widths of all levels except K. The theory that the level width depended on Auger transition probabilities was confirmed experimentally by the work of the author,[5] which showed that the width of the L_I level increased rapidly with atomic number in the range $73 \leq Z \leq 81$ where the probabilities for the Auger transitions $L_I \rightarrow L_{III} M_{IV}$ and $L_I \rightarrow L_{III} M_V$ are known to be swiftly increasing.

Since there are many Auger transition probabilities which vary rapidly with atomic number, it is clear that there should be other levels (in addition to the L_I) which show sudden changes in width from one element to the next. It is the purpose of this paper to investigate the regions in which important variations in Auger transition probabilities occur and to correlate with these variations certain apparently erratic changes in level widths.

II. PROBABLE AUGER TRANSITIONS

According to Coster and Kronig,[1] the probability of an Auger transition in which electron A goes from a state with a wave function $\psi_1(A)$ to a state represented by $\psi_2(A)$, while electron B passes from a state represented by $\psi_1(B)$ to one

[1] D. Coster and R. DeL. Kronig, Physica **2**, 14 (1935).
[2] V. Weisskopf and E. Wigner, Zeits. f. Physik **63**, 54 (1930).
[3] L. Pincherle, Nuovo Cimento (N.S.) **81**, 162 (1935).
[4] E. G. Ramberg and F. K. Richtmyer, Phys. Rev. **51**, 913 (1937).
[5] J. N. Cooper, Phys. Rev. **61**, 234 (1942).

TABLE I. Possible Auger transitions and the elements in which they may occur.

$L_I \rightarrow L_{II}N_I$	below	$Z=70$	
N_{II}	below	75	
N_{III}	below	81	
N_{IV}	below	92	
$L_{III}M_I$	below	31	
M_{II}	below	36	
M_{III}	below	37	
M_{IV}	above	73	
	below	50	
M_V	above	77	
	below	50	
$L_{II} \rightarrow L_{III}M_{IV}$	below	30	
M_V	below	30	
M_V	above	90	
$M_I \rightarrow M_{II}N_{VII}$	below	91	
N_{VI}	below	91	
N_V	below	72	
N_{IV}	below	71	
N_{III}	below	53	
N_{II}	below	53	
N_I	below	47	
M_V	below	34	
M_{IV}	below	34	
$M_{III}N_V$	below	87	
N_I	below	50	
M_V	below	34	
M_{IV}	below	34	
$M_{IV}M_V$	below	44	
M_{IV}	below	43	
M_VM_V	below	45	
$M_{II} \rightarrow M_{III}N_{IV}$	above	$Z=65$	
	below	48	
N_V	above	65	
	below	48	
$M_{IV}N_I$	below	88	
M_V	below	35	
M_{IV}	below	35	
$M_{III} \rightarrow M_{IV}N_V$	below	85	
N_{IV}	below	84	
N_{III}	below	71	
N_{II}	below	65	
N_I	below	55	
M_V	below	36	
M_{IV}	below	36	
M_VN_V	below	91	
N_{IV}	below	89	
N_{III}	below	77	
N_{II}	below	70	
N_I	below	57	
M_V	below	37	
$M_{IV} \rightarrow M_VO_{III}$	below	85	
O_{II}	below	82	
$N_I \rightarrow N_{II}O_{III}$	below	88	
O_{II}	below	85	
O_I	below	79	
N_{VII}	below	80	
N_{VI}	below	80	
N_V	below	53	
N_{IV}	below	53	
$N_I \rightarrow N_{III}N_{VI}$	below	$Z=92$	
N_V	below	53	
N_{IV}	below	53	
$N_{IV}N_V$	below	84	
N_{IV}	below	80	
N_VN_V	below	87	
$N_{II} \rightarrow N_{III}O_{III}$	above	66	
	below	55	
$N_{III}O_{II}$	below	86	
	above	66	
	below	55	
N_{VII}	below	80	
N_{VI}	below	80	
$N_{IV}N_V$	below	60	
N_{IV}	below	60	
N_VN_V	below	62	
$N_{III} \rightarrow N_{IV}O_I$	below	87	
N_{VII}	below	86	
N_{VI}	below	85	
N_V	below	57	
N_{IV}	below	56	
N_VO_I	below	89	
N_{VII}	below	87	
N_{VI}	below	86	
N_V	below	57	
$N_{IV} \rightarrow N_VO_{IV,V}$	below	81	
$N_V \rightarrow N_{VI}N_{VII}$	below	91	
N_{VI}	below	91	
$N_{VII}N_{VII}$	below	91	

described by $\psi_2(B)$, is proportional to the square of the matrix element

$$v=\int \frac{\psi_1^*(A)\psi_2(A)d\tau_1\psi_1^*(B)\psi_2(B)d\tau_2}{r_{12}},$$

where $d\tau_1$ and $d\tau_2$ are volume elements separated by r_{12} and the integration extends over all space. In order to obtain a large value of v, $\psi_1^*(A)$ and $\psi_2(A)$ must overlap considerably as must $\psi_1^*(B)$ and $\psi_2(B)$, while r_{12} should be small in the region of appreciable overlapping. $\psi_1^*(A)$ and $\psi_2(A)$ generally overlap most when both initial and final states of electron A lie in the same shell.

The energy W of the ejected electron is very important in determining the overlapping of $\psi_1^*(B)$ and $\psi_2(B)$. If W is either very small or very large, the overlapping is slight and v will be small. The transition probability as a function of W increases to a maximum and then falls off, so that the probability of an Auger transition in which the ejected electron has a high energy is small.

Many Auger transitions are allowed for some elements and forbidden for others. An Auger transition is possible only when the energy of the initial state is greater than that of the final state (of double ionization) and is most probable when the energy difference is not too great. Consequently, rapid fluctuations in the probability of such a transition are most likely in the atomic number range wherein the transition first becomes possible. In view of this fact it is of considerable value to know the atomic number at which various Auger transitions first become permitted. A systematic investigation was made of all Auger transitions which are allowed for some elements and forbidden for others. The result of

TABLE II. Widths of L series lines in electron volts.

Line	Transition	Ag(47)[a]	Ta(73)	W(74)	Rh(75)	Os(76)	Ir(77)	Pt(78)	Au(79)	Tl(81)[b]	Pb(82)[c]	U(92)[d]
$L\beta_3$	$L_I \rightarrow M_{III}$	6.6	11.7	12.3	13.6	14.7	14.9	17.2	18.4	19.7	18.3	18.8
$L\beta_4$	M_{II}	5.9	14.1	15.1	16.4	17.1	17.7	19.4	20.7	21.6	22.2	32.2
$L\gamma_2$	N_{II}	11.0	11.6	12.1	13.2	14.0	14.6	—	18.1	19.3	19.9	39.4
$L\gamma_3$	N_{III}	10.2	10.0	11.0	12.0	12.6	13.3	15.6	16.4	17.8	19.4	32.4
$L\beta_1$	$L_{II}M_{IV}$	2.4	6.6	6.5	6.5	6.6	6.8	8.3	8.5	9.0	8.4	14.3
$L\gamma_1$	N_{IV}	3.95	9.5	9.3	9.5	9.4	9.6	11.4	11.5	11.7	11.4	15.9
$L\beta_2$	$L_{III}N_V$	3.72	9.8	9.8	9.8	9.9	9.7	11.1	11.2	11.5	11.8	16.1

[a] See reference 6 of text. [b] See reference 5 of text. [c] See reference 9 of text. [d] See reference 7 of text.

TABLE III. Ratios of line widths.

Ratios	Ag(47)	Ta(73)	W(74)	Rh(75)	Os(76)	Ir(77)	Pt(78)	Au(79)	Tl(81)	Pb(82)	U(92)
$L\beta_3/L\beta_2$	1.77	1.20	1.26	1.39	1.49	1.54	1.59	1.72	1.80	1.55	1.17
$L\beta_4/L\beta_2$	1.59	1.44	1.54	1.67	1.73	1.83	1.82	1.96	2.00	1.88	2.00
$L\gamma_2/L\beta_2$	2.96	1.18	1.24	1.35	1.41	1.51	—	1.66	1.71	1.69	2.45
$L\gamma_3/L\beta_2$	2.74	1.02	1.12	1.23	1.27	1.37	1.40	1.49	1.58	1.64	2.02
$L\beta_2/L\beta_1$	1.55	1.49	1.51	1.51	1.50	1.43	1.40	1.35	1.33	1.40	1.12
$L\beta_2/L\gamma_1$	0.94	1.03	1.05	1.03	1.05	1.01	1.00	0.99	1.02	1.04	1.01

this work is summarized in Table I, which lists the transition and the atomic numbers for which it is allowed. It will be observed that certain ones are allowed above one atomic number and below another, while they are forbidden for elements in between.

The atomic number of the element for which the transition is first allowed was obtained by calculating the energy difference between the initial and final states. (A transition is obviously forbidden if the difference is negative.) Values of ν/R for the various states were taken from Siegbahn's *Spectroscopie der Rontgenstrahlen, Zweite Auflage*. The assumption was made that the energy of the final state of double ionization of element Z was equal to the sum of the energy of the inner level for element Z and the energy of the outer level for element $Z+1$. The energy so obtained is a good approximation, although not exactly correct. The uncertainty in the energy of the state of double ionization leads to an uncertainty in the atomic number at which a given Auger transition becomes possible. In the worst cases this atomic number may be incorrect by as much as three or four.

III. WIDTH VARIATIONS AND AUGER TRANSITIONS

From Table I it is clear that there exist many Auger transitions which are allowed for some elements and forbidden for others. Certain of these transitions unquestionably play an important role in determining the widths of x-ray energy levels, while others are doubtlessly negligible. It is not immediately obvious which of the transitions become highly probable, although it would be possible to find out either by lengthy calculations or by detailed experiment. That there already exist sufficient line width data to establish the importance of certain of these transitions will be shown in this paper.

There have been fairly complete studies of the widths of L series lines for several different elements. An exhaustive investigation of the entire L series of silver (47) was made by Parratt.[6] Measurements of the widths of the L lines of uranium (92) are reported by Williams.[7] The gold L series was measured by Richtmyer, Barnes, and Ramberg,[8] while Shrader[9] made a similar study of lead (82). Widths of selected L series lines for elements $73 \leq Z \leq 81$ have been measured by the author.[5] These data reveal many irregular changes in the widths of levels with atomic number. Most of these variations are readily explained in terms of Auger transitions listed in Table I.

[6] L. G. Parratt, Phys. Rev. **54**, 99 (1938).
[7] J. H. Williams, Phys. Rev. **37**, 1431 (1931).
[8] Richtmyer, Barnes, and Ramberg, Phys. Rev. **46**, 843 (1934).
[9] R. E. Shrader, Cornell thesis (1936).

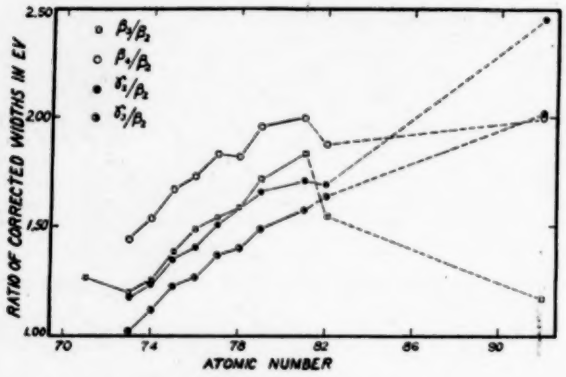

FIG. 1. Ratios of the widths of L_I lines to the width of $L\beta_2(L_{III}\rightarrow N_V)$.

In studying sudden variations in the width of a line as a function of atomic number one must remember that, in general, the width (in electron volts) increases with atomic number. This fact becomes of particular importance when one is considering elements that differ appreciably in atomic number. For example, the L series lines of gold (79) are all wider than the corresponding lines for silver (47), in most cases by a factor of two or three. This width increase for most lines is associated with the normal change with atomic number. One way of treating data which eliminates this problem is to deal with width ratios rather than widths. This essentially amounts to assuming that the "normal" width increase with atomic number is such as to leave the ratios unchanged. Available data indicate that this is a good approximation.

Width ratios have one other great advantage when one is dealing with data taken by several observers, each of whom used different crystals on different spectrometers and then corrected for crystal diffraction patterns on fundamentally different assumptions. That advantage is that the ratios are far less sensitive to crystals, spectrometers, and corrections than are the actual widths themselves. To be sure, the ratios are not independent of corrections for the finite resolving power of the spectrometers, but the percentage variation in the ratios is much less than that in the widths.

In Table II are given the corrected widths in electron volts of seven L series lines for each of eleven elements, and in Table III the ratio of the width of each of these lines to the width of $L\beta_2$ is recorded. $L\beta_2$ is chosen as the reference line because it arises from an L_{III} transition and the width of the L_{III} level is probably the least influenced by Auger transitions. The data on silver are by Parratt,[6] those on lead by Shrader,[9] and those on uranium come from Williams'[7] paper. The line widths of the other elements were measured by the author.[5] It should be mentioned that the type of corrections applied by each of these observers was different. Williams' data were corrected on the assumption that shapes were given by the Gaussian error function and his corrections were much smaller than those applied by the other observers.

In Fig. 1 the ratios of the widths of $L\beta_3$, $L\beta_4$, $L\gamma_2$, and $L\gamma_3$ to $L\beta_2$ are plotted as a function of atomic number. The first four lines all arise from transitions from the L_I state, while $L\beta_2$ comes from an $L_{III}\rightarrow N_V$ transition. There is every reason to believe that the width of $L\beta_2$ is behaving "normally" in this region; that is, neither the initial nor the final states are changing much in width. If this is true, it is clear that the width of the L_I level must be increasing between tantalum (73) and lead (82) since all the lines arising from L_I transitions show large and roughly equal increases in width in this range of atomic numbers. These width increases have been shown[5] to be associated with the rapidly increasing probabilities of the Auger transitions $L_I\rightarrow L_{III}M_V$ (possible above $Z=73$) and $L_I\rightarrow L_{III}M_{IV}$ (possible above $Z=77$).

Since all the lines (except $L\beta_2$) have the same initial state, the four curves should behave similarly unless the width of the final state is varying irregularly with atomic number. The curves do not behave alike above $Z=81$, so the conclusion is that here the widths of the final states must also be varying. In several cases the changes in width ratios are so great that the importance of certain Auger transitions are well established, while in other cases the variations are only of the order of the experimental errors. In such cases the variations may be due to Auger transitions and have been attributed to them, although it is possible that they are due to a fortuitous combination of possible errors.

The line $L\beta_3$ narrows greatly between thallium (81) and uranium (92). Since $L\beta_3$ arises from an $L_I\rightarrow M_{III}$ transition, this means that the M_{III}

level must be decreasing in width. Table I reveals that the Auger transitions $M_{III} \rightarrow M_V N_{IV}$ and $M_{III} \rightarrow M_V N_V$ become possible for elements of atomic number below 90 and are forbidden for elements of higher atomic number. Also the transitions $M_{III} \rightarrow M_{IV} N_{IV}$ and $M_{III} \rightarrow M_{IV} N_V$ are forbidden for uranium and allowed for the other elements. (See Fig. 2, reference 10 and Fig. 1, reference 11.) Judging by the great drop in the relative width of $L\beta_3$ these transitions must account for much of the width of the M_{III} level for elements around $Z=81$.

Since the probability of the transitions will decrease as the energy of the ejected electron becomes too great, the width of the M_{III} level might be expected to be less for Ta(73) than for Tl(81). This argument is supported by the observation that the actual width increase of $L\beta_3$ between these elements is greater than that of any of the other L_I lines. This would be expected if the Auger transitions $M_{III} \rightarrow M_V N_{IV}$ and $M_{III} \rightarrow M_V N_V$ had a maximum probability in the neighborhood of $Z=81$.

Further support for this explanation can be found in the work on $M\alpha$-satellites by Hirsh,[10] who has shown that these satellities have a maximum relative intensity near lead (82). Since these satellites arise from an $M_V N_{IV,V}$ initial state, they will obviously increase in intensity as the Auger transitions $M_{III} \rightarrow M_V N_{IV,V}$ become more probable. Thus the importance of these radiationless transitions is established by independent observations.

The width of $L\beta_4(L_I \rightarrow M_{II})$ appears to be relatively stable between thallium and uranium although data on intermediate elements might indicate width variations associated with the Auger transition $M_{II} \rightarrow M_{IV} N_I$ which is possible[11] for elements of atomic number below 88.

Both $L\gamma_2(L_I \rightarrow N_{II})$ and $L\gamma_3(L_I \rightarrow N_{III})$ are much wider for uranium than might have been expected, showing that the N_{II}, and *particularly* the N_{III}, levels have become very wide. There is nothing in Table I which would predict such an increase. The addition of ten electrons in outer levels between lead and uranium will make many new Auger transitions possible and it is conceivable that one of them might be very probable.

[10] F. R. Hirsh, Phys. Rev. **57**, 662 (1940).
[11] F. R. Hirsh, Phys. Rev. **59**, 766 (1941), Fig. 1.

Figure 2 shows the width ratios $L\beta_2/L\beta_1$ and $L\beta_2/L\gamma_1$. $L\beta_2$ arises from the transition $L_{III} \rightarrow N_V$, while $L\beta_1$ and $L\gamma_1$ have L_{II} as an initial state and their final states are M_{IV} and N_{IV}, respectively. It is immediately clear that these ratios are much more constant than those involving L_I lines. The width ratio $L\beta_2/L\gamma_1$ is almost constant for all the elements listed, but the ratio $L\beta_2/L\beta_1$ decreases with atomic number. There are a number of Auger transitions which may play a part in this. First, $L\beta_1$ may be wider at uranium because the Auger transition $L_{II} \rightarrow L_{III} M_V$ becomes possible above $Z=90$ and may contribute to the width of the L_{II} level. If this is true, the width of $L\gamma_1$ should be similarly influenced, and in order to explain its constancy, it is possible to point out that the N_{IV} level may have narrowed because the transitions $N_{IV} \rightarrow N_V O_{IV,V}$ are forbidden for elements above 81. Part of the decrease for the width ratio $L\beta_2/L\beta_1$ may be due to a narrowing of the N_V level for uranium, since the transitions $N_V \rightarrow N_{VI} N_{VI,VII}$ and $N_V \rightarrow N_{VII} N_{VI,III}$ are impossible for that element. Another factor which contributes to the small ratio for uranium is the smaller correction subtracted from the widths in this case. (Obviously, too small a correction would tend to make this ratio nearer to unity.)

Some interesting changes in the widths of levels occur between elements 73 and 47. For silver the lines $L\gamma_2$ and $L\gamma_3$ are nearly twice as wide as $L\beta_3$ and $L\beta_4$ which indicates that the N_{II} and N_{III} levels are much wider than the M_{II} and M_{III} levels. For elements 73 to 82 the M_{II}

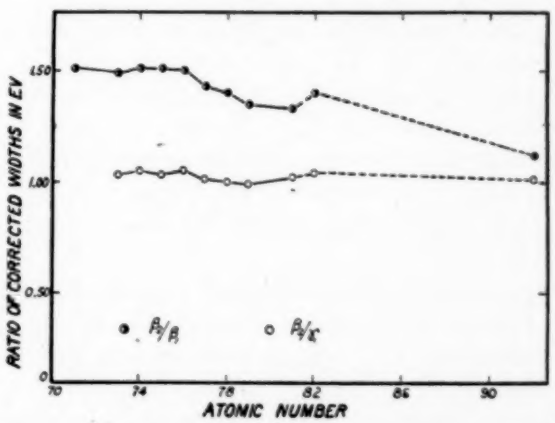

FIG. 2. The width ratios $L\beta_2/L\beta_1$ and $L\beta_2/L\gamma_1$ as a function of atomic number. (Transitions: $L\beta_2$, $L_{III} \rightarrow N_V$; $L\beta_1$, $L_{II} \rightarrow M_{IV}$; $L\gamma_1$, $L_{II} \rightarrow N_{IV}$.)

TABLE IV. Widths of $M\zeta$ in electron volts (after Kiessig).

Element	Width	Element	Width	Element	Width
Sr(38)	1.99	Rh(45)	4.57	Sb(51)	18.5
Zr(40)	2.06	Pd(46)	6.74	Te(52)	18.5
Nb(41)	3.44	Ag(47)	13.6	Ba(56)	7.0
Mo(42)	3.05	Cd(48)	14.8	La(57)	9.1
Ru(44)	3.79	Sn(50)	16.4	Ce(58)	10.6

and M_{III} levels are wider than the corresponding N levels, but for uranium the N levels are again wider. This can be partially explained as follows: (1) For elements of atomic number 70 to 82 the M_{III} level should be wide because of the high probabilities of the transitions $M_{III}\rightarrow M_V N_{IV,V}$ and (possibly) $M_{III}\rightarrow M_{IV}N_{IV,V}$ which have already been mentioned in connection with the small width of $UL\beta_3$. Also, for silver the Auger transitions $M_{III}\rightarrow M_{IV}N_I$ and $M_{III}\rightarrow M_V N_{I,II}$ are impossible, whereas they should contribute to the width of the M_{III} level for elements of higher atomic number. (2) The M_{II} level may be expected to be wide for elements not too far above 70 because of the Auger transitions $M_{II}\rightarrow M_{III}N_{IV}$ and $M_{II}\rightarrow M_{III}N_V$. These transitions are forbidden for elements between (about) 65 and 48. Whether or not they are allowed for silver is doubtful, but judging by the small width of the Ag M_{II} level it seems certain that these transitions are very improbable for silver even if they are possible.

While these Auger transitions may serve to explain why the M levels are wider than the N levels for elements of atomic number between 73 and 82, still the widths of the N_{II} and N_{III} levels for silver are so very great that their excessive widths require further explanation. The N_{II} level is widened by the transitions $N_{II}\rightarrow N_{III}O_{II,III}$ which are possible for elements of atomic number below 55 and by $N_{II}\rightarrow N_{IV,V}N_{IV,V}$ which are allowed below $Z=60$. The great width of the N_{III} level is attributed to the transitions $N_{III}\rightarrow N_{IV,V}N_{IV,V}$ which are possible for elements below $Z=56$.

Line width data by Kiessig[12] support the contention that these transitions must be highly probable for silver (47). In Table IV are the widths of $M\zeta$ for fifteen elements as reported by Kiessig. The line $M\zeta$ arises from a transition $M_V\rightarrow N_{II,III}$. The width increases rapidly from $Z=38$ to $Z=52$, showing that the N_{II} and N_{III} levels are widening rapidly. (The M_V level is "normal" for silver and there is no reason to think that these width changes are due to the initial level.) The width has decreased tremendously at $Z=56$, just as would be expected from a consideration of Auger probabilities. Kiessig did not offer an explanation for the intensity anomaly, but pointed out that the elements at the beginning of the fifth period of the periodic table (36–54) had small $M\zeta$ widths and those at the end had great widths, while the three elements at the beginning of the sixth period again had narrow breadths. Siegbahn and Magnusson[13] had previously found that the $M\zeta$ lines of Br(35) and Rb(37) were very sharp, so that the generalization that the width increased as one went through an atomic period was not justified. Now it seems virtually certain that the above-mentioned Auger transitions provide the correct explanation for this intensity anomaly.

It is not inconceivable that the width increase between element 56 and 58 is due to the increasing probability of $N_{II}\rightarrow N_{IV,V}N_{IV,V}$ but the data do not cover a big enough atomic number range to be conclusive. If the width of $M\zeta$ were shown to be much less above $Z=60$, this explanation would be much better established.

The width of the N_{II} level is consistently wider than that of the N_{III} level for all elements considered here. This is in accord with the general rule that for different levels having the same total quantum number the level width decreases with increasing azimuthal quantum number. An exception to this rule is found in silver where the M_{III} level has a greater width than the M_{II} level. The unexpectedly large M_{III} width may be associated with relatively great probabilities of the transitions $M_{III}\rightarrow M_{IV}N_I$ and $M_{III}\rightarrow M_V N_I$, possible below atomic numbers 55 and 57, respectively.

It is interesting to note that the width ratios $L\beta_2/L\beta_1$ and $L\beta_2/L\gamma_1$ for silver are almost the same as for elements of atomic number 73 to 81. Since all the levels involved in these lines are associated with relatively high azimuthal quantum numbers, the Auger transitions generally

[12] H. Kiessig, Zeits. f. Physik **109**, 671 (1938), and **95**, 555 (1935).

[13] M. Siegbahn and T. Magnusson, Zeits. f. Physik **88**, 559 (1934).

contribute much less to the level widths. The relative constancy of the width ratios for these lines over so great an atomic number range supports the ratio method for handling width data for elements of vastly different atomic number.

IV. CONCLUSIONS

Since the width of a state is inversely proportional to the mean life of atoms in that state, a very probable Auger transition increases the level width. This results in a width increase for all lines which have this level as either an initial or final state. Because Auger transition probabilities frequently vary rapidly as a function of atomic number, one should expect rapid changes in line width. This prediction is verified. In this paper it has been shown that the width variation of $L\beta_3$ for elements $73 \leq Z \leq 92$ can be accounted for in terms of the Auger transitions $M_{III} \rightarrow M_V N_{IV,V}$. Also the anomalous width behavior of $M\zeta$ reported by Kiessig has been shown to be associated with the rapid changes in the Auger probabilities $N_{II} \rightarrow N_{III} O_{II,III}$, $N_{II} \rightarrow N_{IV,V} N_{IV,V}$, and $N_{III} \rightarrow N_{IV,V} N_{IV,V}$ for elements $38 \leq Z \leq 58$. Certain other irregular width variations have been shown to be explicable in terms of Auger transitions. More data on line widths would doubtless reveal other cases in which line widths are increased by Auger transitions.

The author wishes to thank Dr. F. R. Hirsh, Jr., for his encouragement and suggestions.

PHYSICAL REVIEW VOLUME 65, NUMBERS 5 AND 6 MARCH 1 AND 15, 1944

On Apertures of Transmission Type Electron Microscopes Using Magnetic Lenses

L. MARTON AND R. G. E. HUTTER
Division of Electron Optics, Stanford University, Stanford University, California

(Received January 5, 1944)

The numerical aperture of light microscopes is larger than that of electron microscopes at their present state of development by a factor of 100 to 1000. This is due to the fact that electron lenses have higher aberrations than the highly corrected glass lens systems used in modern light microscopes. In the design of an electron microscope care has to be taken therefore that the proper numerical aperture should be used to give the optimum resolution. The majority of transmission type electron microscopes use at present magnetic lenses. For magnetic lenses of the axial field distribution $H(z) = H_0/[1+(z/a)^2]$ optimum conditions for size and location of apertures will be stated. The behavior of the condenser lens-objective lens system with respect to the angular aperture of the illuminating electron beam also will be discussed.

I. THE MAGNETIC LENS OF THE AXIAL FIELD DISTRIBUTION $H(z) = H_0/[1+(z/a)^2]$

THE small values of numerical apertures of electron microscopes can be achieved by allowing only such electrons to take part in the image formation whose paths do not pass through the lenses too far away from the optical axis. These paths are called paraxial. They can be described mathematically as the solutions $r = r(z)$ of the so-called paraxial ray differential equation:

$$\frac{d^2r(z)}{dz^2} + \frac{e}{8mV} H^2(z) r(z) = 0, \qquad (1)$$

where $r = r(z)$ signifies the distance of the electron from the axis at the point z—the axial coordinate; $H(z)$ is the axial field distribution; e/m is the specific charge of the electron, and V is the accelerating potential for the electrons.

It has been shown[1] that for an axial field distribution, very closely approximated in practical magnetic lenses,

$$H(z) = H_0/[1+(z/a)^2]. \qquad (2)$$

The solution of Eq. (1) is given by

$$r(z) = a(1+(z/a)^2)^{\frac{1}{2}} \times \{C_1 \sin [(1+K^2)^{\frac{1}{2}} \operatorname{arc\,cot} (z/a)] + C_2 \cos [(1+K^2)^{\frac{1}{2}} \operatorname{arc\,cot} (z/a)]\}, \qquad (3)$$

[1] Walter Glaser, Zeits. f. Physik **117**, 285 (1941).

where H_0 is the maximum field strength on the axis, $z=\pm a$ is that coordinate where $H(z)=H(\pm a)=\frac{1}{2}H_0$ ($2a$ is termed the half-width of the field curve), and

$$K^2=eH_0^2a^2/8mV \tag{4}$$

is a parameter characterizing the lens strength. C_1 and C_2 are two arbitrary constants of integration, which can be determined so that the path satisfies any initial or boundary conditions.

II. ANGULAR APERTURE. THE CONDENSER LENS-OBJECTIVE LENS SYSTEM

The numerical aperture is defined by

$$N=n\cdot\sin\alpha,$$

where n is the index of refraction and α is the so-called angular aperture, that is, the largest angle formed by light rays which pass the center of the object. In electron microscopes $n=1$ and $\sin\alpha\approx\alpha$ for the values $\alpha=10^{-3}$ to 10^{-2} radian.

Borries and Ruska[2] calculated the angular aperture of a lens system, consisting of a condenser lens and an objective lens, for various lens strength of the condenser lens (Fig. 1a). Their results are given by the following formulas and graphs (Fig. 1b).

$$\alpha_c=\frac{d_{\min}/2}{a+b-(a\cdot b/f_c)}$$

$$\text{for}\quad 0<\frac{1}{f_c}<\left(\frac{a+b}{a\cdot b}-\frac{d_{\min}}{2a^2\alpha_s}\right),$$

$$\alpha_c=\alpha_{c\,\max}=\frac{a}{b}\alpha_s$$

$$\text{for}\quad \left(\frac{a+b}{a\cdot b}-\frac{d_{\min}}{2a^2\alpha_s}\right)<\frac{1}{f_c}<\left(\frac{a+b}{a\cdot b}+\frac{d_{\min}}{2a^2\alpha_s}\right), \tag{5}$$

$$\alpha_c=\frac{d_{\min}/2}{(a\cdot b/f_c)-(a+b)}$$

$$\text{for}\quad \left(\frac{a+b}{a\cdot b}+\frac{d_{\min}}{2a^2\alpha_s}\right)<\frac{1}{f_c}<\infty,$$

where $d_{\min}$ is the diameter of the minimum cross section of the electron beam in front of the cathode (the virtual source), a is the distance of this minimum from the condenser lens, and b is the distance of the object from the same lens. f_c is the focal length of this lens and α_s is the angle given in Fig. 1a.

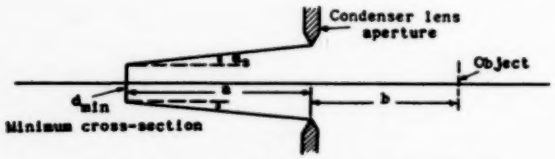

FIG. 1a. Condenser lens. Notation for Eq. (5).

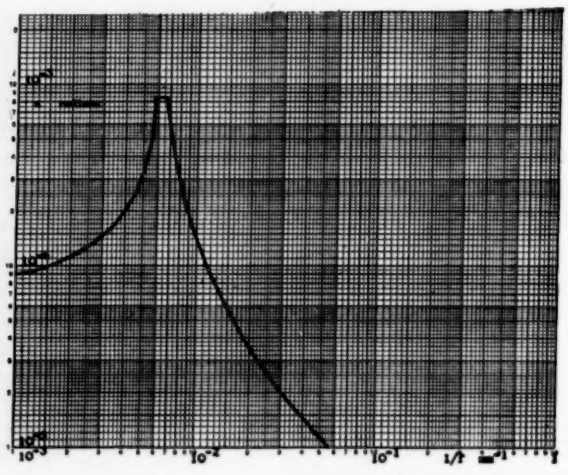

FIG. 1b. Angular aperture in function of the refracting power of the condenser lens according to B. v. Borries and E. Ruska.

In these calculations, of purely light optical character, it was assumed that no other lens was located between the condenser lens and the object. This, however, is no longer true if the object is located so that it is well within the field of the objective lens. Glaser[1] has shown that for the condition of minimum spherical aberration this location is imperative. In this case a part of the field of the objective lens lies between the object and the condenser lens and has a focusing effect on the incoming illuminating electron beam, changing the angular aperture as given by the condenser lens strength alone.

Assuming for both lenses a field form given by Eq. (2) it is possible to recalculate the value of the angular aperture, taking into account the focusing action of the objective lens fragment. It is necessary, however, to assume a field free plane midway between the objective lens and the condenser lens—an assumption normally realized in electron microscopes (Fig. 2).

[2] B. v. Borries and E. Ruska, Zeits. f. tech. Physik **20**, 225 (1939).

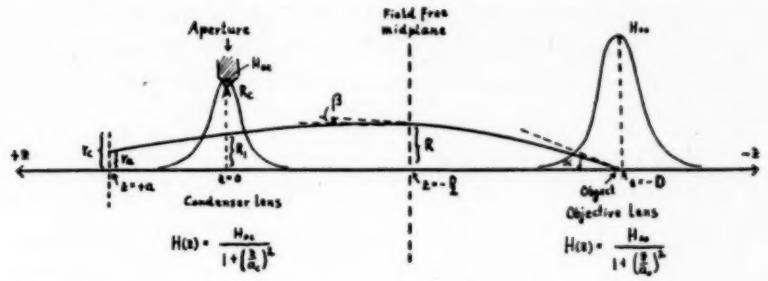

Notation:

H_{0c}, H_{0o} maximum field strengths of the lenses.

$2a_c$, $2a_o$ half-widths of the field strength curves.

$K_{0c}^2 = \frac{eH_{0c}^2 a_c^2}{8mV}$, $K_{0o}^2 = \frac{eH_{0o}^2 a_o^2}{8mV}$ or $\omega_c = (1+K_{0c}^2)^{\frac{1}{2}}$, $\omega_o = (1+K_{0o}^2)^{\frac{1}{2}}$ parameters characterizing the strengths of the lenses.

FIG. 2. Electron path through the condenser lens and objective lens.

The values of ω realized in practice are $1 \leqq \omega \leqq 2$; r_c is the radius of the cross-over disk of electrons in front of the cathode of the electron microscope; R_c is the radius of the condenser lens aperture; R, R_1, r_a are ordinates of the electron path at the abscissas $z=-D/2$, $z=0$, $z=+a$, respectively.

The method for arriving at a solution for the angular aperture α consists of the following steps. Two solutions of the paraxial ray equation, one for each lens, are taken and matched at the field free midplane so that their distances from the optical axis are equal and their slopes are identical. The total path has to pass the center of the object and must also go through a point on the circular disk of the electron cross-over. Among all such paths the one is taken which gives the largest angle α for given lens strengths and position coordinates. This α_{max} is then the angle determining the angular aperture.

Glaser[1] has shown that for minimum spherical aberration the object would have to be very near the center of the objective lens. For the sake of simplicity it is assumed here that the object is at the center of the lens.

Rewriting the formulas of Borries and Ruska in terms of quantities used here, we find the angle α_{max} is given by

$$\tan \alpha_{max} = \frac{-r_a \omega_c}{a_c\{[1+(a/a_c)^2][1+(D/a_c)^2]\}^{\frac{1}{2}} \sin\{\omega_c[\operatorname{arc\,cot}(a/a_c) - \pi + \operatorname{arc\,cot}(D/a_c)]\}}. \quad (6)$$

By varying ω_c between 1 and 2 a variation of α_{max} is obtained which is identical with that given by the previous formulas.

If ω_c becomes

$$\omega_c = \frac{\pi}{\operatorname{arc\,cot}(a/a_c) - \pi + \operatorname{arc\,cot}(D/a_c)}, \quad (7)$$

the cross-over would have its image at the object position, which means that rays leaving the center of the cross-over at any angle would pass through the center of the object at any angle up to 90°. This angle, however, cannot be reached because of the limiting effect of the physical aperture of the condenser lens (Fig. 3).

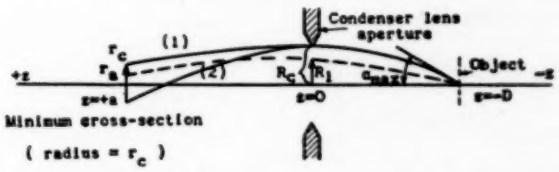

FIG. 3. Limiting effect of the physical aperture of the condenser lens.

There will be a value ω_{c1} which realizes path (1) and a greater value $\omega_{c2}(\omega_{c2}>\omega_{c1})$ which realizes path (2). In order to find the limiting ω_c it is necessary to find the distance R_1, at which any path passes the condenser lens center (where the physical aperture is assumed to be located). R_1 is given by

$$R_1=\frac{a_c}{\omega_c}\left[1+\left(\frac{D}{a_c}\right)^2\right]^{\frac{1}{2}}\tan\alpha\sin\left[\omega_c\left(\operatorname{arc\,cot}\frac{D}{a_c}-\frac{\pi}{2}\right)\right] \tag{8}$$

together with

$$r_c=\frac{a_c}{\omega_c}\left\{\left[1+\left(\frac{a}{a_c}\right)^2\right]\left[1+\left(\frac{D}{a_c}\right)^2\right]\right\}^{\frac{1}{2}}\tan\alpha\sin\left[\omega_c\left(\pi-\operatorname{arc\,cot}\frac{a}{a_c}-\operatorname{arc\,cot}\frac{D}{a_c}\right)\right]; \tag{9}$$

the ratio R_1/r_c can be plotted as a function of ω_c:

$$\frac{R_1}{r_c}=\frac{1}{[1+(a/a_c)^2]^{\frac{1}{2}}}\frac{\sin\{\omega_c[\operatorname{arc\,cot}(D/a_c)-(\pi/2)]\}}{\sin\{\omega_c[\pi-\operatorname{arc\,cot}(a/a_c)-\operatorname{arc\,cot}(D/a_c)]\}}. \tag{10}$$

ω_{c1} and ω_{c2} are the values for which $R_1/r_c=\pm R_c/r_c$. For all values of ω_c, $\omega_{c1}\leqq\omega_c\leqq\omega_{c2}$ the physical aperture becomes the limiting factor for the angular aperture.

Repeating now the same procedure for the case where the fragment of the objective lens is active in forming the angular aperture, we obtain the following expressions:

$$\tan\alpha_{\max}=\frac{(1/a_c)r_a\omega_c[1+(D/2a_c)^2]^{\frac{1}{2}}/[1+(a/a_c)^2]^{\frac{1}{2}}}{(K_1/a_c)\omega_c\cos\{\omega_c[\pi-\operatorname{arc\,cot}(a/a_c)-\operatorname{arc\,cot}(D/2a_c)]\}}, \tag{11}$$
$$+\{(K_1D/2a_c^2)+K_2[1+(D/2a_c)^2]\}\sin\{\omega_c[\pi-\operatorname{arc\,cot}(a/a_c)-\operatorname{arc\,cot}(D/2a_c)]\}$$

where

$$K_1=\frac{a_0}{\omega_0}\left[1+\left(\frac{D}{2a_c}\right)^2\right]^{\frac{1}{2}}\sin\left[\omega_0\left(\frac{\pi}{2}-\operatorname{arc\,cot}\frac{D}{2a_c}\right)\right],$$
$$K_2=\frac{1}{\omega_0}\frac{1}{[1+(D/2a_c)^2]^{\frac{1}{2}}}\left\{\frac{D}{2a_0}\sin\left[\omega_0\left(\frac{\pi}{2}-\operatorname{arc\,cot}\frac{D}{2a_c}\right)\right]+\omega_0\cos\left[\omega_0\left(\frac{\pi}{2}-\operatorname{arc\,cot}\frac{D}{2a_0}\right)\right]\right\}. \tag{12}$$

K_1 and K_2 depend on ω_0, the parameter of the objective lens, and the location of the object; these quantities are plotted in Fig. 4.

In order to determine the range of ω_c values for which the physical aperture of the condenser lens becomes the limiting factor for the angular aperture α the distance R_1 must be determined.

The equation giving R_1 in this case is

$$R_1=\frac{a_c}{\omega_c}\frac{1}{[1+(D/2a_c)^2]^{\frac{1}{2}}}K_1\left\{\frac{\omega_c}{a_c}\cos\left[\omega_c\left(\frac{\pi}{2}-\operatorname{arc\,cot}\frac{D}{2a_c}\right)\right]\right.$$
$$\left.+\left[\frac{D}{2a_c^2}+\frac{K_2}{K_1}\left(1+\left(\frac{D}{2a_c}\right)^2\right)\right]\sin\left[\omega_c\left(\frac{\pi}{2}-\operatorname{arc\,cot}\frac{D}{2a_c}\right)\right]\right\}, \tag{13}$$

and from Eq. (11)

$$r_c=\frac{a_c}{\omega_c}\left[\frac{1+(a/a_c)^2}{1+(D/2a_c)^2}\right]^{\frac{1}{2}}K_1\left\{\frac{\omega_c}{a_c}\cos\left[\omega_c\left(\pi-\operatorname{arc\,cot}\frac{a}{a_c}-\operatorname{arc\,cot}\frac{D}{2a_c}\right)\right]\right.$$
$$\left.+\left[\frac{D}{2a_c^2}+\frac{K_2}{K_1}\left(1+\left(\frac{D}{2a_c}\right)^2\right)\right]\sin\left[\omega_c\left(\pi-\operatorname{arc\,cot}\frac{a}{a_c}-\operatorname{arc\,cot}\frac{D}{2a_c}\right)\right]\right\}\tan\alpha. \tag{14}$$

Forming again R_1/r_c and plotting this ratio as a function of ω, we find the two values ω_c, for which $R_1/r_c = \pm R_c/r_c$. These are called ω_{c1}, ω_{c2}. For all values ω for which $\omega_{c1} \leqq \omega_c \leqq \omega_{c2}$ the angular aperture is determined by the physical condenser lens aperture.

Furthermore, there will be one value $\omega = \omega^*$ for which the denominator in Eq. (11) becomes zero (or $R_1/r_c = +\infty$). For this value ω^* the cross-over of the electrons in front of the cathode is focused on the object. This means that all rays starting at the center of the cross-over will pass through the center of the object. In Eq. (11) r_a and the denominator become zero; hence $\tan \alpha$ is indeterminate, as it should be.

Figures 5 and 6 are obtained if the following values are assumed:

$D = 420$ mm, $a = 250$ mm, $a_c = 3$ mm, $a_0 = 1.5$ mm; $r_c = 0.05$ mm, $R_c = 0.4$ mm, hence $R_c/r_c = 8$; $\omega_0 = 1.5$, $1 \leqq \omega_c \leqq 2$.

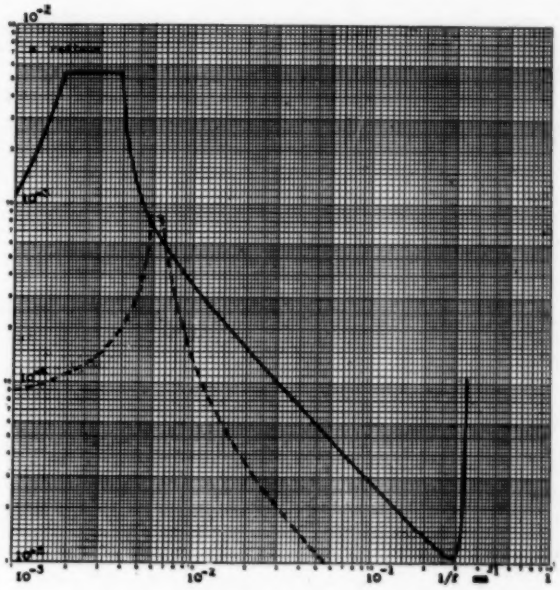

FIG. 5. Angular aperture of the incoming beam in function of the refracting power of the condenser lens.

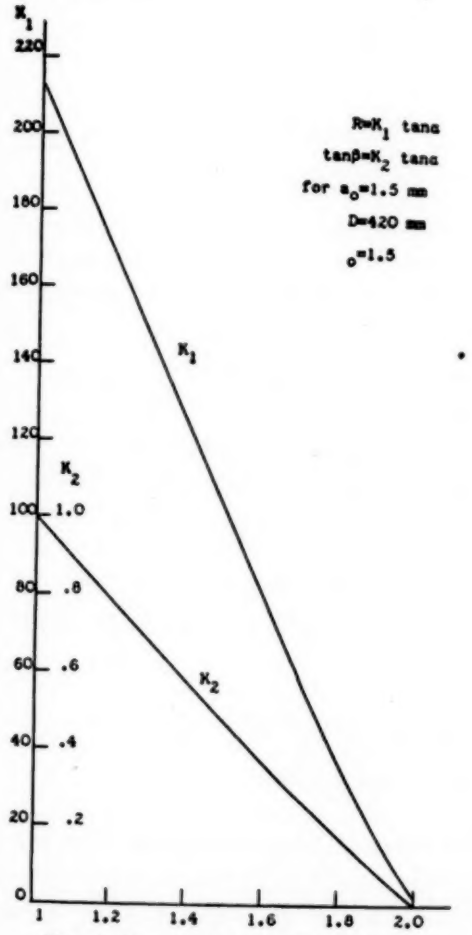

FIG. 4. K_1 and K_2 in function of ω.

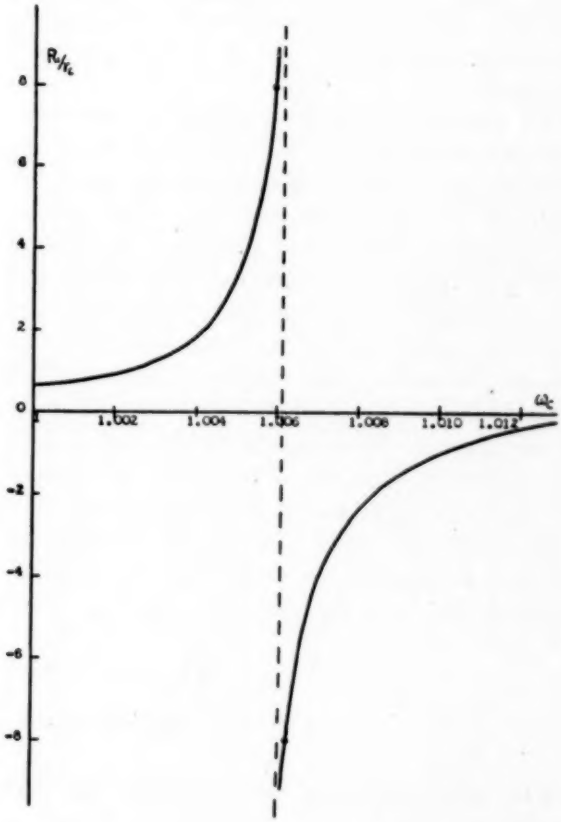

FIG. 6. R_1/r_c as a function of ω_c. [$\omega_{c1} = 1.0059$; $\omega^* = 1.0061$; $\omega_{c2} = 1.0063$.]

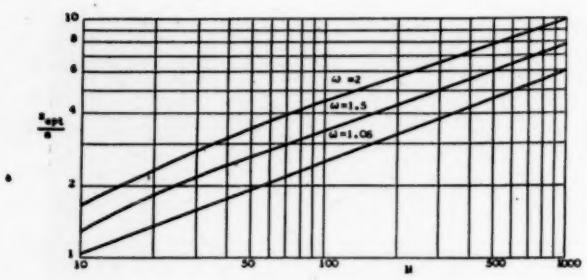

FIG. 7. Location of the aperture on the optical axis in function of the magnification and the lens parameters a and ω.

For the sake of comparison, Fig. 5 shows α_{max} as calculated by means of the indicated methods and as calculated for the same numerical values by the method of v. Borries and Ruska (dotted line).

Contrary to previous assumptions it is shown that the angular aperture cannot be decreased below any prescribed limit by increasing the refracting power of the condenser lens. There exists a definite minimum for α, as observed in electron microscopes, because of the effect of refracting properties of the objective lens fragment.

The formulas derived so far allow the determination of the angular aperture of the incoming electron beam. After passing the specimen the electrons are scattered and diffracted causing the angular aperture to be increased. In order to limit the angular aperture to values prescribed by limitations of the resolving power physical apertures must be used. These apertures are usually located at the center of the objective lens. It is obvious, however, that the diameter of the aperture must become smaller and smaller the nearer the object is to the center of the lens, if it has to achieve the same ray limiting action.

Knowing the exact solution for the electron path it is possible to determine an optimum position and size for such an aperture which achieves the same ray limiting effect. Let

$$y(z)=r(z)/a \quad \text{and} \quad x=z/a; \tag{15}$$

then Eq. (3) can be written as

$$y(z)=(1+x^2)^{\frac{1}{2}}\{C_1 \sin[\omega \operatorname{arc\,cot} x] + C_2 \cos[\omega \operatorname{arc\,cot} x]\}. \tag{16}$$

If the constants of integration C_1 and C_2 are determined so that the path goes through a point $x=x_0$, the x coordinate of the object position, and has there a slope $y'(x_0)=\tan\alpha$, Eq. (3) becomes:

$$y(x)=\frac{1}{\omega}[(1+x^2)(1+x_0^2)]^{\frac{1}{2}} \sin[\omega(\operatorname{arc\,cot} x_0 - \operatorname{arc\,cot} x)] \tan\alpha \tag{17}$$

or

$$y(x)=\frac{\sin[\omega(\operatorname{arc\,cot} x_0-\operatorname{arc\,cot} x)]}{\sin[\operatorname{arc\,cot} x_0]\sin[\operatorname{arc\,cot} x]}\cdot\frac{\tan\alpha}{\omega}. \tag{18}$$

The slope of this path at any point x is given by

$$y'(x_0)=\frac{\tan\alpha}{\omega}\left[\frac{1+x_0^2}{1+x^2}\right]^{\frac{1}{2}} \times\{x \sin[\omega(\operatorname{arc\,cot} x_0-\operatorname{arc\,cot} x)] + \omega\cos[\omega(\operatorname{arc\,cot} x_0-\operatorname{arc\,cot} x)]\}. \tag{19}$$

Let x_m be the x coordinate of the point of maximum deviation of the electron from the axis. Then x_m is given by the transcendental equation:

$$\operatorname{arc\,cot} x_0=\operatorname{arc\,cot} x_m+\frac{\pi}{\omega}-\frac{1}{\omega}\operatorname{arc\,cot}\frac{x_m}{\omega}. \tag{20}$$

The next step is to combine Eq. (8) with the formula for the magnification of the lens.[1]

$$M=\frac{1}{x_0-\cot(\pi/\omega)}\cdot\frac{1}{\sin(\pi/\omega)}. \tag{21}$$

M is then given as a function of x_m and the lens parameter

$$M=\frac{\sin\{\operatorname{arc\,cot} x_m+(\pi/\omega)-(1/\omega)\operatorname{arc\,cot}(x_m/\omega)\}}{\sin\{(1/\omega)\operatorname{arc\,cot}(x_m/\omega)-\operatorname{arc\,cot} x_m\}}. \tag{22}$$

For large values of M ($M>100$) Eq. (22) becomes:

$$M=3\frac{\sin(\pi/\omega)}{(1-\omega^2)}x_m^3. \tag{23}$$

The position coordinate of the maximum path deviation from the optical axis is plotted in Fig. 7 as a function of the magnification for several lens parameters. The value $\omega=1.06$ corresponds

to a weak lens; ($\omega=1$ characterizes a lens of zero refracting power!) and $\omega=2$ to a strong lens. (It has been shown by Glaser[1] that for values $\omega\geqq 2$ an object has two images.)

An aperture placed at $x=x_m$ on the optical axis can have a considerably greater size than one placed at the center of lens and yet have the same ray limiting effect. The size of the aperture for any angular aperture α (as determined for a permissible spherical aberration) can be determined by the use of the formula:

$$\frac{\text{radius of aperture}}{\tan\alpha}=\frac{r_A}{\tan\alpha}=a\left[\frac{(1+x_m^2)(1+x_0^2)}{(\omega^2+x_m^2)}\right]^{\frac{1}{2}}. \quad (24)$$

$2r_A/a\tan\alpha$ is plotted in Fig. 8 as a function of the magnification for various values of ω.

The ordinate of the path at the center of the lens is given by

$$r(0)=\frac{a}{\omega}(1+x_0^2)^{\frac{1}{2}}\sin\left[\omega\left(\operatorname{arc\,cot}x_0-\frac{\pi}{\omega}\right)\right]\tan\alpha. \quad (25)$$

The ratio of $2r_A/2r(0)=d_A/d_0$ is plotted in Fig. 9 as a function of the magnification for various values of ω. It shows the gain in aperture size for an aperture at the optimum position as compared with the customary aperture design at the center of the lens. The ratio is given by

$$\frac{r_A}{r(0)}=\omega\left[\frac{1+x_m^2}{\omega^2+x_m^2}\right]^{\frac{1}{2}}\frac{1}{\sin\{\omega[\operatorname{arc\,cot}x_0-(\pi/2)]\}}. \quad (26)$$

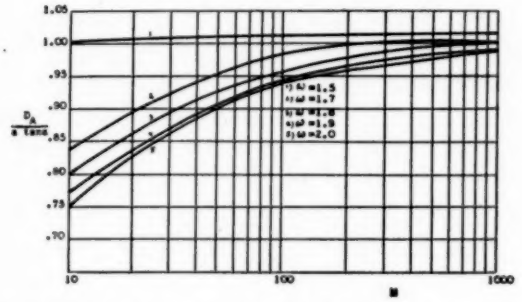

FIG. 8. Reduced aperture size in function of the magnification for various lens strength parameters.

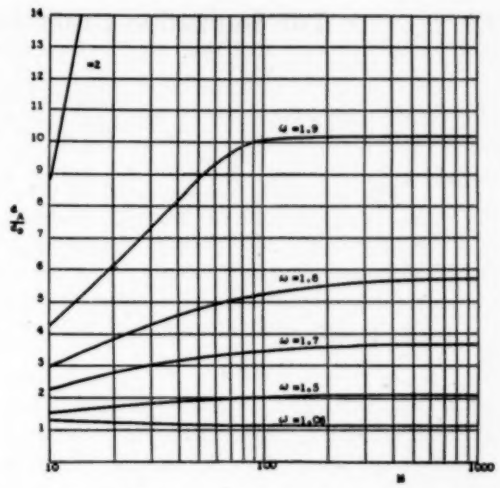

FIG. 9. Ratio of aperture sizes of two equivalent apertures, one located at optimum position (diameter d_A) and the other located at the center of the lens (diameter d_0).

The stronger the lens the more unfavorable is the aperture position at the center of the lens.

Because of the increased size, the difficulties in machining the apertures are reduced. Another advantage results from the location of the aperture outside the lens inasmuch as the removal for cleaning purposes is facilitated. Furthermore, the exact location of the aperture on the axis is not too critical since the path is parallel to the optical axis at the optimum position and hence changes its slope less rapidly than at other positions.

The Ionization Cross Section of the Silver L_{III} State

J. J. G. McCue*
Cornell University, Ithaca, New York
(Received December 31, 1943)

The ionization cross section of the silver L_{III} state has been measured, in arbitrary units, by observing the intensity of the $L\alpha$ doublet radiation from a thin target of silver bombarded by cathode rays whose energies ranged up to nine times the excitation energy of the L_{III} state. The observed data are corrected for the effects of diffusion, rediffusion, and retardation of the cathode rays. The measured values of the cross section agree fairly well with calculations based on the Born approximation, but the agreement is not within the estimated experimental error.

THE dependence of the ionization cross section of an atom on the energy of the impinging electron is a matter that has received considerable attention since it affords a means of testing the applicability of wave mechanics to collision processes on the atomic scale. One can measure the ionization cross section of the inner shell of an atom by observing the intensity of an x-ray spectrum line whose initial state involves ionization of the inner shell in question, the ionization being produced by subjecting the atom to cathode-ray bombardment. The chief difficulty arises from the necessity of using monokinetic cathode rays, but if the target be made in the form of a film, then it can be made thin enough so that the cathode rays pass through it with only a small energy loss, for which a correction can be made. Using such targets, Webster[1-3] and his colleagues have measured the ionization cross section of the silver K shell for electrons whose energies ranged from one to seven times the binding energy of the K electrons. On the publication by Burhop[4] of calculated values of the ionization cross sections for the silver L states, it seemed worth while to measure the cross section for the silver L_{III} state in arbitrary units by using the thin target techniques originated by Webster.

I. THE APPARATUS

The x-ray tube designed especially for this investigation is described elsewhere.[5]

The tube voltage was obtained from a motor generator set coupled to a high voltage transformer and full-wave kenotron rectifier, with a pi-section filter composed of two 0.25-microfarad condensers and a large choke. Tests with a cathode-ray oscilloscope failed to reveal any ripple in the high voltage under operating conditions although a ripple of 50 volts would have been detected.

A Siegbahn-Thoraeus[6] vacuum spectrometer, with a selenite crystal and an ionization chamber, was coupled to the x-ray tube by means of a brass pipe whose axis cut the axis of rotation of the crystal and the center of the target, making an angle of $5°\pm1°$ with the plane of the target. The pipe, which had an inside diameter of 0.5 inch, could be blocked by a movable lead stop. The stop was moved into the beam from time to time during the intensity measurements to keep track of the zero reading of the galvanometer connected to the detecting circuit. Two lead jaws fixed on the front of the ionization chamber limited the width of the beam entering the chamber. The other limiting slit in the system was the focal spot itself. Viewed from the crystal, that is, at an angle of 5° from the plane of the target, the focal spot had a width of the order of 0.5 mm and a height not exceeding 6 mm.

The selenite crystal was 10 mm high and 25 mm long, with its axis of rotation 95 cm from the focal spot and 15 cm from the slit at the ionization chamber. This slit, 14 mm high, was 1.65 mm wide, the width being chosen so as to allow a band of radiation 23 x.u. wide to enter the chamber when the spectrometer was set on the Ag $L\alpha$ line

* Now at the Radiation Laboratory, Massachusetts Institute of Technology, Cambridge, Massachusetts.
[1] Webster, Clark, Yeatman, and Hansen, Proc. Nat. Acad. Sci. **14**, 679 (1928).
[2] Webster, Clark, and Hansen, Phys. Rev. **37**, 115 (1931).
[3] Webster, Hansen, and Duveneck, Phys. Rev. **43**, 839 (1933).
[4] E. H. S. Burhop, Proc. Camb. Phil. Soc. **36**, 43 (1940).
[5] J. J. G. McCue, Rev. Sci. Inst. **14**, 339 (1943).
[6] M. Siegbahn and R. Thoraeus, J. Opt. Soc. Am. **13**, 235 (1926).

at 4150 x.u. This ensured the collection, in the chamber, of all of the Ag $L\alpha$ doublet radiation which the crystal reflected in the first order.[7] Moving the ionization chamber through 3 minutes of arc on either side of the peak of the line decreased the intensity reading by only 1 percent. Therefore slight changes in the position of the focal spot could not introduce any error into the measurements, for the focal spot would have had to move 4 mm to shift the peak of the line 3 minutes.

The ionization chamber that took the place of the plate holder with which the spectrometer was originally equipped was a hollow brass cylinder 12 cm long and of 5 cm inside diameter, with a collecting rod mounted parallel to, but displaced from, the axis of the cylinder. The chamber contained air at atmospheric pressure. Checking the variation of ionization current with x-ray tube current, with the x-ray voltage held constant, showed that in the range of intensities encountered, the ionization current was proportional to the x-ray intensity within the accuracy of the observations, which was about 1 percent.

The ionization current was amplified by an FP-54 electrometer tube operating in a Barth[8] circuit connected to a Leeds and Northrup type R galvanometer whose sensitivity was 4×10^{-10} amp./mm/meter. The over-all sensitivity of the amplifying system was about 30,000 mm/volt with the scale 170 cm from the galvanometer. The non-linearity of its response was detectable, but the range of intensities used was so small that the error introduced by assuming a linear response is less than 0.5 percent. During the course of the measurements, the sensitivity varied somewhat because of changes in the temperature of the battery. Frequent measurements of the sensitivity made possible appropriate correction of the data.

The target consisted of a silver film distilled onto a beryllium disk,[9] 24 mm in diameter and 0.8 mm thick, soldered with Alumaweld to a water-cooled beryllium backing. The interference pattern formed when a glass optical flat lay on the disk showed that the target surface was flat within one wave-length of green light over the area covered by the focal spot, while the interference rings showed that the smoothness of the beryllium surface was about the same as that of plate glass.

The silver, 99.98 percent pure, was melted in a horizontal tungsten trough 10 cm beneath the horizontal polished surface of the beryllium disk; an ionization gauge showed that during the distillation the pressure in the chamber was 3×10^{-5} mm of Hg. Beside the beryllium surface lay a clean, clear-glass microscope-slide. A movable baffle plate allowed the beryllium and glass surfaces to be exposed simultaneously, for an appropriate time, to the silver coming from the trough. Since the heating current in the trough was turned on for only about 2 seconds, the silver condensed on a surface whose temperature was near 20°C.

The thickness of the film was obtained by measuring, at three wave-lengths in the visible spectrum, the opacity of the film on the microscope slide. The data published by Strong and Dibble[10] make possible an estimate of the film thickness when the opacity at these wave-lengths is known. The surface density of the target film according to their curves was 23 micrograms per square centimeter, but the data they obtained by direct weighing indicate that the actual surface density is greater than that shown in their curves; giving equal weights to their two methods of weighing leads to an estimated density of 27 micrograms per square centimeter for the target film. It is sufficient to assume that the volume density of the film was the same as that of massive silver, which implies that the thickness of the target was 260A. A thinner film would have been desirable in some respects, but the thickness of the thinner film would be so uncertain that 260A seemed to represent an optimum thickness.

During the measurements, some contamination of the silver by material from the filament occurred. The portions of the film that could "see" the filament became discolored, but the focal spot was not visibly affected. Tests on the excitation potential of the silver $L\alpha$ lines showed that the cathode rays did not experience any

[7] L. G. Parratt, Phys. Rev. **54**, 99 (1938).
[8] G. Barth, Zeits. f. Physik **87**, 399 (1934).
[9] Beryllium disks were generously furnished by the Brush Beryllium Company.
[10] J. Strong and B. Dibble, J. Opt. Soc. Am. **30**, 431 (1940).

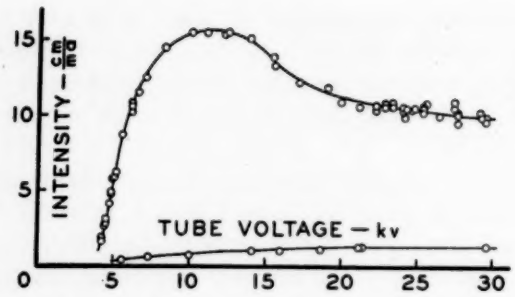

FIG. 1. The observed radiation and the continuous background.

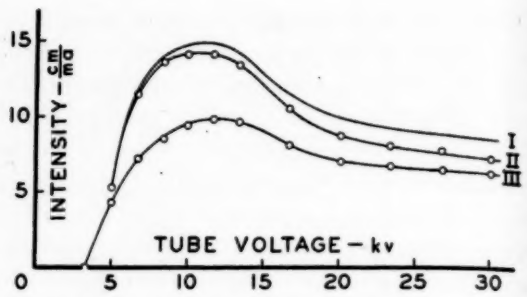

FIG. 2. Specific intensity of the $L\alpha$ doublet. I—uncorrected; II—corrected for fluorescence; III—completely corrected.

serious retardation in a surface film before striking the silver. With a massive silver target that had been used for some time and was very much dirtier than the thin target ever became, $L\alpha$ radiation could be detected when the tube voltage was only 150 volts above the Ag $L\alpha$ excitation potential (3.35 kv). The surface film on the massive target therefore retarded 3.5 kilovolt electrons by not more than 150 volts; the retardation was of course less for cathode rays of higher energy.

The safe limit of power dissipation in the target was about 30 watts. In order to avoid possible injury to the polish of the beryllium surface, it was touched after the polishing operation by nothing but lens paper. There seems to have been enough grease on the beryllium to inhibit good thermal contact between the silver and the backing.

II. THE DATA

After tests had been performed to make certain that the deflection of the galvanometer was proportional to the tube current at constant voltage, and was independent of the size of the focal spot, the intensity of the $L\alpha$ doublet (4.15A) emitted from the film was measured at various voltages from 4 to 30 kv. A set of auxiliary measurements made with the spectrometer set at 4.30A determined the intensity of the continuous radiation in that part of the spectrum. The results appear in the upper and lower curves, respectively, of Fig. 1. The ordinates are centimeters of galvanometer deflection per milliampere of target current, which will be called the "specific intensity." The scattering of the points at the right end of the upper curve is due to unsteadiness in the measuring circuit at the time these points were taken, combined with the fact that the deflections were small because small tube currents had to be used at the high voltages. The difference in the ordinates of the two curves is the specific intensity of the $L\alpha$ doublet radiation from the thin target; it is plotted as curve I in Fig. 2.

III. THE CORRECTIONS

Fluorescence

It is necessary to make allowance for the silver $L\alpha$ radiation that arises from fluorescence of the target foil under the action of the x-ray continuum emanating from the beryllium backing. Let $I(\nu_0, \nu)d\nu$ be the power per unit solid angle emitted by the beryllium disk in the frequency range between ν and $\nu+d\nu$, when ν_0 is the high frequency limit of the continuum. Then the total fluorescent power emitted as $L\alpha$ radiation by the silver foil is

$$u_{L\alpha}\int_{\nu_{L_{III}}}^{\nu_0} d\nu \int_0^{2\pi} d\phi \int_0^{\pi/2} \frac{\mu_{L_{III}}\nu_{L_{III}}}{\mu\nu} I(\nu_0, \nu) \times\{1-\exp(-\mu X_0 \sec\theta)\}\sin\theta d\theta,$$

where $u_{L\alpha}$ = the fluorescence yield of silver for its $L\alpha$ radiation; μ = the absorption coefficient of silver; $\mu_{L_{III}}$ = the part of the absorption coefficient of silver due to absorption by the L_{III} shell; $\nu_{L_{III}}$ = the frequency of the silver L_{III} absorption edge; X_0 = the thickness of the silver foil; θ = the angle between an x-ray and the normal to the silver foil; ϕ = the azimuth measured about the normal to the foil.

If the crystal subtends at the target a solid

angle $\Delta\Omega$, then the fluorescent power striking the crystal is

$$\tfrac{1}{2}u_{ba}\Delta\Omega\int_{\nu_{L_{III}}}^{\nu_0}\frac{\mu_{L_{III}}\nu_{L_{III}}}{\mu\nu}I(\nu_0,\nu)\int_0^{\pi/2}\{1-\exp(-\mu X_0\sec\theta)\}\sin\theta d\theta d\nu.$$

$I(\nu_0,\nu)\Delta\nu\Delta\Omega$ is the power striking the crystal in the range $\Delta\nu$ in the continuum. (A small and easily evaluated correction must be made for the absorption of the continuum in the silver.) This power has been measured, in arbitrary units, for the frequency corresponding to 4.3A. Let ν_e be this frequency, and I_e be the power per unit solid angle per unit frequency interval at ν_e (corrected for absorption in the silver). The arbitrary units used to measure $I_e\Delta\nu$ and the uncorrected power of the $L\alpha$ radiation are the same. Therefore the fluorescence radiation contributed to the observed specific intensity an amount

$$\phi(\nu_0)=\tfrac{1}{2}u_{L\alpha}\int_{\nu_{L_{III}}}^{\nu_0}\frac{\mu_{L_{III}}\nu_{L_{III}}}{\mu\nu}I(\nu_0,\nu)\{1-G(\mu X_0)\}d\nu,$$

where

$$G(\mu X_0)=\int_0^{\pi/2}\exp(-\mu X_0\sec\theta)\sin\theta d\theta.$$

The function $G(y)$ has been tabulated by Gold.[11]

The data on fluorescence yields cited by Compton and Allison,[12] in conjunction with the relative intensity measurements of Parratt,[7] indicate that $u_{L\alpha}=0.17$. Van Dyke and Lindsay[13] have determined $\nu_{L_{III}}$ for silver, and the work of Andrews[14] makes available the values of μ and $\mu_{L_{III}}$ in the pertinent spectral region. The spectral band width admitted to the ionization chamber at ν_e was $\Delta\nu=3.7\times10^{15}$ sec.$^{-1}$.

Kulenkampff's[15] conclusion that $I(\nu_0,\nu)$ is proportional to $\nu_0-\nu$ is based on data corrected for absorption in the target. It implies that the intensity at a given frequency in the continuum varies linearly with tube voltage. Measurements in the present investigation show that the intensity at ν_e, measured at an angle of 85° with the cathode rays, increases less rapidly than the tube voltage up to 20 kv and is constant as the voltage ranges from 20 to 30 kv. Kulenkampff's formula for $I(\nu_0,\nu)$ is therefore not applicable to this case because of absorption of the continuum in the beryllium. Moreover, Kulenkampff worked only with the radiation emitted in a direction perpendicular to the cathode rays, while the fluorescence is excited by radiation passing through the foil in all directions. The numerical calculations show, however, that the foil absorbs strongly only those rays passing through the target rather obliquely. For this reason, and because the cathode rays in the beryllium experience considerable diffusion, it seems safe to ignore the dependence of $I(\nu_0,\nu)$ on θ; the best expression for $I(\nu_0,\nu)$ to use on the basis of available information is $I(\nu_0,\nu)=(\nu_0-\nu)I_e/(\nu_0-\nu_e)$. The function $\phi(\nu_0)$ was evaluated by plotting the integrand of (1) for several values of ν_0 and then integrating with a planimeter. The results appear in column 3 of Table I. The quantity U in the table is the ratio of the tube voltage to the L_{III} ionization potential, while $\phi(\nu_0)$ is expressed in cm of galvanometer deflection per ma of tube current.

Diffusion

The fact that slow cathode rays are likely to experience large deflections in traversing the silver film makes the effective film thickness uncertain at the lowest voltages. For potentials

TABLE I. Observed L doublet intensities, corrections, reduced intensities, and cross sections.

U	I_{obs}	$\phi(\nu_0)$	X_0/X	c_a	c_r	i_0	Q
	cm/ma	cm/ma				cm/ma	
1.5	5.5	0.1	0.58	1.39	0.98	4.3	0.46
2	11.8	0.3	0.62	1.05	0.96	7.2	0.77
2.5	14.0	0.4	0.65	1.01	0.95	8.5	0.91
3	14.7	0.6	0.70	1.00	0.95	9.4	1.00
3.5	14.8	0.7	0.74	1.00	0.94	9.8	1.04
4	14.2	0.8	0.77	1.00	0.93	9.6	1.02
5	11.5	1.0	0.83	1.00	0.93	8.1	0.86
6	9.9	1.2	0.87	1.00	0.93	7.0	0.75
7	9.2	1.2	0.90	1.00	0.93	6.7	0.72
8	8.8	1.2	0.92	1.00	0.93	6.5	0.69
9	8.5	1.3	0.94	1.00	0.92	6.2	0.66

[11] E. Gold, Proc. Roy. Soc. **A82**, 62 (1908).
[12] A. H. Compton and S. K. Allison, *X-rays in Theory and Experiment* (D. Van Nostrand, New York, 1935), pp. 488, 490.
[13] G. D. Van Dyke and G. A. Lindsay, Phys. Rev. **30**, 562 (1927).
[14] C. L. Andrews, Thesis, Cornell, 1938.
[15] H. Kulenkampff, Ann. d. Physik **69**, 548 (1922).

above about 10 kv ($U=3.0$) a satisfactory calculation of the effective thickness of the foil can be made. Throughout the discussion of this and the succeeding calculations the notation of Webster, Hansen, and Duveneck[3] will be followed as closely as possible.

According to Bothe,[16] the most probable deflection experienced by a cathode ray in traversing a thickness x of silver is $\lambda=18.5U^{-1}x^{\frac{1}{2}}$, where λ is in radians, and x is in microns. Let Θ be the deflection of any particular cathode ray at a depth x in the film. For this ray, the path length in a thickness dx at depth x will be dx sec Θ. The effective thickness of the target will therefore be

$$X=\int_0^{X_0}\langle\sec\Theta\rangle_{Av}dx.$$

Here X_0 is the thickness of the film and $\langle\sec\Theta\rangle_{Av}$ is the value of sec Θ, at a particular depth x, averaged over all of the cathode rays. For the distribution-in-angle of the deflected cathode rays, Bothe[16] gives

$$nd\Omega=\frac{n_0}{2\pi\lambda^2}\exp(-\Theta^2/2\lambda^2)d\Omega,$$

where $nd\Omega$ is the number of particles scattered into an element of solid angle $d\Omega$ when n_0 electrons impinge normally on the film. This distribution function leads to a physically absurd result unless Θ remains small. Neher's[17] data indicate that the number of electrons emerging along paths nearly parallel to the foil surface is small, and that

$$nd\Omega\propto\exp(-\Theta^2/2\lambda^2)\cos\Theta d\Omega$$

is more nearly correct. Then

$$\langle\sec\Theta\rangle_{Av}=\frac{\int_0^{\pi/2}\sec\Theta\exp(-\Theta^2/2\lambda^2)\cos\Theta\sin\Theta d\Theta}{\int_0^{\pi/2}\exp(-\Theta^2/2\lambda^2)\cos\Theta\sin\Theta d\Theta}.$$

This reduces to $\langle\sec\Theta\rangle_{Av}=2B(p)/A(p)$, where

$$B(p)=\int_0^{\pi/2p}\exp(-u^2)\sin pudu,$$

$$A(p)=\int_0^{\pi/2p}\exp(-u^2)\sin 2pudu$$

and $p=\lambda\sqrt{2}$.

For small values of p, $B(p)$ and $A(p)$ are approximately equal to $B_\infty(p)$ and $A_\infty(p)$, where

$$B_\infty(p)=\int_0^\infty\exp(-u^2)\sin pudu$$
$$=\exp(-p^2/4)\int_0^{p/2}\exp(s^2)ds$$

and $A_\infty(p)=B_\infty(2p)$. The function $\int_0^{p/2}\exp(s^2)ds$ has been tabulated by Dawson.[18] Investigation shows that $B_\infty(p)$ and $A_\infty(p)$ approximate $B(p)$ and $A(p)$ within 0.1 percent as long as $p\leqq0.5$, but that the approximations become rapidly worse for larger values of p. In the interval $0.6\leqq p\leqq2.0$, the Gauss 4-point numerical method of integration[19] yields values of $B(p)$ and $A(p)$ that are in error by less than 1 percent.

The effective thickness of the target is

$$X=2\int_0^{X_0}[B(p)/A(p)]dx$$
$$=\frac{U^2}{170}\int_0^{4.22/U}p[B(p)/A(p)]dp;$$

X was evaluated for various values of U by further application of the Gauss 4-point method, after determining $pB(p)/A(p)$ for the appropriate values of p. The results appear in the fourth column of Table I.

Retardation

Let $i(U)dx$ be the $L\alpha$ doublet intensity from an ideally thin target of thickness dx. A real target of thickness X will give an intensity $\langle i(U')\rangle_{Av}$, where $U'e$ is the energy of the electron after it has penetrated to a depth x, and $\langle i\rangle_{Av}$ denotes an average of i taken from $x=0$ to $x=X$. To a first

[16] W. Bothe, *Handbuch der Physik XXII/2* (Springer, Berlin, 1933).
[17] H. V. Neher, Phys. Rev. **37**, 655 (1931).
[18] H. G. Dawson, Proc. Math. Soc. London **29**[II], 519 (1897/98).
[19] K. Mader, *Handbuch der Physik, III* (Springer, Berlin, 1928).

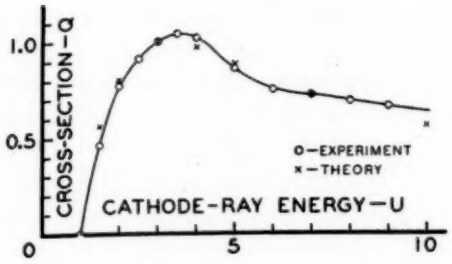

FIG. 3. The ionization cross section of the L_{III} state of silver.

approximation,[3]

$$\langle i(U')\rangle_{Av}=i(U)+\tfrac{1}{2}X\frac{di}{dU}\left(\frac{dU'}{dx}\right)_{U'=U}.$$

The observed intensities, corrected for fluorescence and diffusion of the cathode rays, can be represented to a sufficient degree of approximation by the analytical expression $i(U)=KU^{-1}\log U$. Therefore $\langle i(U')\rangle_{Av}=i(U)+g(U)$, where

$$g(U)=\tfrac{1}{2}KXU^{-2}(1-\log U)\left(\frac{dU'}{dx}\right)_{U'=U}$$

and the observed data, after correction for the effects of fluorescence and diffusion, can be further corrected to compensate for retardation by multiplying them by $c_x=i(U)/[i(U)+g(U)]$. Terrill[20] and Williams[21] have found that, for cathode rays of about the energy used in the present investigation, $(dU'/dx)\propto(1/U')^m$. Terrill finds $m=1$, while Williams gives $m=0.9$, and reports a constant of proportionality much smaller than Terrill's. Since Terrill worked with silver and other metal foils, and Williams' work was done in a cloud chamber, it seems better to use Terrill's results here. Calculation on this basis yields the values of c_x shown in Table I.

Rediffusion

When cathode rays fall normally on a solid body, some of them, experiencing within the body deflections greater than 90°, are "rediffused" so that they appear to have been reflected from the body. The presence of the beryllium backing therefore causes some of the cathode rays to pass through the target twice. The fraction p of electrons experiencing rediffusion when cathode rays are incident normally on a plane surface of a material is called the "rediffusion constant" of the material. Neher's[17] measurements on beryllium show that for 130-kv electrons, $p=0.0248$, and for 70-kv electrons, $p=0.0291$. Using data obtained by Schonland[22] for heavier elements and voltages from 10 to 100 kv, Webster, Clark, and Hansen[2] had previously estimated that $p=0.043$. A reasonable estimate, therefore, is that in the range from 10 to 30 kv $p=0.035$ for beryllium. Following Webster, Clark, and Hansen, let $i(U)=i_0(U)+r(U)$, where $i_0(U)$ is the x-ray intensity per unit length of path of the cathode rays, and $r(U)$ is the intensity per unit thickness of target film. (The diffusion of rediffused electrons is a second-order effect which will be ignored.) It follows[2] that

$$r(U)=2p\int_{1/U}^{1}F(W)\cdot i_0(UW)dW,$$

$pF(W)$ being the fraction of incident electrons which are rediffused with energies between UeW and $Ue(W+dW)$. All of the available evidence[2] on the energy distribution of rediffused electrons indicates that $F(W)=(q+1)(q+2)(1-W)W^q$ is a suitable approximation if q is an appropriate integer. For beryllium $q=3$ seems to be a good choice. An estimate of $r(U)$ satisfactory for the present purpose can be obtained by using for $i_0(UW)$ the empirical approximation $i_0(U)=KU^{-1}\log U$. Setting $c_r=i_0(U)/[i_0(U)+r(U)]$, so that $i_0(U)=c_r\cdot i(U)$, one obtains for c_r the values shown in Table I.

IV. RESULTS

Curve I in Fig. 2 shows the observed specific intensity of the $L\alpha$ doublet (corrected for the continuous background). To the ordinates must be applied first the correction for fluorescence, $\phi(\nu_0)$, and then the corrections for diffusion, rediffusion, and retardation. Curve II in Fig. 2 is a plot of the observed $L\alpha$ intensity minus the intensity due to fluorescence. The ordinates of curve III, the intensities per unit effective target thickness after all corrections have been made, are obtained from those of curve II by multiplying them by $c_r\cdot c_x\cdot X_0/X$. The finally corrected re-

[20] H. M. Terrill, Phys. Rev. **22**, 101 (1923).
[21] E. J. Williams, Proc. Roy. Soc. **A130**, 310 (1930–31).
[22] B. F. J. Schonland, Proc. Roy. Soc. **A108**, 187 (1925).

sults, which are proportional to the ionization cross section Q, are listed under i_0 in Table I and are replotted in Fig. 3, the ordinates here being arbitrary units chosen to make $Q=1$ when $U=3$. The theoretical values of ionization cross section calculated by Burhop[4] are shown as crosses; they are fitted to the experimental curve at $U=3$. Burhop states that his results have been evaluated numerically to "a few percent." The measured values of Q are tabulated in Table I.

There are four sources of error in the experimental results, namely:

(1) the measurement of target potential,
(2) the measurement of tube current,
(3) the measurement of x-ray intensity, and
(4) the corrections.

The target potential was measured with a low voltage laboratory standard voltmeter and wire-wound multiplier. Checks with a potentiometer and Wheatstone bridge showed the calibration of the combination to be correct within 0.25 percent, when account is taken of the corona and surface leakage in the multiplier. Errors in the measurement of target potential therefore make no significant contribution to the experimental error.

The target currents could be read within about 1 percent.

The electrometer tube circuit introduced uncertainty into the intensity measurements through fluctuations and through changes in sensitivity. Frequent checks on the sensitivity ensured that the errors due to changes in sensitivity are certainly less than 2 percent. Fluctuations are partially neutralized by drawing a smooth curve among the points; they render the location of the curve uncertain by not more than 2 percent. This estimate includes an allowance for zero drift.

The geometrical thickness X_0 of the target is uncertain by about 15 percent, but it transpires that a 15 percent error in X_0 causes an error of little more than 1 percent in the measured value of ionization cross section at $U=9$ relative to that at $U=3$. The errors introduced at other values of U between 1.5 and 9 are even smaller. Departures from the assumed law of distribution-in-angle of the diffused cathode rays may introduce further errors, but no estimate of their size can be made except that they are probably not as large as 1 percent. They will therefore be neglected.

The corrections for rediffusion are so small and are based on such accurate information that they do not contribute significantly to the experimental error. The same is true of the corrections for retardation, except for that at $U=1.5$, which renders Q at that voltage uncertain by about 5 percent.

The square root of the sum of the squares of the errors that have been mentioned is 6 percent at $U=1.5$ and 3 percent for the larger values of U. These are the experimental uncertainties in the ordinates of Fig. 3 at small values of U; at large values of U there is in addition the possibility of errors introduced by the assumptions underlying the correction for fluorescence. Concerning these errors, all that can be said is that they are negligible for small values of U, say $U<7$, and that the computed correction for fluorescence is, if anything, too small. (It is perhaps worth mentioning here that Burhop's results were not consulted until after the calculation of the corrections had been completed.) For $U>7$, the curve does not fall off as rapidly as the theory predicts; a 50 percent increase in the correction for fluorescence would be necessary in order to bring the experimental point at $U=9$ into agreement with the theoretical prediction. Without making actual measurements on the intensity of the x-ray continuum from beryllium in directions making various angles with the target, over the range of tube voltages used in the present experiment, one cannot decide with assurance that, for $U=9$, the present correction for fluorescence is in error by less than 50 percent. It should be pointed out, however, that the experimental results of Webster, Hansen, and Duveneck,[3] of Smith,[23] of Tate and Smith,[24] of Webster, Pockman, and Kirkpatrick,[25] and of Webster, Pockman, Harworth, and Kirkpatrick[26] all show that the theoretical calculations (based on the Born approximation) predict cross sections that decrease too rapidly with increasing U when U is large.

In conclusion, it seems of interest to compare

[23] P. T. Smith, Phys. Rev. **36**, 1293 (1930).
[24] J. T. Tate and P. T. Smith, Phys. Rev. **39**, 270 (1932).
[25] Webster, Pockman, and Kirkpatrick, Phys. Rev. **44**, 130 (1933).
[26] Cited by Burhop, reference 4.

the present measurements on the L_{III} state of silver with those of Webster, Hansen, and Duveneck[3] on the K state of the same element. Two facts are clearly shown:

(1) The cross sections for excitation to the K state and the L_{III} state are both greatest for cathode rays whose kinetic energies are about 3.5 times the ionization energy of the state in question.

(2) When $U>3.5$, the decrease in ionization cross section with increasing cathode-ray energy is more rapid for the L_{III} state than for the K state.

ACKNOWLEDGMENTS

The author is very much indebted to Professor C. W. Mason for his great kindness in polishing the beryllium disks, and to Professor L. G. Parratt for suggesting the investigation and patiently guiding its progress.

PHYSICAL REVIEW VOLUME 65, NUMBERS 5 AND 6 MARCH 1 AND 15, 1944

Finite Self-Energies in Radiation Theory. Part III

ALFRED LANDÉ AND LLEWELLYN H. THOMAS
Mendenhall Laboratory of Physics, Ohio State University, Columbus, Ohio

(Received November 10, 1943)

The invariant field theory of Part II is interpreted, in agreement with F. Bopp, as Maxwell's theory with a linear differential relation between the fields E, B and D, H involving a new constant k which measures the reciprocal radius of the electron. The former "mesonic field" of minimum frequency $\nu_0=kc/2\pi$ represents polarization of the vacuum. The electron is a singularity in the D, H field whereas E, B remain finite. Instead of obeying dynamical equations of motion, the electron moves under the condition that the Lorentz force vanishes identically on the singularity, so that no work is done on the particle. All energy is located in the field. In this respect the theory is unitary. Electromagnetic and inert mass are identical. In contrast to Dirac's classical electron which is subject to advanced and retarded potentials and displays self-acceleration, the field theory works with retarded potentials only, and self-acceleration is avoided. Stable equilibrium between electrons and radiation is granted by spontaneous and induced transitions, similar to Einstein's derivation of Planck's radiation formula. In spite of displaying a magnetic moment the electron does not have magnetic self-energy, so that its radius is the ordinary electrostatic radius $1/k=e^2/2mc^2$. In contrast to Born-Infeld's non-linear theory, our field equations allow a Fourier representation as a basis for the quantum theory of Part IV.

1. CLASSICAL FIELD THEORY

THE modification of electrostatics proposed in Part I and its electromagnetic continuation discussed in Part II [1] rest on the assumption that vacuum is polarizable, as described by linear differential relations between the vectors E, B and D, H (for details see Section 6):

$$D=E-k^{-2}\Box E, \quad H=B-k^{-2}\Box B, \qquad (1)$$

where $\Box$ is the Laplace operator in x, y, z, ict. The constant k of dimension $[l^{-1}]$ determines the minimum frequency $\nu_0=kc/2\pi$ of waves of polarization or "meson waves." k also plays the role of the reciprocal electronic radius, although the charges ϵ are condensed in mathematical points only. The simplicity and naturalness of our approach are demonstrated by the fact that the same modification of Maxwell's theory has been proposed independently and simultaneously by F. Bopp.[2] Whereas we began in Part I with a Fourier representation of the field of a point particle with finite self-energy, Bopp started from a formal generalization of the Lagrangian function of the field $E, B=f_{\alpha\beta}$, namely,

$$L=-(1/16)\{(f_{\alpha\beta})^2+k^{-2}(\partial f_{\alpha\beta}/\partial x_\gamma)^2\}+J_\alpha\varphi_\alpha \qquad (2)$$

where J is the 4 current and φ is the 4 potential.

The relation to other field theories (Maxwell, Born-Infeld) become obvious if the vectors E, H of Part II are called E, B, and the vectors E'', H'' are called D, H. Our "meson field" $E'=D-H$

[1] A. Landé, Phys. Rev. **60**, 121 (1941). A. Landé and L. H. Thomas **60**, 541 (1941).

[2] F. Bopp, Ann. d. Physik **38**, 345 (1940).

TABLE I. Notation.

Our former	E, H; V, A	E'', H''; V'', A''	E', H'; V', A'
Bopp	E, B; φ, a	D, H; ϕ, A	F, G; $V/k, U/k$

and $H'=H-B$ then represents the electric and magnetic polarization of the vacuum (see Table I). In contrast to Born-Infeld, our relation between D, H and E, B is *linear* so that it is easy to obtain a Fourier representation (not discussed by Bopp) with subsequent quantization. Infinities are avoided automatically without resorting to arbitrary cutting-off procedures.

The new field theory is unitary insofar as all energy is supposed to be located in the field, without additional "mechanical" energy of particles. Instead of introducing mechanical equations of motion for the electrons, we postulate that the field E and B (which is responsible for Lorentz force and work on the particles) shall vanish at all times on the point singularities themselves. As a consequence of this condition we were able in Part II to derive a quasimechanical equation of motion:

$$m(\ddot{x})_0=\text{external force}+(2\epsilon^2/3c^3)(d\ddot{x}/dt)_0 \quad (3)$$

valid at a particular time ($t=0$). m is an abbreviation for $k\epsilon^2/2c^2$ and represents the electromagnetic mass of the surrounding field.

The simplest solution of the field equations is an electrostatic field of spherical symmetry surrounding a point charge ϵ (II, Section 4):

$$D=\epsilon/r^2, \quad E=\epsilon/r^2-\epsilon(1/r^2+k/r)\exp(-kr).$$

In contrast to D, the field E remains finite at $r=0$, namely, $E=\epsilon k^2/2$. However, similar to Born-Infeld, the field component E_x jumps from the finite value $+|E|$ to $-|E|$ when passing through the singularity, with the average value $E_x=0$ on the singularity itself. This discontinuity preserves the individuality of the particle. The electric field energy of the particle at rest has value $W=k\epsilon^2/2=mc^2$.

Two point charges ϵ_1 and ϵ_2 at distance r have field energy

$$W=k\epsilon_1^2/2+k\epsilon_2^2/2+(\epsilon_1\epsilon_2/r)\cdot[1-\exp(-kr)]. \quad (4)$$

Two opposite charges $+\epsilon$ and $-\epsilon$ therefore yield

$$\begin{aligned} &W=mc^2+mc^2-\epsilon^2/r \text{ for large } r,\\ &W=mc^2kr \text{ for small } r. \end{aligned} \quad (5)$$

Hence, when r decreases from ∞ to 0, field energy of value $2mc^2$ is released. It thus turns out that transformation of mutual electrostatic into radiation energy with neutralization of $+\epsilon$ and $-\epsilon$ (annihilation) is possible already in the classical domain.

Another significant feature of our theory concerns electrons vibrating with high frequencies $\nu>\nu_0=kc/2\pi$. The energy emitted in this case is reduced by a factor (II, Section 6)

$$1-(1-\nu_0^2/\nu^2)^{\frac{1}{2}} \quad (6)$$

as compared with the normal Maxwell-Lorentz radiation. For $\nu\gg\nu_0$ the reduction factor approaches $\nu_0^2/2\nu^2$, so that energy is emitted at the rate ν^2 rather than ν^4 per second, or ν rather than ν^3 per period. This is of importance for the quantum theory of stationary states which always presumes that the energy emission during a single period is small compared with the energy of the state itself.

Our theory in its classical form does not distinguish between self-field and external field, except for the special case of uniform motion. On the other hand, the quantum theory of radiation is dualistic. Here one considers electrons in uniform motion with definite self-energies $W=W_0(1-\beta^2)^{-\frac{1}{2}}$ surrounded by a "pure field" with constant Fourier amplitudes. Transitions between stationary states result from mutual perturbations between pure field and particles. The difficulties of the quantum theory of radiation arise primarily from the task of describing the interaction between external field and mechanical particles in a dualistic fashion, although the classical theory of the electron in the field is unitary. The difficulty is solved in Part IV by considering as zero approximation particles without rest mass which therefore travel with the velocity of light. When the interaction with the field is introduced, stationary states of the particles with any velocity smaller than c become possible. These states may be obtained from states with zero velocity by Lorentz transformations, and the rest mass now has a definite value. Our special type of semi-unitary field theory in which the particles retain their individuality as singularities although all energy is located in the field, offers a satisfactory background from the classical and quantum points of view.

2. THE PROBLEM OF SELF-ACCELERATION

For vanishing external field Eq. (3) reads

$$d\ddot{x}/d(ct)=a\ddot{x} \quad \text{with} \quad a=3mc^2/2\epsilon^2. \tag{7}$$

The solution of this non-relativistic equation is

$$dx/d(ct)=\exp(act)+\beta \tag{7'}$$

where β is the velocity ratio v/c at $t=-\infty$. A free electron thus should be able to accelerate itself from any initial velocity v at $t=-\infty$ to larger and larger velocities, the beginning phase of the process being described by (7'). Relativistic corrections are needed for higher velocities only. Dirac[3] has emphasized the fundamental importance of self-acceleration in his relativistic theory of the classical point electron. There he assumes that the force on the point charge is determined by the difference of retarded and advanced potentials, in order to get rid of the infinite self-energy. As a consequence he obtains self-acceleration. However, the whole idea of a free particle acquiring larger and larger velocities on its own accord is so non-physical that any theory yielding self-acceleration might be rejected almost *a priori*. Yet, self-acceleration is an inevitable consequence of any theory in which the electron is subject to a differential equation of motion of finite order because the equation of motion at the beginning of the process for small velocities is always approximated by (7) with the solution (7'). It is a decisive advantage of the present field theory that the singularity does not obey a differential equation of motion. The force on the electron at t depends on the whole path before t rather than on the motion in the immediate neighborhood of t.

In II, Section 4 we discussed an electron moving with coordinate

$$x=ut+\tfrac{1}{2}ft+\tfrac{1}{6}gt^3 \tag{7''}$$

during a short time t near $t=0$ and with small coefficients u, f, and g whose meaning is $u=(\dot{x})_0$, $f=(\ddot{x})_0$, $g=(d\ddot{x}/dt)_0$ at $t=0$. The self-force was found to be

$$\begin{aligned}\text{self-force}&=-(\epsilon^2k/2c^2)\cdot f+(2\epsilon^2/3c^3)\cdot g\\&=-m(\ddot{x})_0+(2\epsilon^2/3c^3)(d\ddot{x}/dt)_0\end{aligned}$$

where m is an abbreviation for $(\epsilon^2k/2c^2)$ representing the finite mass of the point charge ϵ. Our requirement of a vanishing total force means vanishing self-force for a free electron, so that the latter at $t=0$ satisfies the equation

$$m(\ddot{x})_0=(2\epsilon^2/3c^3)(d\ddot{x}/dt)_0.$$

This equation does not permit conclusions about self-acceleration before or after $t=0$. Whether self-acceleration is possible depends on the question whether the self-field vanishes during an accelerated motion. Before answering this question of dynamics we must first find the correct kinematic description of a relativistically accelerated motion.

Let us assume tentatively that the motion of a certain free particle were actually of the form (7') at least for large negative t and for small values of the initial velocity β. Let us ask also: What is the correct relativistic continuation of this accelerated motion? The answer may be found by relativistic transformations without resorting to dynamics. Since the electron is free, the acceleration at any time must depend only on the proper time s measured on the particle itself. For large negative t, however, t and s are identical provided that $\beta\ll 1$. Instead of (7') we therefore may write relativistically

$$\begin{aligned}dx/d(cs)&=\exp(acs)+\beta,\\d(ct)/d(cs)&=1 \text{ for } s=-\infty.\end{aligned} \tag{8}$$

With reference to a Lorentz system xt in which the electron is at rest at the beginning of the process we also have

$$\begin{aligned}dx_0/d(cs)&=\exp(acs),\\d(ct_0)/d(cs)&=1 \text{ for } s=-\infty.\end{aligned} \tag{8'}$$

Generalizing these equations tentatively for all s values we write

$$\begin{aligned}dx/d(cs)&=S(e^{acs}+b), \quad d(ct)/d(cs)=C(e^{acs}+b),\\dx_0/d(cs)&=S(e^{acs}), \quad\quad d(ct_0)/d(cs)=C(e^{acs}),\end{aligned}$$

where $b(\beta)$ is a function of β which coincides with β for small β, whereas $S(z)$ is a function of z which coincides with z for small z like a sine function, and $C(z)\to 1$ for small z like a cosine function. We now write down relativistic transformation formulae from xt to x_0t_0

$$\begin{aligned}dx&=[dx_0+d(ct_0)\cdot\beta](1-\beta^2)^{-\frac{1}{2}},\\d(ct)&=[dx_0\cdot\beta+d(ct_0)](1-\beta^2)^{-\frac{1}{2}}.\end{aligned}$$

[3] P. A. M. Dirac, Proc. Roy. Soc. **167**, 148 (1938).

Dividing by $d(cs)$ and writing z for e^{acs} we obtain

$$S(z+b)=[S(z)+C(z)\cdot\beta]\cdot(1-\beta^2)^{-\frac{1}{2}},$$
$$C(z+b)=[S(z)\beta+C(z)]\cdot(1-\beta^2)^{-\frac{1}{2}}.$$

These equations represent rotations in Minkowski space. Indeed, if we write

$$(1-\beta^2)^{-\frac{1}{2}}=\cos(ib)=\text{Cosh}(b),$$
$$\beta(1-\beta^2)^{-\frac{1}{2}}=-i\sin(ib)=\text{Sinh}(b), \qquad \text{Tanh } b=\beta,$$

we have

$$S(z+b)=S(z)\text{ Cosh }(b)+C(z)\text{ Sinh }(b),$$
$$C(z+b)=S(z)\text{ Sinh }(b)+C(z)\text{ Cosh }(b).$$

These formulae are valid only if the functions S and C are Sinh and Cosh. The correct relativistic continuation of (7′) in the xt system, therefore, is

$$dx/d(cs)=\text{Sinh }(e^{acs}+b),$$
$$d(ct)/d(cs)=\text{Cosh }(e^{acs}+b), \qquad b=\text{Tanh}^{-1}\beta, \quad (9)$$

where $\beta=v/c$ describes the original constant velocity of the electron in the xt system at $t=-\infty$, and s is the proper time. Equation (9) represents the only accelerated motion possible for a free electron with (7′) as non-relativistic approximation for $t\approx-\infty$. As a consequence we obtain the following invariant description of self-acceleration:

$$d^2x_r/d(cs)^2=a\cdot\exp(acs), \qquad (9')$$

where x_r is the Lorentz system in which the electron is momentarily at rest.

Next let us calculate the self-force according to the field theory if the electron is relativistically accelerated according to (9). In order to simplify the mathematical problem let us discuss only the initial part of the process between $t=-\infty$ and $t=(1/ac)\cdot\ln C$ where C is a small positive number. During this initial phase we may use the approximation (7′). Shifting the zero point of the time scale we may consider the motion

$$d\xi/d(c\tau)=C\exp(ac\tau),$$
$$\xi=(C/a)[\exp(ac\tau)-1] \qquad (9'')$$

during $-\infty<\tau<0$. The zero point of the ξ axis coincides with the position of the electron at $\tau=0$. Furthermore, instead of discussing the self-force during the whole time $\tau<0$, we calculate it at $\tau=0$ itself. In the original time scale this is the time $t=(1/ac)\ln C$ where C is any small number, so that what applies to $t=0$ also applies to a continuity of times t in the original time scale.

In order to find the self-force of the motion (9″) at $\tau=0$ we apply the method of retarded potentials (Part II, Section 4) and proceed in three steps.

(1) If the exponential function in (9″) is expanded into a series we have

$$\xi=(C/a)[ac\tau+\tfrac{1}{2}(ac\tau)^2+\tfrac{1}{6}(ac\tau)^2].$$

If we omit all higher terms, the result was already found in II, Section 4:

$$\text{Self-force}=-(\epsilon^2k/2c^2)(\ddot{\xi})_0+(2\epsilon^2/3c^3)(d\ddot{\xi}/d\tau)_0$$
$$=-\epsilon^2a^2C[(k/2a)-(2/3)].$$

The self-force vanishes for $a=0$ (uniform motion) and also for $a=3k/4$ (self-accelerated motion), that is, for $a=3mc^2/2\epsilon^2$ which is Dirac's value.

(2) If the next expansion term $(ac\tau)^4/24$ is added to the series, the self-force becomes infinite for every value of a except $a=0$.

(3) If the complete exponential function $\exp(ac\tau)$ is used the self-force becomes *finite* again due to the fact that successive expansion terms contribute infinite terms of opposite signs. The resulting self-force according to the method II, Section 4 is

$$-e^2C\cdot\int_0^\infty J_1(kR)\{(aR^{-1}e^{-aR})+(a^{-1}R^{-3}e^{-aR})$$
$$-(R^{-3}a^{-1})+(R^{-2}e^{-aR})\}d(kR)$$

or after integration:

$$\text{Self-force}=$$
$$-\epsilon^2a^2C\left\{\frac{(a^2+k^2)^{\frac{1}{2}}-a}{a}-\frac{(a^2+k^2)^{\frac{1}{2}}-k^2}{3a^3}+\frac{1}{3}\right\}.$$

If we had used the exact relativistic motion (9) rather than (9″), the bracket would contain an additional term linear in the small quantity C. For small but finite C the self-force vanishes only if the bracket is zero. The latter, however, does not vanish for $a=3k/4$ nor for any other value of a save $a=0$ (or $a\approx0$ if the small correction term linear in C is added). That is, our field theory does not allow self-acceleration in its beginning phase. Therefore, the whole process of self-acceleration is not compatible with the

field theory. It will be noticed that the bracket in the last equation for the self-force would vanish for $a=3k/4$, if the positive root $(a^2+k^2)^{\frac{1}{2}}$ were replaced by the negative root. However, because of our application of retarded potentials the root appears with positive sign, and we arrive at the gratifying result that self-acceleration is impossible in our field theory.

3. NEGATIVE ENERGY DENSITY

It seems impossible to devise a field theory of charged particles without violating the requirement that the density of the field energy ought to be larger in the presence of a field than without field, that is, be positive definite in the presence of a field. As an example we mention Born-Infeld's field theory which leads to negative energy densities[4] wherever the vectors D and B have certain large values. (In our theory negative field energy is connected with large frequencies $\nu>\nu_0=kc/2\pi$ rather than with large field intensities). Dirac[3] in his classical theory of the electron simply assumes that an infinite amount of negative energy of unknown origin is condensed near the point electron so as to counterbalance somehow the infinite positive Maxwell energy. He thereby denies that the mass of the electron is of electromagnetic origin.

The negative energy density of the meson field in our theory seems to lead to certain difficulties. Consider an electron vibrating with a frequency ν larger than ν_0 for a limited time only. As shown in Part II, it then emits a group of Maxwell waves E, B and a group of meson waves of polarization $D-E$, $H-B$. The two groups travel with different group velocities and become separated at some distance from the source. The Maxwell group carries more energy than was emitted by the electron; the meson group with its negative energy re-establishes the energy balance. A resonator exposed to the Maxwell group alone then might transform the Maxwell energy into mechanical energy of the resonator, thereby reducing the energy remaining in the field to larger and larger negative values. This objection does not hold, however, in our unitary theory where all energy is located and conserved in the field, and the work on the resonating charged particle is zero. From the energetic point of view our position with respect to negative field energy is the same as that of an observer above sea level who discovers that weights may be dropped below zero level at the expense of other weights raised above sea level. Difficulties appear, however, if one tries to derive a statistical distribution of photons and mesons over positive and negative levels, at least if he wants to apply the same statistical methods which had been developed for positive levels.

In case of Boltzmann statistics the relative number of particles on two energy levels is

$$\bar{n}_1/\bar{n}_2=\exp\,(W_2-W_1/kT),$$

and remains unchanged if both energies are counted from a new zero point. Bose statistics, however, yield the following formula for the average number of particles of energy W:

$$\bar{n}=1/[\exp\,(W/kT)-1],$$

where W is an absolute energy value without an additional constant. $\bar{n}_1/\bar{n}_2$ depends on the absolute position of the zero energy. Furthermore, Bose's formula is meaningless for negative values of W unless a new interpretation of a "negative number of particles" is invented. However, one must remember that Bose particles are "particles" only in a very restricted sense, and that the success of Bose's procedure is more or less accidental. Bose showed that the same Planck radiation law which was derived from an equilibrium between radiation and radiating matter (Planck's and Einstein's derivations) could also be obtained from certain statistics applied to "particles without individuality." We cannot expect that a modified Planck law (asked for by modified field theories) should still be derivable from Bose's corpuscular method. This applies in particular to our case where "pure field" and "electronic field" are undistinguishable within the range $1/k$ of the electronic "radius." Radiation of wave-length $\lambda=2\pi/k$ may be treated in connection with electrons responsible for the radiation equilibrium, similar to Einstein's derivation of Planck's law, as follows.

[4] M. Born, Proc. Roy. Soc. **143**, 410 (1934). See also W. Heitler, *Quantum Theory of Radiation* (Oxford University Press, 1936), Eq. (5), p. 237.

4. MODIFIED EINSTEIN EQUILIBRIUM

An electron vibrating with frequency $\nu > \nu_0 = kc/2\pi$ emits negative meson energy at the ratio of $(1-\nu_0^2/\nu^2)^{\frac{1}{2}}$ to 1 in comparison to the normal Maxwell radiation, according to (6). This ratio has another significant meaning. The number of Jeans proper vibrations per unit cube and per wave-length interval $d\lambda$ is

$$dZ = (8\pi/\lambda^2)d(1/\lambda).$$

Since $c/\lambda = \nu$ for Maxwell waves, and

$$c/\lambda = (\nu^2 - \nu_0^2)^{\frac{1}{2}}$$

for meson waves, we obtain the following numbers of levels within the same $d\nu$:

$$dZ'' = 8\pi\nu^2 d\nu/c^3 \text{ for photons } h\nu \qquad (10)$$
$$dZ' = (8\pi\nu^2 d\nu/c^3)(1-\nu_0^2/\nu^2)^{\frac{1}{2}} \text{ for meaons } (-h\nu).$$

dZ' and dZ'' turn out to have the same ratio as the numbers of mesons and photons emitted "spontaneously" by the vibrating electron during a certain time. Hence, if a group of electrons has emitted just one photon onto every one of the dZ'' levels within $d\nu$, the same group of electrons has also emitted just one meson onto every one of the dZ' meson levels within $d\nu$. The total number of photons and mesons emitted is proportional to $(dZ''+dZ')$ whereas the total energy emitted is proportional to $h\nu\cdot(dZ''-dZ')$.

After this preparation let us discuss Einstein's derivation of Planck's radiation law, modified by our field theory. Two electronic energy levels W_a and $W_b < W_a$ may be occupied by N_a and N_b electrons, respectively. Electronic transitions between the two levels produce emissions and absorptions of quanta $+h\nu$ and $-h\nu$ to and from the Jeans radiation levels within a certain resonance interval $d\nu$ containing dZ'' photon levels and dZ' meson levels. An electronic transition from W_b to the higher level W_a corresponds to an increase of the electronic amplitude of vibration and to a decrease of the Maxwell field strength $|E''|$ (=absorption of photons) and to an increase of the meson field strength $|E'|$ (=emission of mesons). In terms of statistics this means that the probability of an electronic transition from W_b to W_a ought to be proportional to the difference of the numbers $n''dZ''$ of photons and the number $n'dZ'$ of mesons ready to be absorbed from the resonance interval $d\nu$:

$$P_{ba} = N_b[n''dZ'' - n'dZ'].$$

Opposite transitions $a \to b$ induced by the radiation will be proportional to the same difference, whereas spontaneous transitions will be proportional to $1\cdot dZ'' - 1\cdot dZ'$ [see (6) and (10)] so that

$$P_{ab} = N_a[(n''+1)dZ'' - (n'+1)dZ'].$$

In case of equilibrium we must have $P_{ab} = P_{ba}$ in the average, that is,

$$N_b/N_a = \frac{(\bar{n}''+1)dZ'' - (\bar{n}'+1)dZ'}{\bar{n}''dZ'' - \bar{n}'dZ'}.$$

The bars indicate average numbers of photons and mesons per level. If equilibrium shall apply to photon processes alone and to meson processes alone we must have

$$N_b/N_a = (\bar{n}''+1)/\bar{n}'' = (\bar{n}'+1)/\bar{n}',$$

hence, $\bar{n}'' = \bar{n}'$. That is, the average number of photons and mesons per Jeans level must be equal. If the electrons are subject to Boltzmann statistics $N = \text{const.}\exp(-E/kT)$ we obtain the following value for the average number of photons and mesons per level:

$$\bar{n}'' = \bar{n}' = [\exp(h\nu/kT) - 1]^{-1}. \qquad (10')$$

The total radiation energy within $d\nu$ has density

$$w_\nu d\nu = \bar{n}''h\nu dZ'' + \bar{n}'(-h\nu)dZ' = (w_\nu'' - w_\nu')d\nu$$
$$= \frac{8\pi h\nu^2 d\nu}{c^3}\,\frac{1}{\exp(h\nu/kT)-1} \times [1-(1-\nu_0^2/\nu^2)^{\frac{1}{2}}]. \qquad (10'')$$

For $\nu > \nu_0 = kc/2\pi$ Planck's radiation formula is multiplied by the same factor (6) which already occurs in the classical energy emission of an electron for $\nu > \nu_0$. The result is obtained without applying statistics to the pure radiation.

5. STABILITY OF EQUILIBRIUM

In order to show that the equilibrium is stable consider small deviations from the average numbers

$$n'' = \bar{n}'' + \delta'', \quad n' = n' + \delta',$$
$$N_a = \bar{N}_a + \Delta, \quad N_b = \bar{N}_b - \Delta$$

which are related by the condition

$$\Delta = Z'\delta' - Z''\delta''$$

where Z' and Z'' are the number of radiation levels involved (formerly called dZ' and dZ''). Photonic processes lead to an increase of the number of photons, $d(n''Z'')/dt = P_{ab} - P_{ba}$ whereas $dZ' = 0$, that is,

$$d(n''Z'')/dt = (\bar{N}_a + \Delta)(\bar{n}'' + \delta'' + 1)Z'' - (\bar{N}_b - \Delta)(\bar{n}'' + \delta'')Z''.$$

The terms of zero order in the deviations cancel, and the second-order terms shall be neglected. This leaves the first-order terms:

$$d(\delta''Z'')/dt = -(\delta''Z'')(\bar{N}_b - \bar{N}_a) + \Delta \cdot (2\bar{n}'' + 1)Z''.$$

Mesonic processes yield similarly $d(n'Z')/dt = P_{ba} - P_{ab}$ and $dZ'' = 0$, that is, after removing second- and zero-order terms:

$$d(\delta'Z')/dt = -(\delta'Z')(\bar{N}_b - \bar{N}_a) + \Delta(2\bar{n}' + 1)Z'.$$

At last, the electronic number N_a increases with probability $P_{ba} - P_{ab}$, that is, after removing second- and zero-order terms:

$$d\Delta/dt = -\Delta\{(2\bar{n}'' + 1)Z'' - (2\bar{n}' + 1)Z'\} + (\bar{N}_b - \bar{N}_a)(\delta''Z'' - \delta'Z').$$

The last bracket is $-\Delta$. Writing C for the positive constant $\bar{N}_b - \bar{N}_a$, we thus obtain

$$(\alpha) \quad d\Delta/dt = -\Delta\{C + (2\bar{n}'' + 1)Z'' - (2\bar{n}' + 1)Z'\}$$

together with the former results

$$(\beta) \quad d\delta''/dt = -\delta''C + \Delta \cdot (2\bar{n}'' + 1),$$
$$(\gamma) \quad d\delta'/dt = -\delta'C + \Delta \cdot (2\bar{n}' + 1).$$

The factor of $-\Delta$ in (α) is positive since $C > 0$, and $\bar{n}'' = \bar{n}'$, as well as $Z'' > Z'$. Thus the absolute value of Δ will always decrease. The terms with Δ in (β) and (γ) will therefore shrink to zero after some time, and from thereon the absolute values of δ'' and δ' will always decrease. A small deviation from the average values $\bar{n}''$, $\bar{n}'$, $\bar{N}_a$, $\bar{N}_b$ thus tends to disappear automatically according to the transition probabilities accepted before, and the equilibrium turns out to be stable.

6. FIELD EQUATIONS

We now return to our former notation E, H for Maxwell's field E, B, and E'', H'' for Maxwell's D, H (Table I). Both fields shall be derived from potentials V, A and V'', A'', respectively:

$$E = -\nabla V - \dot{A}/c, \qquad H = \nabla \times A; \tag{11}$$

$$E'' = -\nabla V'' - \dot{A}''/c; \qquad H'' = \nabla \times A''. \tag{11'}$$

However, only the potential V'', A'' shall always obey the Lorentz condition:

$$(\nabla \cdot A) + \dot{V}/c = R, \tag{12}$$

$$(\nabla \cdot A'') + \dot{V}''/c = 0 \tag{12'}$$

where R on the right of (12) may be any scalar function of $xyzt$, to be restricted later. In our applications we usually consider the special case $R = 0$ only. As a consequence of (11), (12) one obtains field equations for E, H and E'', H'':

$$\nabla \times E + \dot{H}/c = 0, \qquad (\nabla \cdot H) = 0; \tag{13}$$

$$\nabla \times E'' + \dot{H}''/c = 0, \qquad (\nabla \cdot H'') = 0; \tag{13'}$$

$$\nabla \times H - \dot{E}/c = -\Box A + \nabla R, \qquad (\nabla \cdot E) = -\Box V - \dot{R}/c; \tag{14}$$

$$\nabla \times H'' - \dot{E}''/c = -\Box A'', \qquad (\nabla \cdot E'') = -\Box V''. \tag{14'}$$

The right-hand sides of (14') represent 4π times the current j/c and density ρ of the true charge (which later on is supposed to be condensed to world lines only). The right-hand sides of (14) represent 4π times the free current and density. $\Box A$ and $\Box V$ have the dimensions of potentials divided by the square of a length. They may be written in the form

$$-\Box A = k^2 A', \qquad -\Box V = k^2 V'; \tag{15}$$

$$-\Box A'' = 4\pi j/c, \qquad -\Box V'' = 4\pi\rho; \tag{15'}$$

thereby defining a new "potential" A', V'. Hence $(k^2 A' + \nabla R)$ is 4π times the free current density, and $(k^2 V' - \dot{R}/c)$ is 4π the free charge density. As a consequence of (14) (14') we obtain continuity equations for free and true charge:

$$(\nabla \cdot A') + \dot{V}'/c = -\Box R/k^2, \tag{16}$$

$$(\nabla \cdot j) + \dot{\rho} = 0. \tag{16'}$$

From the potentials A', V' we may also derive a new "field" E', H':

$$E'=-\nabla V'-\dot{A}'/c, \quad H'=\nabla\times A'. \tag{17}$$

(13) and (14′) are Maxwell's equations. It has been assumed that both fields $E, H(=E, B)$ and $E'', H''(=D, H)$ are derived from potentials, and that V'', A'' satisfy the Lorentz condition.

We now postulate a new relation between the two potentials, namely,

$$V''=V-\Box V/k^2, \quad A''=A-\Box A/k^2 \tag{18}$$

from which follows

$$E''=E-\Box E/k^2, \quad H''=H-\Box H/k^2 \tag{19}$$

or $D=E-\Box E/k^2$ and $H=B-\Box B/k^2$ in the usual notation. Eliminating $\Box A$ and $\Box V$ from (15) and (18) we obtain

$$A=A''-A', \quad V=V''-V'. \tag{20}$$

Hence (12) must be the difference of (12′) and (16). That is, the right-hand side R of (12) must satisfy the condition

$$-\Box R+k^2R=0. \tag{21}$$

From (20) we learn that

$$E=E''-E', \quad H=H''-H' \tag{22}$$

or $E=D-E'$ and $B=H-H'$ in the usual notation, which shows that the fields E' and H' determine an electric (P) and magnetic (M) polarization of the vacuum

$$E'=4\pi P, \quad H'=-4\pi M. \tag{22′}$$

Equation (16) now reduces to

$$(\nabla\cdot A')+\dot{V}'/c=-R. \tag{23}$$

The field equations for E' and H' according to (17) and (23) read

$$\nabla\times E'+\dot{H}'/c=0, \quad (\nabla\cdot H')=0; \tag{24}$$

$$\nabla\times H'-\dot{E}'/c=-\Box A'-\nabla R, \quad (\nabla\cdot E')=-\Box V'+\dot{R}/c. \tag{24′}$$

Subtraction of (15) from (15′) yields, because of (20),

$$-\Box A'+k^2A'=4\pi j/c, \quad -\Box V'+k^2V'=4\pi\rho. \tag{25}$$

Equation (25) together with (15′)

$$-\Box A''=4\pi j/c, \quad -\Box V''=4\pi\rho \tag{25′}$$

shows that the true charge is the common source of the two otherwise independent fields E'', H'' and E', H'. True charge shall be condensed on singular world lines only.

The absolute values of the potentials A', V' have a physical meaning without additional constants since they occur in the field equations (14) whose right-hand sides read

$$k^2A'+\nabla R \quad \text{and} \quad k^2V'-\dot{R}/c. \tag{26}$$

They represent 4π times the free current and free charge density.

Since the fields $E=E''-E'$ and $H=H''-H'$ determine the Lorentz force and work, the energy-momentum tensor T must be the difference $T=T''-T'$. In particular, the density of energy and flux are

$$w=w''-w', \quad S=S''-S', \tag{27}$$

where

$$w'=(1/4\pi)\{\tfrac{1}{2}(E'^2+H'^2+k^2A'^2+k^2V'^2) +R\dot{V}'/c-\dot{R}V'/c+\tfrac{1}{2}R^2\}, \tag{28}$$

$$S'=(c/4\pi)\{[E'\times H']+k^2V'A'+V'\nabla R+\dot{A}'R/c\},$$

and

$$w''=(1/4\pi)\tfrac{1}{2}(E''^2+H''^2), \quad S''=(c/4\pi)[E''\times H'']. \tag{28′}$$

Equation (28) contains the right-hand side R of (12) and is more general than the expressions for w' and S' of Part II where we considered the case of $R=0$ only.

Meson waves in vacuum may have longitudinal field components. Indeed, consider the special case

$$A_x'=a_x'\sin(2\pi\nu t+2\pi x/\lambda), \quad A_y'=0, \quad A_z'=0, \quad V'=v'\cdot\sin(2\pi\nu t+2\pi x/\lambda).$$

The amplitudes a_x' and V' are not restricted by (12). The field is

$$E_x'=-(a_x'\nu/c+v'/\lambda)2\pi\cos(2\pi\nu t+2\pi x/\lambda), \quad E_y'=E_z'=H_x'=H_y'=H_z'=0,$$

representing a longitudinal electric wave. In case of Maxwell waves we would have $a_x''=-v''$, and $E_x''=0$. Maxwell waves do not have longitudinal components for two reasons: first, because $\lambda=c/\nu$, and second, because of the

Lorentz condition (12′). Meson waves do not have to satisfy the Lorentz condition, and their relation between λ and ν is

$$(\nu/c)^2=1/\lambda^2+(kc/2\pi)^2. \tag{29}$$

7. ELECTRIC POLE AND MAGNETIC DIPOLE

In Part II we discussed the potential and field of an electric point charge ϵ. The field equations allow the following solution:

$$\begin{aligned} V''&=\epsilon/r\,, \quad V'=(\epsilon/r)\exp(-kr), \\ E_r''&=\epsilon/r^2, \quad E_r'=\epsilon(1/r^2+k/r)\exp(-kr). \end{aligned} \tag{30}$$

At large distance this is the ordinary Coulomb field of a point charge ϵ. In a similar way we now discuss the field of a magnetic dipole of moment μ. The field equations for $R=0$ allow the solution:

$$\begin{aligned} &A_x''=0, \quad A_y''=\mu\frac{\partial}{\partial z}\left(\frac{1}{r}\right), \quad A_z''=-\mu\frac{\partial}{\partial y}\left(\frac{1}{r}\right) \\ &A_x'=0, \quad A_y'=\mu\frac{\partial}{\partial z}(e^{-kr}/r), \\ &\qquad\qquad A_z'=-\mu\frac{\partial}{\partial y}(e^{-kr}/r) \end{aligned} \tag{31}$$

with the magnetic fields

$$\begin{aligned} &H_x''=\mu\left(\frac{3x^2}{r^5}-\frac{1}{r^3}\right), \quad H_y''=\mu\frac{3xy}{r^5}, \\ &\qquad H_z''=\mu\frac{3xz}{r^5}, \\ &H_x'=\mu\left\{\left(\frac{3x^2}{r^5}-\frac{1}{r^3}\right)+k\left(\frac{3x^2}{r^4}-\frac{1}{r^2}\right)\right. \\ &\qquad\qquad \left.+k^2\left(\frac{x^2}{r^3}-\frac{1}{r}\right)\right\}e^{-kr}, \\ &H_y'=\mu\left\{\frac{3xy}{r^5}+k\frac{3xy}{r^4}+k^2\frac{xy}{r^3}\right\}e^{-kr}, \\ &H_z'=\mu\left\{\frac{3xz}{r^5}+k\frac{3xy}{r^4}+k^2\frac{xz}{r^3}\right\}e^{-kr}. \end{aligned} \tag{31′}$$

For large r this is the ordinary Coulomb field of a dipole of moment μ parallel x. Although the field $H=H''-H'$ does not vanish for $r=0$, the Lorentz force $\mu\partial H/\partial x$ vanishes for $r=0$. The classical field theory remains unitary if we postulate as before that the electron moves so that the total Lorentz force and work on the singularity are always zero.

In order to find the energy of the magnetic field we use (27), (28) for the energy density $w=w''-w'$ with function $R\equiv 0$. Integration over space yields

$$W_{\text{mag}}=\mu^2k^3\tfrac{1}{9}.$$

The field energy of the point dipole is **finite** due to magnetic polarization of the vacuum.

If the electron really had a magnetic self-energy like this, the common electric and magnetic radius $1/k$ at which Coulomb's law breaks down would be determined by the equation

$$mc^2=\tfrac{1}{2}\epsilon^2k+\tfrac{1}{9}\mu^2k^3.$$

Substituting the quantum values

$$\mu=\epsilon\hbar/2mc, \quad \epsilon^2=\alpha\hbar c, \quad \alpha=1/137, \tag{32}$$

this would yield the following equation for $\delta=2mc^2/\epsilon^2k$:

$$\frac{\delta}{2}=\tfrac{1}{2}+\tfrac{1}{9}(\alpha\delta)^{-2}$$

solved by $\delta=16.47$; that is, $1/k=16.47\,(\epsilon^2/2mc^2)$. The radius would be more than sixteen times the electric radius, and the magnetic energy more than fifteen times the electric energy.

However, results obtained from substituting quantum values into classical formulae do not mean very much. Take the example of the ratio of spin M to magnetic moment μ which according to quantum theory and experience is $\mu/M=\epsilon/mc$ corresponding to a g factor 2. In the classical field theory the spin is due to the radial electric field of the pole ϵ and the longitudinal field of the dipole μ which together produce angular momentum about the dipole axis, proportional to the product $\epsilon\mu$. In case of a point pole and point dipole with surrounding Coulomb fields, M becomes infinite. If instead we take a "model" in which the field is present outside the radius $1/k$ only, M becomes $2\epsilon\mu k/3c$. In our invariant field theory in which Maxwell and meson terms are subtracted the spin happens to be **zero**. It is not surprising that the classical theory cannot yield the correct spin, because the angular moment rests on the exact knowledge of per-

pendicular components of E and H simultaneously which cannot be measured without uncertainty. The actual value $M=\frac{1}{2}\hbar$ is just halfway between the field value $M=0$ and the "normal" value $M=\hbar$.

We learn, however, from these considerations that the ratio of magnetic moment to spin and also to magnetic energy varies widely with the special theory under consideration. The "model" with fields outside $1/k$ yields

$$W_{el}=\tfrac{1}{2}\epsilon^2 k, \quad W_{mag}=\tfrac{1}{3}\epsilon^2 k^3, \quad M=\tfrac{2}{3}\epsilon\mu k/c, \quad 1/k=23.3\epsilon^2/2mc^2.$$

Quantum theory and experience, however, yield (see Part IV):

$$W_{el}=\tfrac{1}{2}\epsilon^2 k, \quad W_{mag}=0, \quad M=\tfrac{1}{2}\hbar, \quad 1/k=\epsilon^2/2mc. \tag{33}$$

The result that the magnetic energy and magnetic mass are zero in spite of the presence of a magnetic moment μ is suggested already by the simple formula $\mu=\epsilon\hbar/mc$; if m in this formula should depend on μ implicitly, the ratio between electric and magnetic energy would have complicated values [like 16.47 (see above)]. Also, the radius $1/k$ would be much too large as soon as the magnetic energy plays any considerable part in the self-energy [even with so small a factor as $\frac{1}{9}$ (see above)]. Already the discussion of various classical models and field theories shows that it is well possible already on a classical basis to construct a dipole moment whose surrounding magnetic energy happens to vanish.

The satisfactory result of Part IV that the electron does not have magnetic self-energy arising from its magnetic moment, and that its radius is the electrostatic radius $1/k=\epsilon^2/2mc^2$, is explained in the following way. In the first place, the only sources of the field according to the field equations (25), (25′) are the electric charges, and there are no retarded potentials from magnetic poles or dipoles. Turning to the Fourier representation of Part II, Section 7, the Hamiltonian consists of terms referring to the particles alone, to the field alone, and perturbation terms. In our unitary theory the terms referring to the particles alone vanish [first two terms in II, (26)]. The part of the "mutual" energy which is proportional to ϵ^2 may be interpreted as electromagnetic "self-energy." It arises from scalar and vector potentials, but for a particle at rest the contribution of the scalar potential [last term in first line of II, (26)] is of opposite sign and half as large as the contribution of the vector potential [second line in II, (26)]; the resultant energy is $-\frac{1}{2}k\epsilon^2+k\epsilon^2=\frac{1}{2}k\epsilon^2$. If the particle is in an external field one also obtains mutual energy terms proportional to ϵ, namely, for a particle at rest $\epsilon\cdot(V'-V'')_{ext}$ and also, if Dirac's quantum method is applied, the scalar product $(\mu\cdot H''-H')$ where μ stands for $\epsilon\hbar/2mc$ as though the electron had a dipole moment μ. There are no terms, however, proportional to μ^2 which could be interpreted as magnetic self-energy. In spite of displaying spin and magnetic moment μ, the electron at rest has only electrostatic self-energy, and the mass is $m=\frac{1}{2}\epsilon^2 k/c^2$.

The Accommodation Coefficient of Helium on Platinum*

PAULINE ROLF†
Bryn Mawr College, Bryn Mawr, Pennsylvania
(Received December 20, 1943)

The accommodation coefficient of helium on platinum has been measured at 77, 193, 273, and 373°K; and the values obtained at these temperatures for a clean platinum surface are 0.090, 0.043, 0.071, and 0.072 (±0.004), respectively. When the platinum is allowed to remain in contact with the helium for twenty-four hours or more, the accommodation coefficient values increase to 0.43, 0.071, 0.170, and 0.170 (in the same temperature order). Little adsorption occurs at 193°K, but strong van der Waals adsorption appears at 77°K and activated adsorption at the higher temperatures.

THE accommodation coefficient a of a gas striking a solid surface is defined by the following equation:

$$a=Q'/Q,$$

where Q' is the actual average energy exchange and Q is the energy exchange that would occur if the gas molecules, on the average, attained on collision the temperature of the solid surface. Since the accommodation coefficient is not independent of temperature, closely approaching solid and gas temperatures are understood.

The differential equation for the temperature distribution along a wire carrying a current and losing heat to its surroundings by radiation, conduction through the ends of the wire, and conduction to gas molecules impinging on its surface is:

$$d^2t/dx^2=At-B,^{1,2} \quad (1)$$

where

$$A=(1/K\pi r^2L)[8\pi e\sigma rT^3L+2(2\pi)^{\frac{1}{2}}aprL(R/MT)^{\frac{1}{2}}-I^2R_0cL] \quad (2)$$

and

$$B=I^2R_0/K\pi r^2L \quad (3)$$

are constants. The quantities involved are defined as follows:

I—current passing through wire,
R_0—resistance of wire at bath temperature,
e—emissivity of Pt at bath temperature,
K—thermal conductivity of Pt at bath temperature,
σ—Stefan-Boltzmann constant—5.722×10^{-12} watt cm^{-2} deg.$^{-4}$,
R—gas constant—8.314 joules °C^{-1},
c—temperature coefficient of resistivity,
r—radius of wire,
L—length of wire,
T—temperature of surrounding bath,
M—molecular weight of gas,
p—pressure of gas,
a—accommodation coefficient.

The solution of Eq. (1) for $A>0$ is:

$$t=\frac{B/A}{e^{\sqrt{A}L}-e^{-\sqrt{A}L}}\times[-(1-e^{\sqrt{A}L})e^{\sqrt{A}x}+(1-e^{\sqrt{A}L})e^{-\sqrt{A}x}]+B/A \quad (4)$$

and the average temperature of the wire is:

$$\bar{t}=B/A[f(A)-1], \quad (5)$$

where

$$f(A)=\frac{4-2(e^{\sqrt{A}L}+e^{-\sqrt{A}L})}{\sqrt{A}L(e^{\sqrt{A}L}-e^{-\sqrt{A}L})}. \quad (6)$$

Upon equating the heat supplied to the wire to the heat losses from the wire, the following equation results:

$$\frac{f(A)}{1-c\bar{t}}=-1+\frac{8\pi e\sigma rT^3Lm}{R_0c}+\frac{2(2\pi)^{\frac{1}{2}}aprL(R/MT)^{\frac{1}{2}}m}{R_0c}, \quad (7)$$

where

$$m=(R-R_0)/Q=R_0c\bar{t}/Q \quad (8)$$

* This paper represents the publication in part of a dissertation submitted to the faculty of Bryn Mawr College in partial fulfillment of the requirements for the degree of Doctor of Philosophy.

† Now with Institutum Divi Thomae, Cincinnati, Ohio.

[1] J. K. Roberts, Proc. Roy. Soc. **A135**, 192 (1932).

[2] B. Raines, Phys. Rev. **56**, 691 (1939).

is a constant for a given bath temperature T, provided the power input is not too great.

Following the method of Cox,[3] one observes that the right-hand side of Eq. (7) is independent of the temperature rise; and, therefore, for zero power input,

$$f(A_0) = -1 + 8\pi e\sigma r T^3 L m/R_0 c + 2(2\pi)^{\frac{1}{2}} a p r L (R/MT)^{\frac{1}{2}} m/R_0 c. \quad (9)$$

Also, for zero power input, Eq. (2) for A becomes

$$A_0 = \frac{8\pi e\sigma r T^3 L - (2\pi)^{\frac{1}{2}} 2 a p r L (R/MT)^{\frac{1}{2}}}{K\pi r^2 L}. \quad (10)$$

And it can be seen from Eq. (9) that

$$-f(A_0) = 1 - (m/R_0 c) K \pi r^2 L A_0, \quad (11)$$

which defines a series of straight lines depending on the parameter,

$$N = (m/R_0 c) K \pi r^2 L. \quad (12)$$

At any fixed bath temperature K and c are known and m and R_0 are determined from the experimental data. Hence N is determined. Then, from the graphical simultaneous solution of (6) and (11), A_0 can be determined. When applied to a run in vacuum ($p < 1\times10^{-6}$ mm Hg) the second term in Eq. (10) falls out, and one can solve directly for the emissivity e. For a run in the presence of gas ($1\times10^{-3} < p < 1\times10^{-2}$ mm Hg) a can be evaluated from A_0, once the emissivity is determined by a run in vacuum at the same bath temperature. This method of calculating at zero power input has increased the precision and materially reduced the work of determining the accommodation coefficient from the experimental data.

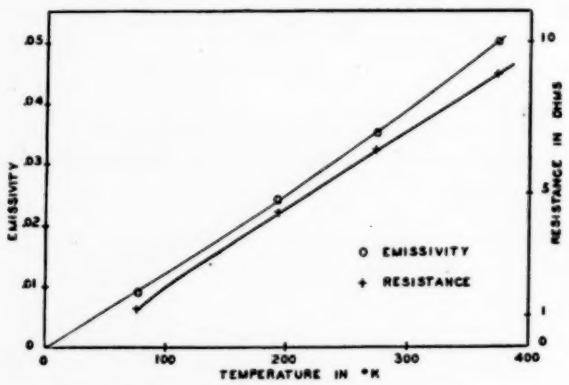

FIG. 1. Emissivity and resistance of platinum filament *vs.* temperature.

EXPERIMENTAL PROCEDURE

The vacuum system was a standard gas circulating system similar to those used by other workers in the field with the exception that all stopcocks directly in the path of the helium were replaced by mercury cut-offs. This was done to prevent contamination of the gas by stopcock grease. The helium was purified by high voltage discharge in a misch metal bottle. Pressures in the experimental tube were measured by a McLeod gauge connecting directly to the tube through a necessary mercury trap. The pressures read were corrected for the difference in temperature between the tube and the McLeod gauge.[4] Stepwise variations of pressure in the experimental tube were obtained by use of a mercury control. This consisted of two concentric glass tubes, the outer one connected to a lift containing mercury, the inner one containing a series of small holes of leak dimensions growing larger toward the bottom.

The experimental tube was somewhat pot-bellied in shape, being $3\frac{1}{2}$ cm wide at its widest point slightly below the center. This was to allow sideward sag of the platinum wire when it was flashed. The platinum (obtained from Baker and Company and of 99.99 percent purity) was in the form of a filament (14.23 cm long at room temperature, 2.65×10^{-3} cm in radius) supported vertically by tungsten leads without the use of springs. Since the flashing temperature of platinum (about 1200°C) is low, springs were unnecessary; and considerably greater accuracy can be obtained by their elimination.

The potential drop across the tube and across a ten-ohm standard resistance in series with it was measured with a Leeds and Northrup Type K potentiometer. Readings were taken with the current flowing first in one and then in the reverse direction to eliminate errors due to thermal e.m.f.'s. From these readings the resistance of the tube and its power input were determined.

The temperature of the medium surrounding the platinum was set by the use of fixed tempera-

[3] M. Cox, Phys. Rev. **64**, 241 (1943).

[4] O. Reynolds, Phil. Trans. **170**, 727 (1879).

TABLE I. Data under vacuum conditions.

Temperature °K	77.4	193.2	273.2	373.1
Resistance R_0 ohms	1.2562	4.4172	6.4475	8.9620±0.0001
Resistivity ρ ohm cm $\times 10^{-6}$	1.95	6.85	10.0	13.9 ±0.1
Thermal conductivity K watts/cm °C	0.796	0.679	0.695	0.715 ±0.005
Temp. coeff. resistivity $c=1/R_0 dR/dT$ °C$^{-1}\times 10^{-3}$	23.1	5.70	3.90	2.81 ±0.01
Emissivity e	0.009	0.024	0.035	0.050 ±0.001

ture thermostating baths. Ice, solid carbon dioxide and acetone, liquid air, and boiling water were used.

VACUUM DATA

Initially the resistance of the wire at 0°C was 6.4780 ohms, and the emissivity was equal to 0.057 (a thermal conductivity of 0.695 watt/cm °C is assumed).[5] The platinum was flashed first at 1000°C, then at 1200°C. At intervals the tube was thermostated and readings of R_0, e, and a were taken. After 100 hours of flashing, the ratio m/R_0 had become constant within its uncertainty, but the resistance at 0°C continued to decrease slowly; and it did not reach stability until after a thousand hours of flashing had elapsed.

Once stability had been attained at 0°C, runs were made at other temperatures. Reference to the equations will show that at zero gas pressure both the emissivity and the thermal conductivity of platinum enter. A search of the literature indicated some confusion in the values of the thermal conductivity of platinum. The best values appeared to be those by Holm,[5] whose work was done on platinum of 99.95 percent purity, and whose results are given by:

$$K=0.699[1+2.83\times 10^{-4}(T-292.7)] \text{ watt/cm°K.}$$

This formula was determined for temperatures above 0°C, so that its use at −80°C without substantiating data is to be questioned. But use of the calculated value (0.679) at this temperature leads to a value of the emissivity which falls on a smooth curve between the higher temperature values and the known value of zero at 0°K. The emissivity-temperature relationship is shown in Fig. 1. At 77.4°K the radiation loss (which is proportional to T^3) has become so low that it can be neglected, and the thermal conductivity is the only unknown. Unfortunately there is a limiting value of N for very small A_0 where the two expressions of $-f(A_0)$ are tangent over a considerable range, and there is quite a lack of precision. This value of N equals $L^2/2$. It is necessary, therefore, to use slightly different methods of computation at this temperature. Two were tried—first, using a non-zero power input Q and the corresponding average temperature $\bar{t}$; second, expanding $-f(A_0)$ in terms of power series in A_0 and neglecting all powers of A_0 higher than the first. The two methods gave the same value of K.

Figure 1 also includes a graph of the variation of the resistance of the platinum wire with absolute temperature (over the range 200–400°K it is close to a straight line). The vacuum data are summarized in Table I.

GAS DATA

Workers[1,2,6] in the field have long ago discovered that the accommodation coefficient is a function of the surface of the metal. In order to have meaning a must be measured on the metal itself: That is, the surface must be free of adsorbed or combined films. A clean surface can be obtained by flashing the metal at high temperatures in vacuum. But, unfortunately, as soon as the metal is allowed to cool in the presence of a gas, the surface becomes contaminated. Whether the contamination is due to adsorption of the impinging molecules of the pure gas or to the adsorption of minute impurities from the gas, the effect is practically the same. The accommodation coefficient will increase in value as time elapses. It is necessary then to extend the data back to the time of zero contamination. Two methods have been used to obtain this. The first, initiated

[5] R. Holm and R. Stormer, Wiss. Veroff. a. d. Siemens-Konzern 9, 2, 312 (1930).

[6] W. C. Michels, Phys. Rev. 40, 472 (1932).

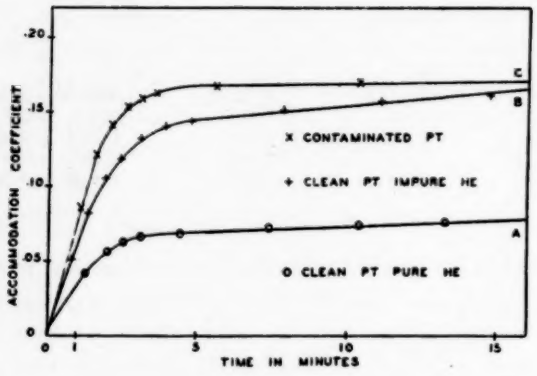

FIG. 2. Accommodation coefficient of helium on platinum *vs.* time after gas admission, 0°C, for clean and dirty platinum, pure and impure helium.

by Roberts,[1,7,8] consists of flashing the metal in vacuum, letting in the gas (metal still flashing) until equilibrium pressure is obtained, then suddenly cutting the flashing current off and taking readings of resistance against power input from that moment on. The second, used by Mann and Newall[9] and Raines,[2] consists of flashing the wire in vacuum until a clean surface is obtained, then letting in the gas and taking resistance-power readings from the time of entrance of the gas. Both methods were tried in this work under comparable conditions (hours aging of wire, gas purity, and pressure, etc.). It was noticed that at equal times after zero (10 min. or more) the first method invariably gave a higher accommodation coefficient than the second. On runs by the first method alone, a_0 increased whenever gas pressure was increased or the platinum was allowed to flash for longer times in the presence of the gas. There seemed to be only one reasonable explanation of this: namely, that residual impurities in the helium (despite the fact that the gas appeared pure viewed through a pocket spectroscope) were adsorbed upon the platinum when it was flashed in their presence, and, therefore, the first method gave a value of a_0 characteristic of an already contaminated surface. For this reason it was discarded, and the second method used throughout the remainder of the work.

Plotted in Fig. 2 are three curves representing the accommodation coefficient against time after the entrance of the gas for three runs at 0°C. Curve *A* was done with spectroscopically pure helium on platinum that had been flashed for many hours in vacuum before the run was taken and was presumably clean of adsorbed impurities. Curve *B* was taken with a clean wire but impure helium. Curve *C* was done in the following manner. The platinum was allowed to remain in the presence of the helium until a stable accommodation coefficient $a_\infty = 0.166$ was reached. The tube was then evacuated and a resistance-power measurement determined for $p < 1 \times 10^{-6}$ mm Hg. Then the gas was allowed to re-enter (no flashing had been done) and resistance-power measurements taken against time. Curve *C* shows the resulting accommodation coefficient. It is noticeable that it immediately rises from a zero value to the previously determined value of a_∞. But mere evacuation will not remove a film from a metal. Therefore the plotted values of a in the first few minutes after the gas entrance are not true measures of the accommodation coefficient. During this time the wire is cooling from its equilibrium temperature in vacuum to a lower temperature determined by ap, and an unsteady state exists. The equations for the determination of a assume a steady state (no time term), so that the apparent accommodation coefficient determined by them is not true until the temperature of the wire has ceased to lag behind the value determined by the energy losses.

Reference to curve *B* shows, however, that the fastest change in the accommodation coefficient is occurring in the early time intervals when the cooling lag is present. For the above reason it was decided to use logarithmic extrapolation of the accommodation coefficient to zero time, following the procedure suggested by Michels.[10] That this extrapolation is not always too good is only to be

TABLE II. Accommodation coefficient of He on Pt at zero time (a_0), some twenty minutes later (a_{eq}), and after twenty-four hours (a_∞).

Temp. °K	a_0	a_{eq}	a_∞
77.4	0.090	0.42	0.43
193.2	0.043	0.045	0.071
273.2	0.071	0.080–0.113	0.170
373.1	0.072±0.004	0.110	0.170

[7] J. K. Roberts, Proc. Roy. Soc. **A129**, 146 (1930).
[8] J. K. Roberts, Proc. Roy. Soc. **A142**, 518 (1933).
[9] W. B. Mann and W. C. Newall, Proc. Roy. Soc. **A158**, 397 (1937).
[10] W. C. Michels, Phys. Rev. **52**, 1067 (1937).

expected. The presence of more than one impurity with different rates of film build-up is logical; an actual saturation effect (that is—entrance of the impurity within the body of the platinum) is possible.

The accommodation coefficient data are summarized in Table II for the four different bath temperatures used. By a_0 is meant the accommodation coefficient at zero time, and the values of it given in the table were obtained by logarithmic extrapolation except at 193.2°K where no adsorption occurred until many hours had passed. By a_{eq} is meant the value of the accommodation coefficient obtained some ten to twenty minutes after the entrance of the gas. At this time the value of the accommodation coefficient is changing very slowly. By a_∞ is meant the accommodation coefficient 24 hours or more after the gas has been let in. Figure 3 shows representative runs at each temperature for thirty minutes after gas admission. Although the curves have been shown extrapolated to zero time the values of accommodation coefficient obtained by such extrapolation mean little because of the cooling lag of the platinum present in the first few minutes, and the actual values of a_0 were obtained by linear logarithmic extrapolation.

There are some points of interest in the accommodation coefficient data obtained. The values of a_0 at 273°K and 373°K, i.e., 0.071 and 0.072, respectively, are in fair agreement with the classical value[10] of 0.078 determined from

$$4mM/(m+M)^2,$$

where m and M are the atomic weights of platinum and helium. The low value of a_∞ (0.170) at these temperatures indicates a tightly bound adsorbed film on the platinum and, therefore, activated adsorption of minute impurities present in the helium. At 77.4°K the high value of a_∞ (0.43) combined with the fact that the best straight line logarithmic extrapolation was found at this temperature strongly indicates van der Waals adsorption of helium.

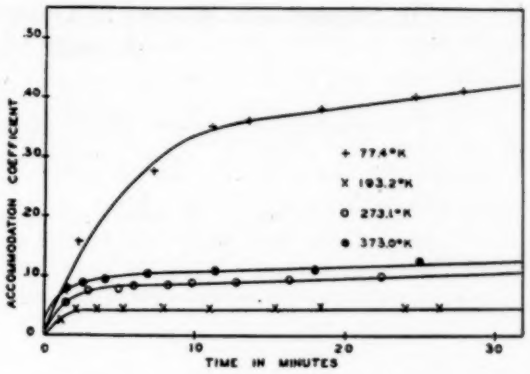

FIG. 3. Accommodation coefficient of helium on platinum *vs.* time after gas admission for various bath temperatures.

In Table III are presented values of the accommodation coefficient of helium on several metals found by other authors. Comparison of the values of a determined in this work with those determined by Mann[11] (He on Pt) are difficult because at no time in the latter's work did the filament temperatures run below 100°C. In the one comparable case (both bath and filament temperatures at 100°C) agreement is obtained for a_0 (0.07 against 0.072). There seems to be little correlation between the present work and the other two sets of data (He on Ni[2] and W[1]) shown in Table III. In the case of the nickel data which were determined by experimental means very similar to this work no attempt was made to allow for a possible lag in cooling of the nickel when the gas was admitted. None of the three sets of data presented in Table III shows the characteristics of the helium on platinum accommodation coefficient data discovered in this work, i.e., a region of strong van der Waals adsorption at very low temperatures, followed by a region of no adsorption and finally an extended region of activated adsorption as the temperature is increased.

TABLE III. Accommodation coefficients of He on Ni, W, and Pt.

Temp. °K	Accommodation coefficients found by other workers					
	He on Ni[a]		He on W[a]		He on Pt[b]	
	a_0	a_∞	a_0	a_∞	a_0	a_∞
77.4	0.048	0.410	0.025	—	0.04*	—
195	0.060	0.423	0.046	—	—	—
273	0.071	0.360	0.057	0.19 (295°K)	0.03†	—
373	0.077	0.343	—	—	0.07	0.25

[a] See reference 1.
[b] See reference 11.
* Bath temperature 80°K, filament temperatures 100°C and up.
† Bath at room temperature, filament between 100°C and 1000°C.

[11] W. B. Mann, Proc. Roy. Soc. **A146**, 776 (1934).

On Supersonic Waves in Cylindrical Tubes and the Theory of the Acoustic Interferometer

P. E. KRASNOOSHKIN
Laboratory of Oscillations, Physical Research Institute, Moscow State University, U.S.S.R.

(Received May 6, 1943)

A theory of the Pierce acoustic interferometer is given which takes into account the non-uniformity of the acoustic field. This leads to an interpretation of the satellite peaks observed in the experiments of Pielemeier and others, and to an improved formula for the determination of the absorption coefficient from the observational data.

1. INTRODUCTION

THE successful application of the Pierce acoustic interferometer to the determination of supersonic sound velocities is well known. Many attempts have been made to apply it to the measurements of absorption coefficients as well, but the accuracy obtained has appeared exceedingly low. L. Mandelstam has concluded that the most likely cause for this is the non-uniformity of the sound field, for which no correction has been made. Ordinary methods of reduction of the experimental data have assumed that the quartz plate used as a radiator vibrates like a piston, giving rise to a purely plane wave. However, real plates do not come up to this ideal, usually exhibiting a rather irregular form of vibration.

The present paper deals with the theory of the interferometer, taking into account this more complex pattern of the acoustic field, and describes a new method of reduction of the experimental data which is believed to be more accurate and general in application than those previously employed.

Before attacking the general theory, it may be desirable to give a brief description of the principle of the interferometer and of the manner in which it is employed. A cylindrical metal tube of arbitrary sectional form is closed at one end by a quartz plate driven by an electrical sine wave generator, and at the other by a movable piston used as a reflector. The whole volume of gas in the tube is set into vibration, in virtue of which there is an acoustic reaction on the sound source. The observational result is a reaction curve in which some quantity measuring the acoustic output of the source is plotted as a function of the distance between the emitter and reflector plates. The reduction of the observations consists of the deduction of the ultrasonic velocity and the absorption coefficient from the form of this curve. In order to study this latter problem we must find an analytical expression for the acoustic reaction on the emitter in terms of the velocity of sound on the one hand, and in terms of parameters describing the form of the vessel and the character of the vibration of the quartz plate on the other.

2. GENERAL THEORY

A rigorous solution of this theoretical problem would be extremely difficult. In our analysis we shall consider the various types of waves which may be generated in such a system, and their effect on the output of the source. This mathematical theory is similar in principle to the theory of electrical wave guides.

If, at a given frequency, the absorption may be considered as small and the transverse dimensions of the cylinder as large, we may follow Kirchhoff[1] in neglecting viscosity and heat losses on the surface of the cylinder, and consider it as infinitely rigid, perfectly smooth, and absolutely thermonegative. By virtue of these conditions, we assume the existence of a velocity potential satisfying the equation

$$\nabla^2\varphi+k_0^2\varphi=0 \qquad (1)$$

throughout the interior of the cylinder. Here $k_0=\beta_0-i\alpha_0$ is a complex wave factor for the unconfined medium ($\beta_0=\omega/v_0$), and the time factor $e^{i\omega t}$ is understood.

With the z axis parallel to the generators of the

[1] G. Kirchhoff, Pogg. Ann. **132**, 177 (1868).

cylinder, the reflecting surface in the plane $z=0$, and the radiating surface in the plane $z=L$, the boundary conditions take the form

$$\partial\varphi/\partial n=0, \quad \text{on the side walls of the cylinder,} \tag{2}$$

$$\partial\varphi/\partial z=0, \quad \text{in the plane } z=0, \tag{3}$$

$$\partial\varphi/\partial z=F(x, y), \quad \text{in the plane } z=L, \tag{4}$$

where $F(x, y)$ gives the normal component of the velocity on the surface of the radiator.

Following Rayleigh's method[2] we look for particular solutions of Eq. (1) in the form of progressive plane waves propagated in the z direction, by setting

$$\varphi=\psi(x, y)e^{\pm imz}, \tag{5}$$

where ψ satisfies the condition

$$\frac{\partial^2\psi}{\partial x^2}+\frac{\partial^2\psi}{\partial y^2}+(k_0^2-m^2)\psi=0 \tag{6}$$

with $f=k_0^2-m^2$, and where it will be assumed that f is real.

Supposing this equation solved, with boundary condition (2), we find the types of waves which may be propagated along the cylinder without change of type, corresponding to a discrete set of values f_j, $j=0, 1, 2, \cdots$ for f, with associated values for the wave factor $m_j=\beta_j-i\alpha_j$. Under the conditions assumed, the different solutions of Eq. (6) will form an orthogonal set of functions when integrated over the cross section of the cylinder, and we shall suppose further that they have been normalized.

The types of waves permitted vary with the form of the bounding cylinder, as do their phase velocities and attenuation coefficients. The wave $f_0=0$ corresponds to an ordinary uniform plane wave; the greater being the value of f_j, the more complicated the wave pattern becomes.

Separating the real and imaginary parts of $m_j^2=k_0^2-f_j$, we obtain

$$2\beta_j^2=(\beta_0^2-\alpha_0^2-f_j)+[(\beta_0^2-\alpha_0^2-f_j)^2+4\alpha_0^2\beta_0^2]^{\frac{1}{2}}, \tag{7}$$

$$2\alpha_j^2=-(\beta_0^2-\alpha_0^2-f_j)+[(\beta_0^2-\alpha_0^2-f_j)^2+4\alpha_0^2\beta_0^2]^{\frac{1}{2}}. \tag{8}$$

[2] Lord Rayleigh, *Theory of Sound*, Vol. 2, Section 301.

The typical form of dependence of β_j and α_j on the value of f_j is shown in Fig. 1. The waves for which f_j is of the order of β_0^2 have such large attenuation that they practically disappear within a few wave-lengths, while if $\alpha_0=0$, waves for which $f_j\geqslant\beta_0^2$ are not propagated at all. This type of attenuation is not due to adsorption in the medium, but to interference effects of primary waves from the source and their reflected waves from the sides of the cylinder. It is this

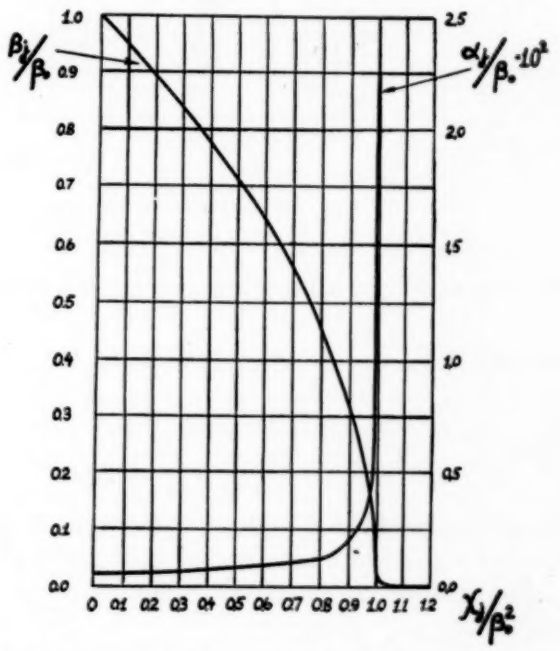

FIG. 1. Attenuation and phase velocity of corrugated waves in tubes for $\alpha_0/\beta_0=6\times10^{-4}$.

effect which constitutes the basis for the present theory.

The general solution of Eq. (1) is obtained as a linear superposition of all of these special waves

$$\varphi=\sum\psi_j(x, y)[c_j'\exp(im_jz)+c_j''\exp(-im_jz)]. \tag{9}$$

From the form of this solution, boundary condition (2) is satisfied automatically. Condition (3) will be satisfied by taking $c_j'=c_j''=c_j$.

We assume that, whatever the form of vibration of the source, $F(x, y)$ of condition (4) can be expanded in a series of the form

$$F(x, y)=\sum A_j\psi_j(x, y) \tag{10}$$

from which, restoring the time factor, our general

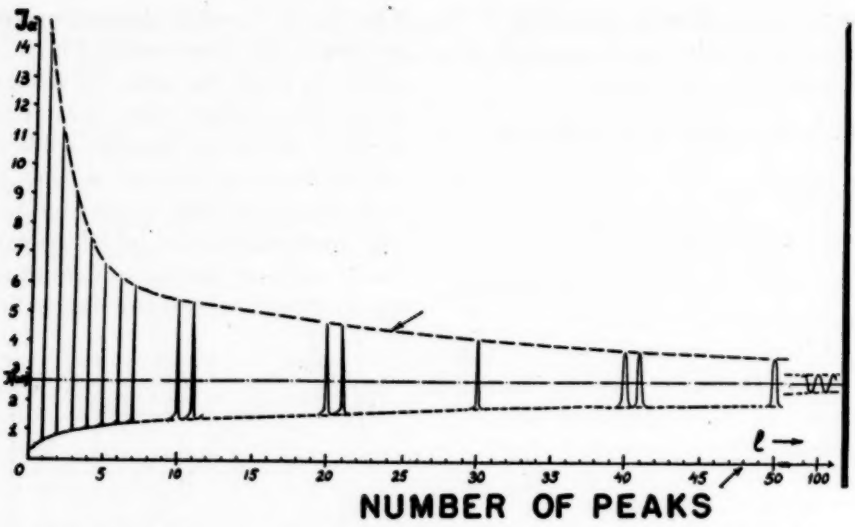

FIG. 2. The elementary reaction curve for air at a frequency of 100,000 cycles.

solution satisfying all conditions turns out to be

$$\varphi=\Re\left\{e^{i\omega t}\sum\frac{A_j\psi_j}{im_j}\times\frac{\exp(im_jz)+\exp(-im_jz)}{\exp(im_jL)-\exp(-im_jL)}\right\},\quad(11)$$

where the symbols $\Re$ and $\Im$ will be used to indicate the real and imaginary parts, respectively.

The acoustic output of the radiator is

$$\frac{dw}{dt}=\int\int\rho\left(\frac{\partial\varphi}{\partial t}\right)_{z=L}\cdot\left(\frac{\partial\varphi}{\partial z}\right)_{z=L}dS\quad(12)$$

in which ρ is the density of the medium. The integral is to be extended over the surface of the radiator.

By substitution of Eq. (11) in (12), taking advantage of the orthonormal character of the ψ's, and performing a time average in the usual fashion, we get

$$\left\langle\frac{dw}{dt}\right\rangle_{Av}=\frac{1}{2}\rho\omega\sum\frac{A_j^2}{\beta_j^2+\alpha_j^2}\times[\beta_j\Im(\cot m_jL)+\alpha_j\Re(\cot m_jL)].\quad(13)$$

To a sufficient approximation, the terms containing the factors $\alpha_j\Re(\cot m_jL)$ can be neglected, as they are small for both small and large values of α_j, since for large values of α_j

$$\Re(\cot m_jL)\sim\exp(-2\alpha_jL).$$

In the remaining expression we need consider only the terms for which $|\beta_j|\gg|\alpha_j|$ in which we can put

$$\omega\beta_j/(\beta_j^2+\alpha_j^2)\approx\omega/\beta_j=v_j.$$

If the variation in the output of the sound generator over a resonance curve is small, we may assume that the experimentally measured plate current of the power tube which drives the oscillator is a linear function of the acoustic power output, and we can take as a measure of the observed curve the remaining quantity

$$\left\langle\frac{dw}{dt}\right\rangle_{Av}\cong I(L)=\sum\rho v_jA_j^2\Im(\cot m_jL).\quad(14)$$

3. DISCUSSION

The simplest case is that in which the radiator vibrates like a piston, as is usually assumed, so that only A_0 differs from zero. This reduces $I(L)$ to the form

$$I(L)=\rho v_0A_0^2[1+\exp(-2\alpha_0L)\cdot\cos 2\beta_0L]\quad(15)$$

for large values of L. The reaction curve for the ordinary theory is shown in Fig. 2. According to Eq. (14) the complete reaction curve is made up of a superposition of curves of this type.[3-5]

In order to explain the usual form of observed

[3] W. H. Pielemeier, Phys. Rev. **34**, 1187 (1929).
[4] J. S. Hubbard, Phys. Rev. **38**, 1011 (1931).
[5] L. Beliavskaya, Bull. Acad. Sci. U.S.S.R., No. 7 (1935).

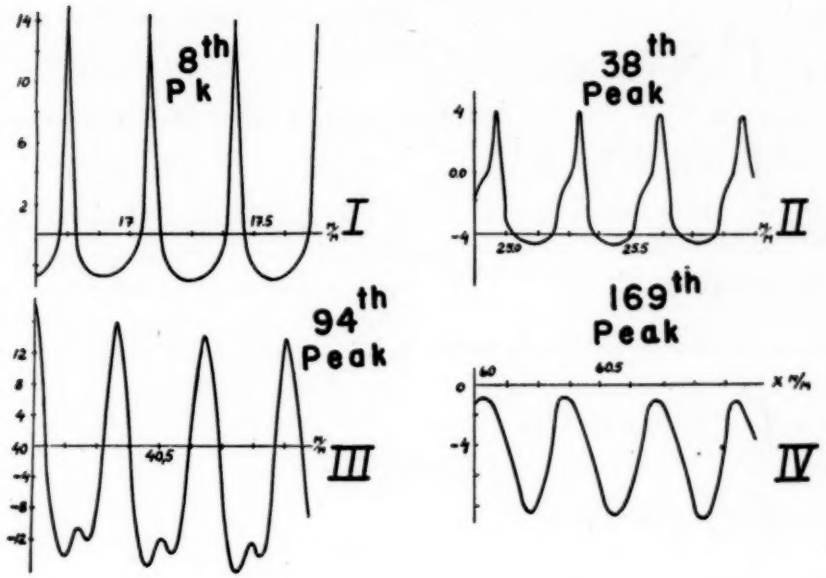

FIG. 3. The satellites after Pielemeier.

reaction curve, it is necessary to assume that in most cases the acoustic field set up consists of a group of waves forming a narrow wave packet. The presence of absorption diminishes the resolving power of the interferometer, so that the fine structure remains unresolved.

In particular cases, in which there are two dominant groups of waves, satellites may be observed, which gives us an explanation of the subsidiary peaks which have been observed by many authors.[3, 6–8] Figure 3 represents such a curve taken from the work of Pielemeier.[3] The measurement of the intervals indicates that the major peaks correspond to waves of high index f_j, while the minor peaks correspond to the nearly plane wave. This is peculiar to Y-cut crystals; for X-cut crystals the approximately uniform plane wave predominates.

Since only the peaks without satellites are used in the experimental work on absorption coefficients, we confine our attention to them. According to our theory, we consider them to be made up of a group of waves forming a single wave packet. We shall now show that the apparent absorption coefficient of such a wave packet arises from two independent causes: (a) the true absorption of the medium, and (b) an apparent absorption arising from the mutual interference effects of the waves comprising the packet. The separation of the two effects will lead us to our improved formula for the reduction of the experimental data.

For large values of $\alpha_0 L$, when the dominating part of the acoustic reaction on the source may be attributed to the first reflected wave, expression (14) takes the form

$$I(L)=\sum \theta_j[1+\exp(-2\alpha_j L)\cos(2\beta_j L)] \quad (16)$$

with

$$\theta_j=\rho v_j A_j^2.$$

Replacing the line spectrum by a continuous wave group, we get

$$I(L)\backsimeq\int_{\beta_0}^{0}\theta(\beta)[1+e^{-2\alpha L}\cos(2\beta L)]d\beta.$$

If we transfer the origin to the center of the packet β_c, and assume the whole spectrum to be confined within the interval $\beta_c \pm b$, we get

$$I(L)\backsimeq C'(L)$$

$$\times\exp(-2\alpha_c L)\cos(2\beta_c L+\varphi)+\text{const.}, \quad (17)$$

[6] E. Klein and W. D. Hershberger, Phys. Rev. **37**, 760 (1931).
[7] R. Alleman, Phys. Rev. **55**, 87 (1939).
[8] W. H. Pielemeier, J. Acous. Soc. Am. **9**, 600 (1938).

where

$$C'(L)\cos\varphi=\int_{-b}^{+b}\theta_s(\xi)\cdot\cos 2L\xi\cdot d\xi,$$
$$C'(L)\sin\varphi=\int_{-b}^{+b}\theta_a(\xi)\cdot\sin 2L\xi\cdot d\xi, \tag{18}$$

$$\theta_s(\xi)=\tfrac{1}{2}[\theta(\xi)+\theta(-\xi)],$$
$$\theta_a(\xi)=\tfrac{1}{2}[\theta(\xi)-\theta(-\xi)]. \tag{19}$$

These equations may be inverted in the form

$$\theta_s(\xi)=\cos\varphi\cdot\int_0^\infty C'(L)\cdot\cos 2\xi L\cdot dL,$$
$$\theta_a(\xi)=\sin\varphi\cdot\int_0^\infty C'(L)\cdot\sin 2\xi L\cdot dL. \tag{20}$$

It is evident that the relation between the form of the spectrum $\theta(\xi)$ and that of the reaction curve envelope $C'(L)$ is similar to that connecting the optical spectrum and the visibility curve of the Michelson interferometer.

Since a large variety of forms of the function $\theta(\xi)$ may produce effectively the same enveloping function $C'(L)$, it is not surprising that observed reaction curves may be approximated rather well by an over-all exponential decay curve of the form e^{-2aL}.

4. REDUCTION OF THE EXPERIMENTAL DATA

It is customary, in the reduction of experimental observations, to choose those reaction curves which may be represented with sufficient accuracy for large L by an expression of the form

$$\exp(-2\alpha_e L)\cdot\cos(2\beta_e L+\varphi). \tag{21}$$

By comparison with the theoretical curve (15) for a uniform plane wave, it is normally assumed that (a) the experimental decay coefficient α_e is equal to α_0 for the uniform wave, and (b) $\beta_e=\beta_0$, so that the wave-length of the uniform wave is equal to twice the distance between adjacent maxima.

By comparison with our more complete formula (17), we see that the dependence on L is determined in part also by the variation of the envelope function $C'(L)$. If we suppose that the over-all variation of the reaction curve is exponential in character, we must put

$$C'(L)=C_0\cdot e^{-2aL} \tag{22}$$

so that the apparent decay constant becomes

$$\alpha_e=\alpha_c+a. \tag{23}$$

The absorption coefficient α_c arises from direct absorption in the medium, while the absorption represented by the coefficient a is due to interference effects within the wave packet, the resultant absorption being due to the combination of the two effects.

Substituting (22) in (20) we find

$$\theta_s(\xi)=\cos\varphi\cdot\frac{a}{a^2+\xi^2}$$

so that

$$a=\Delta\xi$$

is the half-width of the symmetrical part of the packet.

Now we can express $\Delta\xi$ in terms of the width Δf, for according to (7) and (8)

$$2\beta_c\Delta\xi=\Delta f$$

so that to a first approximation

$$a=\Delta f/8\beta_c\cong\Delta f/8\beta_0. \tag{24}$$

The value of Δf is characteristic of the form of the vibrations of the source and the geometry of the interferometer, but does not depend on the properties of the medium in it.

According to Eq. (8), if $f_c/\beta_c^2<\frac{1}{2}$, we have

$$\alpha_c\cong\alpha_0[1+(f_c/2\beta_0^2)], \tag{25}$$

so that, if the width of the symmetrical part of the packet Δf and the position of its center f_c are known, the coefficient of attenuation α_0 referred to the supposed homogeneous plane wave may be deduced from the apparent absorption coefficient by means of the formula

$$\alpha_0=\frac{\alpha_e-(\Delta f/8\beta_0)}{1+(f_c/2\beta_0^2)}, \tag{26}$$

while the corresponding wave-length is given by the formula

$$\lambda_0=\lambda_e/[1+(f_c/2\beta_0^2)] \tag{27}$$

in terms of the apparent wave-length λ_e.

Since many authors reduce their results to a calculation of $\alpha_0\lambda_0^2$, we have the corresponding formula

$$\alpha_0\lambda_0^2=\frac{[\alpha_e-(\Delta f/8\beta_0)]\cdot\lambda_e^2}{[1+(f_e/2\beta_0^2)]}. \quad (28)$$

As far as can be judged, the corrections involving Δf and f_e are appreciable, and with an ideal uniform plane wave the ultrasonic interferometer would give a much less rapid attenuation than that usually measured.

The determination of Δf and f_e for a given apparatus may be carried out by observation of the reaction curve of a gas with known values of v_0 and α_0. The coefficient a obtained by the method of Lubny-Herzyk[9] may be used in (24) to determine Δf. With Δf known, f_e may be determined by measuring α_e and then using (25) with $\alpha_e=\alpha_0-a$.

In conclusion I should like to express my deep gratitude to L. Mandelstam, under whose guidance this work has been done, and to K. Theordortchik for his exceptional attention to the present investigation.

[9] E. Pumper, J. Phys. U.S.S.R. **1**, No. 5–6 (1939).

PHYSICAL REVIEW VOLUME 65, NUMBERS 5 AND 6 MARCH 1 AND 15, 1944

Ambiguities in the X-Ray Analysis of Crystal Structures*

A. L. PATTERSON
Department of Physics, Bryn Mawr College, Bryn Mawr, Pennsylvania

(Received November 23, 1943)

The intensities of the x-ray reflections from a given crystal of a known substance depend on the vector distances between the atoms and not directly on the coordinates of the atoms. The problem of uniqueness in the x-ray analysis of a crystal structure thus depends on the uniqueness of the determination of the arrangement of a periodic set of points in space by its vector distance set. In this paper a large number of cases is presented in which two, and sometimes three or four, non-congruent sets of points are homometric, i.e., have the same vector distance set. Although the investigation is largely based on a discussion of one-dimensional cyclotomic sets, i.e., those in which the points divide the period on the line into rational fractions, it is shown that there are many families of non-cyclotomic pairs and multiplets and that each of these families has its counterpart in two and three dimensions. The significance of these results for practical crystal analysis is discussed.

INTRODUCTION

IT is well known that the F factors of x-ray analysis are completely determined in magnitude and in phase by the coordinates of the atoms in the crystal and by the f factors of the individual atoms. The absolute values of the F factors are, however, given by

$$|F(h_i)|^2=\sum_{s,t=1}^{N}\sum f_s f_t \exp 2\pi i\mathbf{h}\cdot(\mathbf{r}_t-\mathbf{r}_s), \quad (1)$$

in which f_s and $\mathbf{r}_s$, respectively, are the f factor and the coordinate vector for the sth atom and

$$\mathbf{h}=\sum h_i\mathbf{b}_i. \quad (1a)$$

In this latter equation the quantities h_i are the Miller indices for the plane in question and the vectors $\mathbf{b}_i$ are the reciprocal lattice vectors. The intensities in the x-ray diffraction pattern thus depend only on the vector distances between atoms and on the f factors, since in Eq. (1) the coordinate vectors $\mathbf{r}_s$ do not enter alone, but only in the form of the differences $\mathbf{r}_t-\mathbf{r}_s$.

We shall not concern ourselves here with the problem of determining the distances from the values of $|F(h_i)|^2$ since this has been discussed in detail elsewhere.[1] We shall investigate the problem of the determination of the coordinate

* A preliminary report of this work was presented at the Ann Arbor Meeting of the American Society for X-Ray and Electron Diffraction in June, 1943.

[1] A. L. Patterson, Zeits. f. Krist. **90**, 517 (1935); D. Harker, J. Chem. Phys. **4**, 381 (1936); M. Avrami, Zeits. f. Krist. **100**, 381 (1939); S. H. Yu, Nature **149**, 638 (1942) and **150**, 151 (1942).

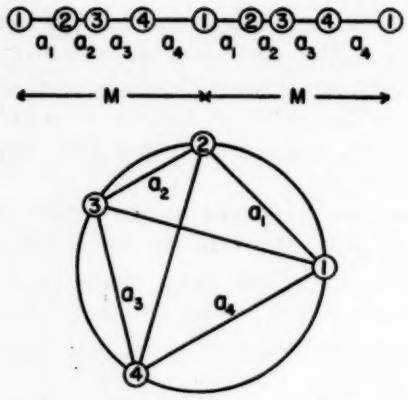

FIG. 1. Sample periodic set on a line, and the representation of its distance set on a circle.

vectors $\mathbf{r}_s$ from the values of the vector distances $\mathbf{r}_t - \mathbf{r}_s$, since it is apparent that a knowledge of these distances is the most information which we can possibly obtain from the x-ray diffraction data alone.

It is well known that the methods of crystal analysis introduce a center of symmetry and that two structures which can be related to one another by a center of symmetry give the same diffraction effects. Any two structures which are congruent in the sense that they can be brought into coincidence with one another by a translation, a rotation, a reflection, or some combination of these operations give the same x-ray pattern. We shall then say that a structure analysis is unique if all the structures which can be derived from it are congruent to one another.

That the distance vectors do not determine all structures uniquely is known from the work of Pauling and Shappell[2] who found that the special point 24(*d*) of the space group $T_h^7 - Ia3$ (for the values $+x$ and $-x$ of the parameter x) presents two non-congruent structures which have the same x-ray intensities and consequently the same distance vectors. It has been shown[3] that this property is also exhibited by a corresponding special point for the space group $O_h^{10} - Ia3d$. Most of the further preliminary discussion of the problem[3,4] must now be withdrawn, however, in the light of the results presented here.

We are thus concerned with the discussion of the cases of ambiguity which may arise in the determination of the arrangement of a set of points from a knowledge of the vector distances for these points. We shall omit discussion of the finite problem,[5] and confine our attention to the case of an infinity of points arranged periodically. We first consider periodic distributions of points on a line; later we shall refer to problems in two and three dimensions.

DISTANCE ARRAYS

Consider a set of N line lattices of points represented by the coordinates $x_i + kM$ $(i = 1, 2, \cdots N)$ with k any integer. These N sets of points can be equally well represented by the symbols x_i (mod M), and together form a periodic set of period M. The discussion of periodic sets of this type is facilitated by making the transformation

$$\theta_i = 2\pi x_i / M.$$

We can then represent the set on the line by points on the circumference of a circle, the angular coordinate of the ith point being θ_i. A sample set on the line and its representation on a circle are shown in Fig. 1.

It is easy to see that the distances A_{ij} (mod M) for a periodic set on the line are given by the

TABLE I. Survey of cyclotomic sets (r points on a period divided into n equal parts). The number of possible arrangements was obtained by first considering the number of r partitions of n. The number of cyclic arrangements (clock order neglected) of each r partition was then considered. In all, 2664 cases ($4 < r < n/2$, $n \leq 16$) were investigated. 390 pairs, 7 triplets, and 3 quadruplets were found.

	Possible arrangements								Number of pairs				
n	$r=1$	2	3	4	5	6	7	8	4	5	6	7	8
8	1	4	5	8	5	4	1	1	1	—	—	—	—
9	1	4	7	10	10	7	4	1	0	—	—	—	—
10	1	5	8	16	16	16	8	5	0	3	—	—	—
11	1	5	10	20	26	26	20	10	0	0	—	—	—
12	1	6	12	29	38	50	38	29	1	3	15	—	—
13	1	6	14	35	57	76	76	57	1	0	1	—	—
14	1	7	16	47	79	126	133	126	0	6	6	48	—
15	1	7	19	56	111	185	232	232	0	5	23	9	—
16	1	8	21	72	147	280	375	440	2	10	31[a]	42[b]	183[c]

[a] 3 triplets are here counted as pairs. If all pairs of the triplets are counted, 6 pairs should be added.
[b] 4 triplets are here counted as pairs. If all pairs of the triplets are counted, 8 pairs should be added.
[c] 3 quadruplets are here included as far as their complementary pairs are concerned. If the four non-complementary pairs of each quadruplet are included 12 pairs should be added.

[2] L. Pauling and M. D. Shappell, Zeits. f. Krist. **75**, 128 (1930).
[3] A. L. Patterson, Nature **143**, 939 (1939).
[4] A. L. Patterson, Phys. Rev. **55**, 682 (1939).
[5] Many results concerning this and related problems are discussed by S. Piccard: *Sur les ensembles des distances des ensembles des points d'un espace euclidien*, Mémoires de l'Université de Neuchatel, **13** (1939).

expressions

$$A_{ij}=x_j-x_i \quad (i,j=1,2,\cdots,N). \tag{2}$$

We shall define as a simple translation a_i (mod M) the translation which joins any point x_i with the point next in order of numbering. It then follows that

$$a_i=x_{i+1}-x_i=A_{i,i+1} \tag{3}$$

and hence that

$$A_{ij}=a_i+a_{i+1}+\cdots+a_{j-1} \quad (i<j). \tag{4}$$

All the distances A_{ij} for a four-point set such as that illustrated in Fig. 1 can then be exhibited in the array:

$$\begin{array}{cccc} 0 & a_1 & a_1+a_2 & a_1+a_2+a_3 \\ -a_1 & 0 & a_2 & a_2+a_3 \\ -a_1-a_2 & -a_2 & 0 & a_3 \\ -a_1-a_2-a_3 & -a_2-a_3 & -a_3 & 0 \end{array} \tag{5}$$

in which all operations are to be carried out (mod M).

We call an array of the type of (5) a distance array, and now list a few of its properties:

(A) The ith row represents the coordinates of the points of the set referred to the ith atom as origin. All rows thus represent the same set of points.

(B) The ith column represents the coordinates of the set obtained from that of the ith row by an inversion in the ith point. All columns represent the same set of points and one which is the inverse of that represented by the rows.

(C) Every entry in the $(i+1)$th row is obtained from the corresponding entry in the ith row by subtracting a_i.

(D) Every entry in the $(i-1)$th column is obtained from the corresponding entry in the ith column by subtracting a_i.

(E) The distance array obtained by interchanging the ith and jth row and then interchanging the ith and jth column will represent the original set with a different numbering of the points.

(F) Any distance array is fully determined by any row or any column combined with a knowledge of the modulus M.

(G) Any distance array is determined by its simple translations a_i provided their order is known.

(H) If a set A is represented by a given distance array, then any set B congruent to A can be represented either by the same array or by the array obtained from it by interchanging rows and columns.

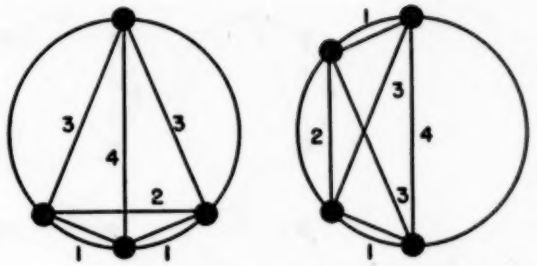

FIG. 2. A simple homometric pair. The distances are the same but the points are in different arrangements.

We shall say that two arrays are equivalent if they represent congruent sets. It then follows that any array can be transformed into any equivalent array by some succession of the operations referred to under (E) and (H).

If we are given the distances of an array such as (5), but have no knowledge of their order within the array, it is always possible to find at least one arrangement of these distances in an array of the type (5). Routines can be established which will do considerable preliminary sorting. This sorting can be completed by trial and error methods which must in the end be successful since the numbers to be arranged came originally from a distance array. In general this sorting process will have several possible solutions, corresponding to different numberings of the set. If all the arrays which can be obtained from a given set of distances are equivalent, we can then say that the structure defined by these arrays is uniquely determined by its distances in the sense that we have defined uniqueness for an x-ray crystal analysis. That this uniqueness does not hold for all sets on the line is demonstrated by the counter-example exhibited in Fig. 2. The two sets shown there have the same set of distances but are not congruent, hence the distance array for this set is not unique. We say that two arrangements which are non-congruent but possess the same set of distances form a homometric pair[3] of arrangements.

CYCLOTOMIC SETS

The discovery of the homometric pair illustrated in Fig. 2 suggested that further pairs of

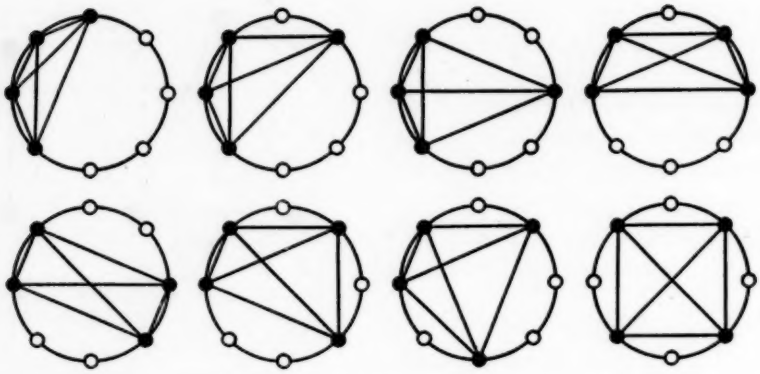

FIG. 3. The cyclotomic sets $n=8$, $r=4$. It will be noted that the third and fourth sets of the top line are complementary and therefore form a pair (that of Fig. 2). All other sets are congruent to their complements and no two have the same distance set.

the same type might be found by arranging points on the circle at r of the n vertices of an inscribed regular polygon. Sets obtained in this manner we call cyclotomic sets.

The results obtained in the examination of 2664 cyclotomic sets are exhibited in Table I. We have found 390 homometric pairs, 7 sets of homometric triplets, and 3 sets of quadruplets. These figures are by no means final although the examination was quite carefully carried out. No theory seems to exist for the number of non-congruent cyclotomic sets, and it is very easy to omit one or more cases despite a careful systematization of the search.

In the course of the examination of the cyclotomic sets a number of interesting results have been obtained. Two of these results must be

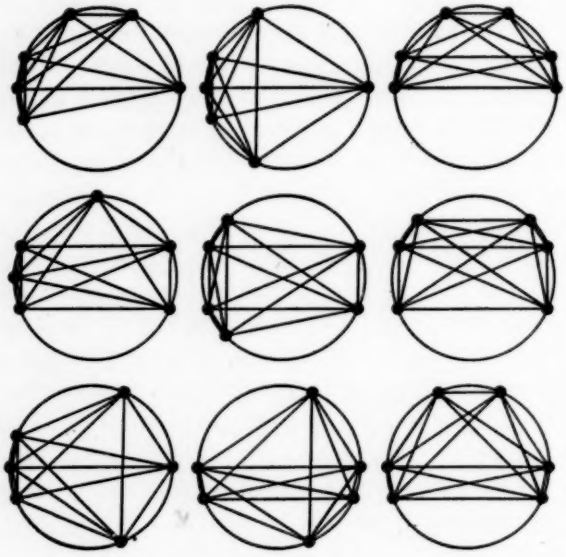

FIG. 4. Three homometric triplets from the cyclotomic sets: $n=16$, $r=6$. The three sets in each horizontal row form a triplet. Note the invariant subsets of each triplet, and of each pair in each triplet.

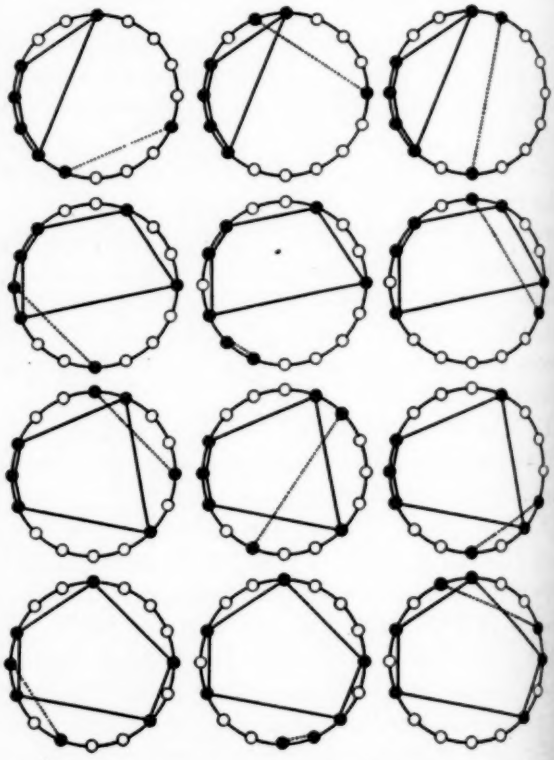

FIG. 5. Four homometric triplets from the cyclotomic sets: $n=16$, $r=7$ (full circles). Most of the distance lines are omitted for clarity. An invariant subset for each triplet is outlined in full lines. Variant points are connected by dotted lines. The open circles will form four homometric triplets from the cyclotomic sets: $n=16$, $r=9$.

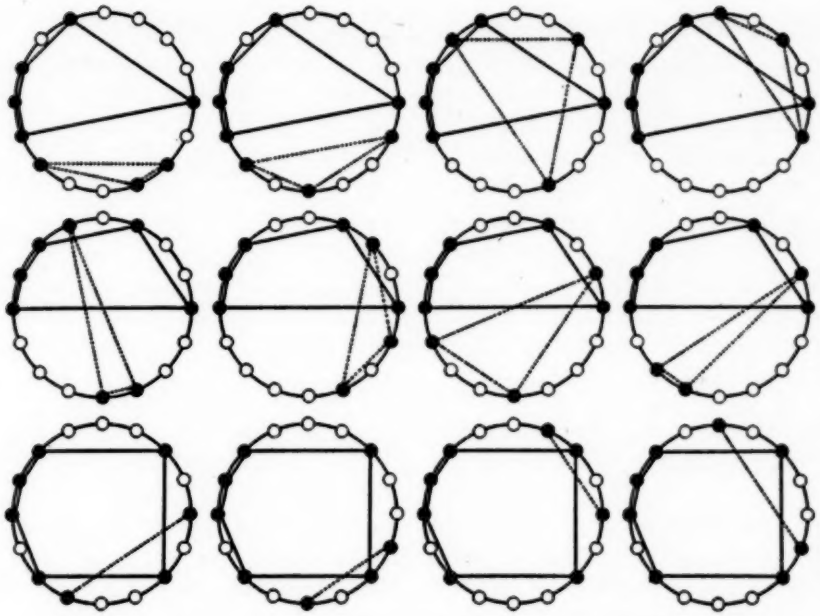

FIG. 6. Three homometric quadruplets from the cyclotomic sets: $n=16$, $r=8$ (full circles). Most of the distance lines are omitted for clarity. An invariant subset for each quadruplet is outlined in full lines. Variant points are connected by dotted lines. Examination of the open circles will show that the first two and the last two of each quadruplet form complementary pairs.

mentioned here, but the proofs will be left for a more detailed discussion elsewhere.

If we consider a set A consisting of r points located on an n cyclotomy, then the set A' consisting of the n-r points of the cyclotomy which are not occupied by A is called the complementary set to A. It can be shown (i) that if two sets A and B form a homometric pair then A' and B' also form a homometric pair, and (ii) that every cyclotomic set with n even and $r=n/2$ is either congruent to its complementary set or it forms a homometric pair with it.

The first of these results cuts down considerably the number of cyclotomic sets which need investigating since the homometric pairs for $(n-r)$ points on an n cyclotomy can be deduced from those for r points. The second of these results enables us to determine by inspection many of the homometric pairs for $r=n/2$. The case of $r=4$ and $n=8$ is illustrated in Fig. 3. There is one homometric pair (that of Fig. 2) and the two members are complementary to one another. All other sets are congruent to their complements and no two have the same distance set.

Figures 4 and 5 exhibit the triplets found on $n=16$ for $r=6$ and $r=7$, respectively, and Fig. 6 shows the quadruplets found on $n=16$ for $r=8$.

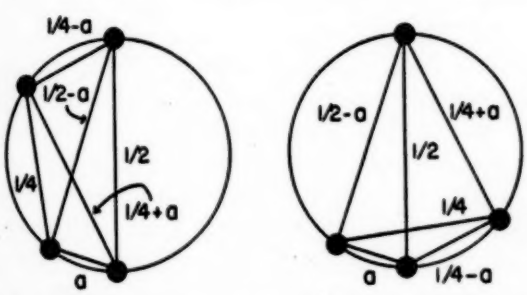

FIG. 7. Homometric pair (4 points) with one variable parameter, obtained by generalization of the set of Fig. 2. ($M=1$, $a<\frac{1}{4}$.)

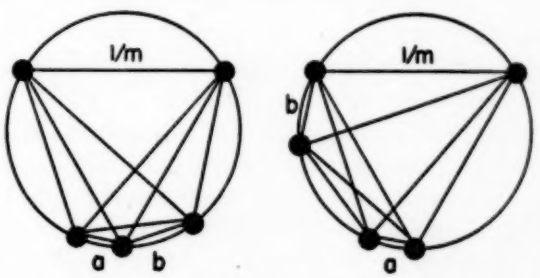

FIG. 8. Homometric pair ($m+2$ points) with one variable parameter, obtained by generalization of the set of Fig. 2. [$M=1$, $a+b=(2m)^{-1}$; $a<(2m)^{-1}$.] The set is illustrated for $m=3$ but it may be constructed on any regular polygon.

TABLE II. Generalized five-point pairs. Each horizontal line gives the simple translations for one pair. a and b are variable parameters.

a_1	a_2	a_3	a_4	a_5	a_1'	a_2'	a_3'	a_4'	a_5'
a	b	$1/2-2a-2b$	$2a+b$	$1/2-a$	a	$1/2$	b	$1/2-2a-2b$	$a+b$
a	b	$1/2-2a-b$	$2a+b$	$1/2-a-b$	a	$a+b$	$1/2-b$	b	$1/2-2a-b$
a	$1/5-a$	a	$2/5-a$	$2/5$	a	$1/5-a$	$1/5$	a	$3/5-a$
a	$1/5-a$	$1/5$	$1/5+a$	$2/5-a$	a	$1/5$	$1/5-a$	$1/5$	$2/5$
a	$1/5-a$	$1/5+a$	$1/5$	$2/5-a$	a	$1/5$	$1/5$	$1/5-a$	$2/5$
a	$1/6$	$1/6-a$	$1/3$	$1/3$	a	$1/6-a$	$1/6+a$	$1/3$	$1/3-a$
a	$1/4$	$1/4-a$	$3/8$	$1/8$	a	$1/4-a$	$1/8+a$	$1/8$	$1/2-a$
a	$1/8$	$1/8-a$	$1/4+a$	$1/2-a$	a	$1/8-a$	$1/8+a$	$1/4-a$	$1/2$
a	$1/4-a$	$1/4+a$	$3/8$	$1/8-a$	a	$1/4$	$1/8-a$	$1/8$	$1/2$

The appearance of these quadruplets indicates that homometric pairs may be formed with sets other than the non-congruent complementary sets.

In many of the multiplets so far studied there are subsets which remain unchanged in going from one member of the multiplet to another. These invariant subsets can easily be recognized by the reader in the sets of Figs. 2 and 4. In Figs. 5 and 6, in which most of the distance lines have been omitted for clarity, invariant subsets are outlined in full lines, while the variant points are connected by broken lines. The choice of an invariant subset in a multiplet is not necessarily unique.

GENERALIZATION OF THE CYCLOTOMIC SETS

The study of the cyclotomic sets soon made it apparent that these were special cases of much more general types of pairs. The four-point pair of Fig. 2 immediately permitted generalization[6] in the manner shown in Fig. 7. We were thus led to an infinity of cyclotomic pairs connected by a continuum of pairs which do not fall in the cyclotomic class. Another type of generalization based on the pair of Fig. 2 is exhibited in Fig. 8. It can be developed from any regular polygon and can thus occur for $(m+2)$ points. Many other general types of pairs have been discovered and only a partial report can be given at the present time. Table II lists the five-point families found by generalization of the cyclotomic pairs of Table I. It may well be incomplete. Over thirty six-point families have been discovered by an incomplete investigation of the pairs of Table I. Their listing must be postponed, however, until an adequate classification system has been developed. The triplets and quadruplets of Figs. 4–6 also produce families of multiplets, but the detailed discussion is incomplete and must be withheld at the present time.

An exhaustive study of all possible pairs and other multiplets seems to be of extreme difficulty. There is obviously a limit to the number of families of multiplets which can occur for a given number of points, but so far it has not been possible to set up a theory which will establish this limit.

EXTENSION TO TWO AND THREE DIMENSIONS

Little has been done so far on the extension of the study to two and three dimensions. It is easy to show that every one-dimensional family of pairs has its counterpart in two- and three-dimensional periodic sets. As a modulus **M** we can use any translational group or translational subgroup of any lattice in the plane or in space. In the construction of the distance array we use the vectors $\mathbf{a}_1$, $\mathbf{a}_2$, $\mathbf{a}_3$, etc., instead of scalars and carry out all our calculations vectorially using **M** as modulus. Corresponding to every homometric pair which we can obtain on the line there will be at least one homometric pair in space. We are assured of this because every translation group in space is either a line lattice, or it contains infinitely many line lattices as subgroups. We can use any such line lattice as a modulus **M′** and calculations (mod **M′**) will also be valid (mod **M**). The vectorial calculation (mod **M′**) is then exactly parallel to the scalar calculation (mod M). In the pairs (mod M) we simply replace fractions of M by fractions of **M′**, and replace disposable scalar parameters by disposable vector parameters. These new solutions

[6] This generalization was suggested by Dr. P. Erdős who also provided helpful discussion of several other points.

are by no means trivial since the vector parameters are no longer confined to the direction of the line lattice **M′**. An example of a two-dimensional pair in which the modulus **M′** is the diagonal line lattice of the primitive cell is exhibited in Fig. 9. It is based on the one-dimensional family of Fig. 7.

It is obviously a restriction to use as modulus a translation subgroup **M′** rather than the full translation group **M**. If this restriction is removed homometric pairs may appear in the plane or in space which have no counterpart on the line. We have been able to show that the two three-dimensional pairs already discussed[2,3] can be based on a two-dimensional modulus **M′** which is a subgroup of a three-dimensional lattice **M**.

CONCLUSION

The picture presented in this paper is somewhat pessimistic as far as x-ray analysis is concerned. It must be remembered, however, that in very few cases are the atoms of a crystal all of one kind, and it seems very probable that the presence of a second kind of atom will often[7] resolve ambiguities which might occur in the location of the first if taken alone. A detailed examination must ultimately be made of all the cases in three dimensions in which ambiguities can occur for arrangements of one and of several kinds of atoms.

Before a particular structure can be determined by x-ray data alone, a complete examination of all ambiguities which can arise in that structure must be available. In addition, it must be remembered that, owing to experimental inaccuracy, x-ray analysis does not usually give all the distances or information equivalent to a knowledge of all the distances. Such a lack of information can lead only to further ambiguity. It seems therefore that x-ray analysis must be used in combination with all other available physical, chemical, and morphological data in the determination of the structure of the solid state. That x-ray analysis can in special cases stand alone is undoubted,[8] but each of these special cases requires its own investigation, not only of the geometry of the situation in question, but of the accuracy of the methods in use, to avoid the possibility of ambiguity.

The writer wishes to express his indebtedness to Mr. John C. Oxtoby of the Department of Mathematics of Bryn Mawr College for his continued interest and his invaluable aid in the development of the mathematical background for this paper.

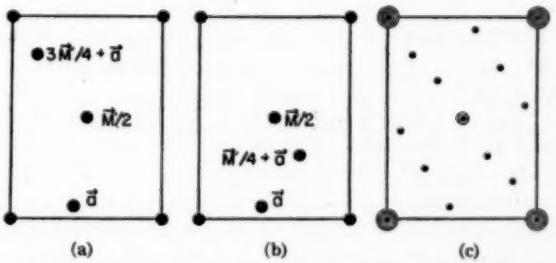

FIG. 9. (a) and (b). Homometric pair in two dimensions derived from the pair of Fig. 7. The modulus **M′** is the diagonal of the unit cell. The lattice **M** is not necessarily orthogonal. (c) Distance vector map for the pair of (a) and (b).

[7] Pauling and Shappell, reference 2, have shown that a second kind of atom in certain special positions of T_h^7-Ia3 does not resolve the ambiguity exhibited by that group.

[8] Reference is made of course to the structures of many elements and simple compounds and to such investigations of more complicated compounds as those of Dickinson and Raymond on hexamethylenetetramine, West on potassium dihydrogen phosphate, and Robertson on the phthalocyanines.

Letters to the Editor

PROMPT publication of brief reports of important discoveries in physics may be secured by addressing them to this department. The closing date for this department is the third of the month. Because of the late closing date for the section no proof can be shown to authors. The Board of Editors does not hold itself responsible for the opinions expressed by the correspondents. Communications should not in general exceed 600 words in length.

Anomalous Rate of Nuclear Disintegration Effected by Cosmic Rays

A. P. ZHDANOV, N. A. PERFILOV, AND M. Y. DEISENROD
Radium Institute of the Academy of Sciences of U.S.S.R., Kasan, U.S.S.R.
January 26, 1944

THE disintegration of atom nuclei by cosmic rays may be only rarely observed in the Wilson chamber, and the method of thickly coated photographic plates first proposed and worked out[1] at the Radium Institute of the Academy of Sciences of U.S.S.R. has proved to be more effective. Applying this method to a series of experiments,[2] we succeeded in observing many individual cases of nuclear disintegration. The rate of nuclear disintegration at sea level is about 8×10^{-3} an hour per 1 cm² of the photoplate area and shows a rapid increase depending on altitude and reaching, for example, at 7000 m, an amount 50 times as large, as that at sea level.[3] This paper records some preliminary data obtained in the case of an exceedingly high rate of nuclear disintegration we observed late in 1942.

The investigation was made in the following way: Thickly coated (70μ) plates with the emulsion sensitive to the charged particles analogous to the emulsion E_3 applied so far[1] were prepared for a series of tests to be carried out on November 19, 1942. The plates developed three days after their preparation (and not radiated at all) upon being examined under the microscope were found to contain an enormous quantity of forks, which because of a great range of particles had necessarily to be attributed to the nuclear disintegration from cosmic rays. This conclusion is also supported by the outward appearance of tracks, for the emulsion E_3 as it was formerly reported[3] possesses a property contributing by their appearance to the discrimination of tracks of mesotrons, protons, α-particles, and other particles capable of higher ionization. It was noted earlier[4] that the property of this emulsion allowed us to point out the possibility of registering mesotrons and of evaluating the mass of these particles. Yet in the plates developed on the day following their preparation, the number of similar disintegrations fully coincided with the above-mentioned "normal" rate for sea level. Further plate development (within different intervals up to 1½ months) led to the observation of a greatly increased number of nuclear disintegrations. The examination of plates also showed the presence of a whole series of characteristic anomalies. Thus, for example, the former studies (carried out both at our Institute and in other laboratories) have shown that at sea level there prevail disintegrations involving three heavy charged particles, the number of ejected particles slowly increasing with the altitude; the quantity of single heavy tracks is much higher than that of forks. In our case the greatest percent of disintegrations is obtained from fourfold forks, and the quantity of single tracks is obviously smaller than that of disintegrations.[5] Side by side with single tracks and forks of a small number (2–5) of tracks one may observe (mostly on plates developed in December) an increased number of disintegrations with the ejection of many particles and characteristic showers consisting of a great quantity (up to some score) of heavy particles that are analogous to the shower of about 100 particles which was registered in 1938 on the plates sent up in an airplane to the altitude of 9000 m.[3,6] An illustration thereof is given in a stereomicrophotograph of disintegration with the ejection of 20 heavy charged particles in Fig. 1 and an example of a shower of 50 particles (protons) in Fig. 2.

It is necessary, however, to point out the great fluctuations in the distribution of nuclear disintegrations on the plate area. For example, on some plates with the area of 10 mm² the magnitude of the rate amounts to the value 10^3 as high as that of the aforesaid "normal" value. Nevertheless, the greatest rate seems to have taken place during the period from November 23 till December 1. But it is only after a detailed and painstaking investigation of the plates under a microscope that we may come to a final conclusion.

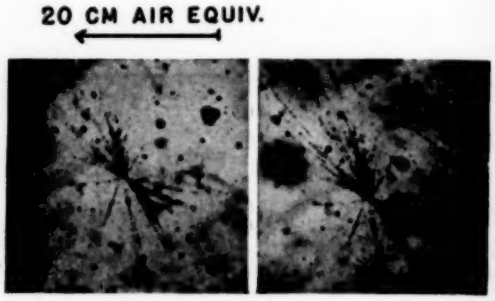

FIG. 1. Example of disintegration involving 20 heavy particles.

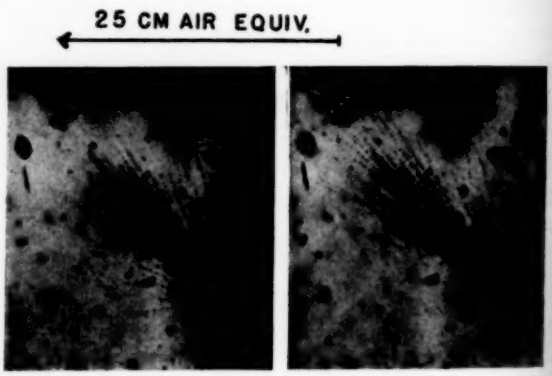

FIG. 2. A shower of 50 particles (protons).

The question becomes complicated due to the presence of an abnormal concentration of forks in the proximity of big showers—the fact noted at an earlier[6] period and graphically seen when drawing a topographic map of the distribution of nuclear disintegrations.[3] Doubtlessly the reason that called forth this anomalous phenomenon is a rough increase of the intensiveness of those components of cosmic radiation that are responsible for nuclear disintegrations. Considering this, it is of great interest to find out whether the increase is a general one and how long it will last (it may be the result of a cosmic catastrophe and thus a similar anomaly could be observed in other places of the globe), or whether it is a local one stipulated, for instance, by the passage of some superpowerful torrent of cosmic particles or, finally, whether it is a result of a combination of both alternatives.

We may hope that a further detailed statistical investigation of plates will bring some answer to these questions.

[1] L. Myssowsky and P. Tschishow, Zeits. f. Physik **44**, 408 (1927); A. Jdanov, J. de phys. et rad. **6**, 233 (1935).
[2] See M. Shapiro, Rev. Mod. Phys. **13**, 58 (1941) for a summary.
[3] A. Jdanov, Bull. Acad. Sci. U.S.S.R. **4**, 266 (1940); Comptes rendus Acad. Sci. U.S.S.R. **28**, 109 (1940).
[4] A. Filippov, A. Jdanov, and I. Gurevich, Comptes rendus Acad. Sci. U.S.S.R. **18**, 181 (1938); J. Phys. U.S.S.R. **1**, 51 (1939); A. Jdanov, Comptes rendus Acad. Sci. U.S.S.R. **20**, 645 (1938); **22**, 163 (1939).
[5] If one takes into consideration only those disintegrations and single tracks where the range is more than 10 cm of air equivalent.
[6] A. Jdanov, Nature **143**, 682 (1939).

The Method of Shower Anticoincidences for Measuring the Meson Component of Cosmic Radiation

VIKRAM SARABHAI
Department of Physics, The Indian Institute of Science, Bangalore, India
January 24, 1944

THE meson intensity measured in counter experiments where absorbers are used to filter out the soft electronic component refers only to fast mesons. The slow mesons which get cut out by the absorber can so far be estimated only indirectly, as, for instance, by the method adopted by Auger[1] and Greisen.[2] There is evidence, however, that the proportion of slow mesons increases rapidly with altitude, and it would be of great advantage if there were a direct method for measuring the total meson intensity. Bhabha[3] has recently suggested on grounds of reducing the weight of lead carried by balloons measuring the meson intensity in the stratosphere that the production of secondaries by the electronic component can be used to advantage in cutting them out. But this principle could be used for the more important purpose of bringing for the first time the slow mesons in the field of direct experimental observations. While a great proportion of cosmic-ray electrons in the atmosphere are already associated with other ionizing particles, the number so associated can be increased by a lead plate of thickness corresponding to the maximum of the Rossi curve. By means of an anticoincidence arrangement working along with a vertical counter telescope, it is possible to exclude events in which associated particles arrive in the telescope. This can be done with side anticounters arranged as shown in Fig. 1*a*, but here the

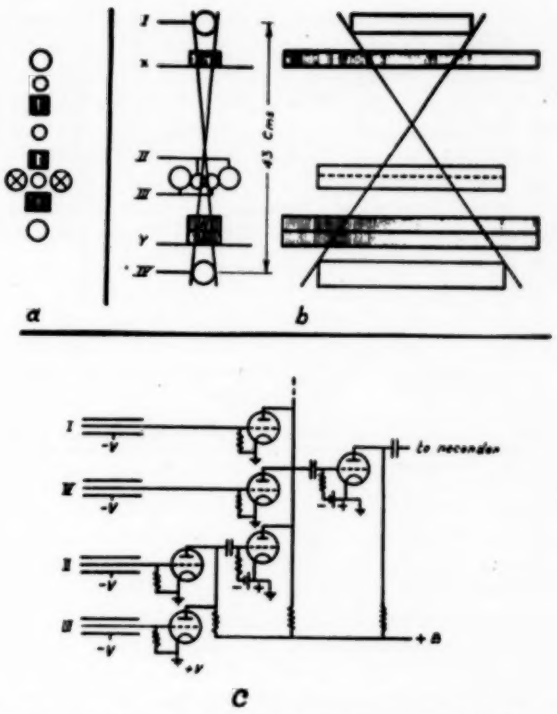

FIG. 1. *a*. Arrangement showing anticounters outside the main cone of measured radiation. *b*. Arrangement used for measuring shower anticoincidences. *c*. Basic circuit for registering shower anticoincidences.

main cone of measured radiation is not utilized for detecting the showers and those that are generated in the lead above on account of their narrow angular spread might avoid detection. The actual arrangement used is shown in Fig. 1*b*, where the sets of counter II and III are used to register the showers. A shower coincidence II, III gives rise to an antipulse which is fed to the coincidences of the main telescope formed by counters I, IV. The lead placed in position *X* is to increase the associated soft particles, and the lead placed in position *Y* is to study the absorption of the radiation without interfering with the efficiency of shower anticoincidences. The basic circuit used has been shown in Fig. 1*c*.

Preliminary results obtained with this arrangement of the total intensity given by coincidences I, IV and the meson intensity given by shower anticoincidences I, IV-(II, III) at various altitudes up to 13,900 ft. in Kashmere illustrate the working of the arrangement. Figure 2 shows the absorption curve at two altitudes of these two counting rates with lead placed at positions *X* and *Y*. The difference between the two curves diminishes rapidly with increasing thickness of lead absorber as the electronic component gets progressively absorbed; and while the slope of the total intensity curve increases with diminishing thickness of lead, the slope of the meson intensity curve varies in an opposite direction. The tendency of the shower anticoincidence curve to become horizontal for zero thickness of lead is a striking indication of the fact that it measures chiefly the meson intensity. The altitude intensity curves from readings at 4 elevations in Kashmere at geomagnetic

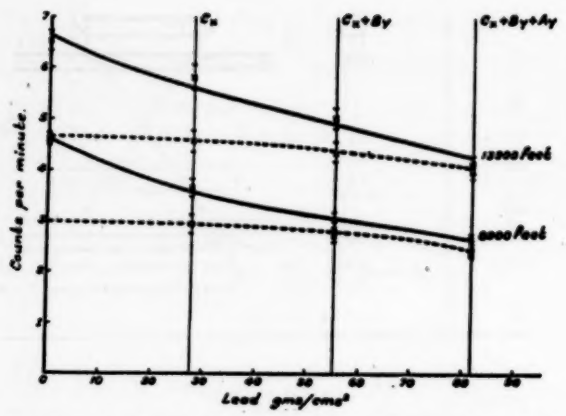

FIG. 2. Curves showing for two altitudes the absorption of the total intensity measured by coincidence rate I, IV (full line) and the meson intensity measured by shower anticoincidence rate I, IV-(II, III) (broken lines).

latitude 25°N show that above 10,000 ft. the meson intensity increases less rapidly than the total intensity and the atmospheric shower intensity. At 13,900 ft. the proportion of mesons was 64 percent of which about 18 percent consisted of slow mesons, but the accuracy of these estimates is not high. A full report of the results obtained at Kashmere and repeated with the same arrangement at Bangalore will appear shortly.[4]

The errors in this experiment might be due to three causes. Firstly, due to the contribution of side showers to the double coincidences that were measured. This would give an under-estimate of the proportion of electrons. Secondly, due to electrons of low energy which do not produce large enough showers to be detected and cut out by the anticoincidence arrangement, and lastly, due to mesons which are associated by other mesons or knock-on electrons and which get cut out by the anticoincidence arrangement. These two errors will tend to give an over-estimate of the proportion of slow mesons. With the help of an accurate experiment that is now being performed with quadruple coincidences measuring the vertical intensity, it is hoped to correct for these errors.

I am indebted to Professor Sir C. V. Raman for supprt and assistance, and to Professor Bhabha for helpful discussions. The Kashmere trip would not have been possible but for the willing help given by the state officials and friends.

[1] P. Auger, Phys. Rev. 61, 684 (1942).
[2] K. Greisen, Phys. Rev. 63, 323 (1943).
[3] Bhabha, Proc. Ind. Acad. Sci. (A), in press.
[4] Sarabhai, Proc. Ind. Acad. Sci. (A), in press.

Configurations of a Binary Mixed Crystal

R. EISENSCHITZ
Davy Faraday Laboratory of the Royal Institution, London, England
January 31, 1944

IN a recent paper Ashkin and Lamb[1] applied the matrix method of statistical mechanics to mixed crystals, especially to the order-disorder equilibrium. In their theory any configuration of the crystal is specified as usually by the kind of atom (A or B) by which every lattice point is occupied. The matrices by which the correlations in the lattice are determined appear to be "degenerated" at low temperatures; the quotation mark indicates that it is the absolute and not the algebraic value of the highest proper value which matters. By this method information is obtained on the superstructure, whereas the evaluation of the specific heat curve seems to be difficult.

In this note an alternative specification of configurations is discussed which is equivalent to the above specification. In a simple cubic lattice of a binary alloy such as β-brass, there are two possible values for the bond energy ϵ, namely, $\epsilon=0$ and $\epsilon=\varphi$ corresponding to bonds between atoms of different kinds and the same kind, respectively. φ is assumed to be positive. The configurations may accordingly be specified by the pattern of bonds, i.e., by the value of ϵ for every bond in the lattice. Not every pattern of bonds corresponds to an atomic configuration; only those patterns are admissible in which there is an even number of "O bonds" on every closed contour of bonds in the lattice. Every pattern which complies with that condition corresponds to two atomic configurations which are transformed into each other by interchanging all A atoms with B atoms and vice versa. The set of all admissible patterns corresponds to the set of all atomic configurations in which not only the positions of A and B atoms but also their ratio is varied.

Instead of making statistics over atomic configurations, it may be made over the admissible patterns of bonds. The central problem is the enumeration of those admissible patterns for which the number of "φ bonds" and accordingly the configurational energy is given. In a square of four nearest neighbors those patterns are admissible in which the number of O bonds is 0 or 2 or 4. There are altogether 8 patterns of this kind. If a pattern of bonds in the lattice is admissible, then every square necesssarily exhibits one of these 8 patterns. This necessary condition is also sufficient. Assuming that the number of O bonds is even in every square of four nearest neighbors, it is proved in the following that this number is even on every closed contour of bonds in the lattice.

In proving this, at first a square net in the plane is considered. Set $q=\int(1-\epsilon/\varphi)ds$ a contour integral taken counterclockwise over the circumference of one square. This integral is equal to a sum of four terms which are 0 for every φ bond and ±1 for every O bond. Let Q be the sum of all q taken over an area which is enclosed by any arbitrary contour of bonds in the net. Then all bonds in the interior of this area contribute 0 to the sum of contour integrals. Q is equal to the contour integral $\int(1-\epsilon/\varphi)ds$, which is taken over the boundary and equal to a sum of as many terms as there are bonds in the boundary. Since, according to premises, every square contributes in even number to Q, Q is even and so is the sum taken over the boundary. As that sum consists only of terms equal to 1, 0, -1, the number of its non-vanishing terms is necessarily even. There is accordingly an even number of O bonds on the boundary, whatever the contour may be like.

In a lattice of three dimensions an arbitrary closed contour of bonds is considered to be the boundary of a large number of surfaces which are formed by squares between nearest neighbors in the lattice. Two of these surfaces define a closed surface and accordingly the direction of an outer normal for each square on either surface. Having assigned on one surface an outer normal to each square, q is defined as contour integral taken counterclockwise over one square as seen from the outer normal and Q is defined as the sum of all q taken over the surface. According to the above argument, the number of O bonds on the contour is then seen to be even.

So far the number ν of A atoms in the lattice of n atoms is regarded as variable so that the configurational partition function is

$$P=\sum_{\nu=0}^{n} p(\nu),$$

where $p(\nu)$ is the partial sum over the configurations with ν A atoms. The partition function of an equimolecular alloy is

$$P^*=\sum_{\nu=0}^{n} p(\nu)\cdot\exp(-\alpha\nu),$$

where the parameter α is determined by

$$n/2=-\partial \log P^*/\partial\alpha.$$

Since $p(\nu)=p(n-\nu)$, it follows from the former equation that $\alpha=0$ for all temperatures. The specific heat curve of an equimolecular alloy is accordingly equal to the specific heat curve of an alloy with variable composition.

The writer[2] recently applied the matrix method to the statistical calculation of the specific heat. The configurations of the lattice are specified in this calculation by the pattern of bonds and only such patterns are admitted in which every square has an even number of O bonds. It appears that in this case the matrices show no "degeneracy." While no information is obtained on the superstructure, the specific heat is evaluated for all temperatures; it has no singularity. A note on the corresponding result for a two-dimensional net has been published previously.[3]

[1] J. Ashkin and W. E. Lamb, Phys. Rev. **64**, 159 (1943).
[2] In print in the Proceedings of the Royal Society.
[3] R. Eisenschitz, Nature **147**, 779 (1941).

Relativity and Supplementary Indeterminacy

G. WATAGHIN
Department of Physics, São Paulo University, São Paulo, Brazil
February 5, 1944

IN recent years experimental evidence has been accumulated concerning the production of groups of mesotrons in one collision and processes in which the hypothetical neutrinos take part.[1] It was pointed out[2] that in view of the irreversibility of many of the processes observed with cosmic rays the statistical mechanics of an assemblage of particles having an average energy per particle $E\gtrsim 200$ mc² is quite different from the usual one. For instance, the introduction of temperature and entropy is not allowed in the cases in which statistical equilibrium is impossible. New limitations arise because of the following circumstances: In a collision accompanied by the production of several mesotrons, the rest mass of the group changes, and the control of the conservation laws of momenta and spins appears limited by the decay processes and fluctuation of the number of created mesotrons and neutrinos. The wave properties of particles, based on diffraction and interference phenomena, are also altered and probably unobservable in high energy collisions, in accordance with the non-linear character of the laws (differential equations, interaction operators) governing such collisions. The representation of high frequency photon-field (for $h\nu>200$ mc²) as a system of harmonic oscillators, and the statistical laws of Planck, Fermi, Bose at extremely high temperatures are invalidated for similar reasons. From the foregoing considerations, it follows that the behavior of high energy particles (observed as cosmic rays in a terrestrial frame of reference) is qualitatively different from the usual one, in accordance with the idea of supplementary indeterminacy.[3]

In the theory of relativity we must distinguish the postulate of general covariancy referring to an arbitrary transformation of coordinates (mathematical symbols used to denominate the events in S_4) from the equivalence of different physical reference frames, each individualized by a system of measuring devices (diffraction gratings, microscopes).[4] Obviously our possibilities of building a reference frame corresponding to a given mathematical transformation are limited (we cannot use rigid bodies or apparatus moving with $v>c$). Let us consider a terrestrial frame of reference (neglecting the rotation) as a local "co-moving" frame in the Friedman universe in expansion. The velocities of the receding nebulae and the cosmic rays are distributed around the earth with spherical symmetry. Let us consider another Lorentz observer moving with an ultra-relativistic velocity βc $[(1-\beta^2)^{-\frac{1}{2}}>1000]$. Any particle of the apparatus used by this second observer will constitute for the terrestrial observer a high energy particle capable of producing a cascade shower or a mesotron shower. Now we introduce the assumption that the "ultra-relativistic" frames of reference are not equivalent to the co-moving ones because the apparatus moving with the velocity of high energy cosmic rays could not function or could not be used as measuring devices in the actual world. Thus we can exclude from our relativity postulate such non-allowed reference systems.

In this way we overcome the incompatibility between the relativity and the theory of a world in which a universal length marks the lower limit for measurement of intervals and a supplementary indeterminacy exists in the region of high energies and momenta.

[1] See cloud-chamber photographs of groups of three, five, seven, mesotrons; experiments with counters on mesotron showers produced in air, lead, and also in clay, underground; high altitude researches on the production of protons, neutrons, and mesotrons in lead and paraffin. Some of the secondary protons and neutrons behave like primaries and thus generate mesotron showers.
[2] G. Wataghin, Phys. Rev. **63**, 137 (1943), and **64**, 248 (1943).
[3] Nature **142**, 393 (1938).
[4] Zeits. f. Physik **66**, 650 (1930); Comptes rendus **207**, 421 (1938).

On the Spin of the Meson

S. K. Chakrabarty and R. C. Majumdar
University College of Science and Technology, Calcutta, India
February 14, 1944

THE phenomena of large bursts under thick layers of a material consisting of more than 200 particles, which are produced almost entirely by mesons of energies greater than 10^{10} ev provide a very feasible means for the determination of the spin of the meson. Christy and Kusaka[1] calculated the frequency of large bursts produced by mesons and concluded that the results for a meson of mass 177 times that of electron and spin zero are in satisfactory agreement with the observation of Schein and Gill.[2] Similar calculations made by one of us (S.K.C.)[3] showed that the conclusions of Christy and Kusaka cannot be maintained and that the observational results fitted well with the results of calculations for a meson of spin 1 when one took the bremsstrahlung cross section, after taking into consideration the effect of radiation damping in it, as given by Wilson.[4] The reasons for arriving at such opposite conclusions were discussed in (C) (see reference 3). It now appears to us that the analyses of Wilson contain some errors, and the correct expression for it may somewhat modify the results obtained (C) in this particular case. By introducing properly the effect of the radiation damping on the emission of photons by mesons, we obtain the differential cross section $\phi(\epsilon)d\epsilon$ for the emission of a photon of energy lying between ϵW and $(\epsilon+d\epsilon)W$ by a meson of spin 1 and energy W, as given by the following expressions:

$$\phi(\epsilon)d\epsilon=\bar{\phi}d\epsilon[C_0f_0(a)-C_1f_1(a)+L(W,b)], \quad \text{for} \quad a\leqslant 1 \quad (1)$$

and

$$\phi(\epsilon)d\epsilon=\bar{\phi}d\epsilon\left[C_0\left\{\frac{\pi}{2}\log a+f_0\left(\frac{1}{a}\right)\right\}-C_1\left\{\frac{\pi^2}{6}+2\log^2 a-f_1\left(\frac{1}{a}\right)\right\}+L(W,b)\right] \quad \text{for} \quad a\geqslant 1 \quad (2)$$

where

$$L(W,b)=2C_1\log^2\left(\frac{a}{b}\right)-C_0f_0(b)+C_1f_1(b)+\left\{\frac{(3C_2+8)\beta}{3b}+2C_1\log(1+b^2)-C_0\tan^{-1}b\right\}\log\left(\frac{a}{b}\right)-\frac{(9C_2+26)\beta}{9b}$$

$$f_0(a)=a\left(1-\frac{a^2}{3^2}+\frac{a^4}{5^2}-\cdots\right),$$

$$f_1(a)=a^2\left(1-\frac{a^2}{2^2}+\frac{a^4}{3^2}-\cdots\right), \quad a=W\beta/\kappa MC^2,$$

$$C_0=\frac{2-2\epsilon+7\epsilon^2}{12\beta}-(C_2+4)\beta,$$

$$C_1=\frac{(34-34\epsilon+7\epsilon^2)\epsilon}{48(1-\epsilon)}+2b\beta,$$

$$C_2=\frac{(14-14\epsilon+\epsilon^2)\epsilon^2}{24(1-\epsilon)^2}-8b^2,$$

$$\beta=(5/288)^{\frac{1}{2}}\alpha\approx 9.63\times 10^{-4}, \quad b=\frac{\epsilon\beta}{2(1-\epsilon)},$$

$$\bar{\phi}=\alpha Z^2\gamma_0^2(m/M)^2, \quad \alpha=e^2/\hbar C.$$

κ is 1 or $5Z^{\frac{1}{2}}/\pi$ according to whether we take for the lowest value of the impact parameter the Compton wave-length (Wilson) or the nuclear radius (Christy and Kusaka). The cross section for the case of spin 0 will, however, not be appreciably affected by the inclusion of the effect of radiation damping. Whether the frequency of bursts calculated with (1) and (2) will still compare favorably with that obtained in (C) cannot be stated without making a long and tedious calculation.

While this calculation is in progress we meanwhile point out that the frequency of bursts produced by the pseudoscalar mesons of spin 0 can be made to agree with the observation of Schein and Gill by a suitable adjustment of its mass. From Eq. (18a) in (C) the total probability $B(N)$ of getting a burst containing more than N particles below an infinitely thick layer of lead, for different values of γ, the ratio between the mass of the vector and pseudoscalar mesons, have been calculated. The mass of the vector meson has been taken as in (C) to be 177 times the electron mass. The results obtained for two different values of γ are given in Table I. On comparing these values with the observations of Schein and Gill we find that the agreement is satisfactory when $\gamma\approx 2.5$. Moreover, our calculations show that in order to obtain the correct sign and magnitude of the quadrupole moment of the deuteron in the theory of Møller-Rosenfeld and Schwinger,[6] we shall have to take $\gamma\approx 2.5$. (Pauli and Kusaka[7] find this ratio to be greater than 2.) These results therefore speak in favor of the theory of Møller and Rosenfeld as modified by Schwinger. The analysis will be shortly published in detail.

TABLE I. Values of $B(N)\times 10^9$ for a pseudoscalar meson.

γ \ N	100	200	400	600	800	1000	1200	1600
2.5	355.5	99.75	28.00	13.41	7.976	5.191	3.733	2.203
3.0	527.0	147.4	41.30	19.76	11.74	7.639	5.492	3.239

[1] R. F. Christy and S. Kusaka, Phys. Rev. **59**, 405, 414 (1941).
[2] M. Schein and P. S. Gill, Rev. Mod. Phys. **11**, 267 (1939).
[3] S. K. Chakrabarty, Ind. J. Phys. **16**, 377 (1942). To be quoted as (C).
[4] A. H. Wilson, Proc. Camb. Phil. Soc. **37**, 301 (1941).
[5] C. Møller and L. Rosenfeld, Nature **144**, 476 (1939).
[6] J. Schwinger, Phys. Rev. **61**, 387A (1942).
[7] W. Pauli and S. Kusaka, Phys. Rev. **63**, 400 (1943).